In vivo mechanical loading combined with cell therapy in a bone tissue engineering scaffold

PAR

Tanja Cloé HAUSHERR

ÉCOLE POLYTECHNIQUE
FÉDÉRALE DE LAUSANNE

Suisse
2016

*"**K**nowledge **i**s **l**imited. **I**magination **e**ncircles **t**he **w**orld."*

*A*lbert *E*instein

Acknowledgements

precious advices and the good moments we shared together. A special warm and kind thank to Lee for her precious time in having read and corrected a part of my thesis before submitting it.

A huge thank to all students I supervised during my thesis, Axelle Justafré, Florence Gavin, Iris Rentsch, Serge Metrailler, Sophie Aebischer, Rebekka Anker, Tiffany Thebault and Thaïs Clouet. Their great work had nicely contributed to my thesis, and I learned a lot with them and gained in experience while teaching them.

What would be a PhD student life without friends, fellows and buddies? A lot of pain, loneliness and boring moments… Therefore, huge and great thanks to my friends within and out of the LBO lab: Philippe Abdel-Sayed, Salim Darwiche, Valérie Lavanchy-Parvex, Antoine Dewarrat, Priscilla Briquez, Ziad Julier, Kay Bartholdi and Nathalie Brandenberg. Thanks for all the shared funny moments, laughers, and joy as well as the upside and downside of a PhD student's life. You all made my PhD journey full of surprises, unexpected events and enlightenment, thanks for these great experience and adventure!

Special thanks to Priscilla Briquez who was very brave to read and correct thoroughly my entire thesis before its submission. The discussions as well as your precise comments and corrections were really valuable!

And last but not least, I want to warmly thank my friends and family, especially my parents, Christine and Rolf Hausherr, for their unconditional support, presence and advices all along my studies and PhD, and by supporting me in every decisive paths I decided to follow. I am mostly who I am thanks to them. Furthermore, I want to thank as well my sister Jennifer Guyon and family (especially for her help and enlightenment during two surgery sessions) and my brother Yann Hausherr for fantastic discussions and air changes when needed, filled with a lot of laughers and love.

Finally, I want to thank my partner Miguel Torres with all my gratitude for his unconditional support by his love, calm, understanding and patience on this long and not always easy PhD journey. And most of all, I want to thank our wonderful daughter Katnyss and her baby brother-to-be for having given me the strength, joy and energy filled with love and giggles that accompanied me through this adventure.

Abstract

Bone defects generate a worldwide high demand for bone repair and reconstruction. The incidence of bone defect repair in our aging society is expected to increase in the next decades. As bone auto- and allografting solutions often suffer from limited supplies, there is a clinical need for alternative bone substitutes, challenging researchers in bone tissue engineering to find novel approaches. To address this challenge, several biomaterials have been combined with different approaches, such as various biomolecules delivery, cell therapy or the application of mechanical loading. In the present PhD thesis, we assessed for the first time the effect of temporal onsets of mechanical loading combined with cell therapy in a tissue engineering scaffold implanted in a bone site. For this purpose, we used a poly(L-lactic acid)/ß–tricalcium phosphate scaffold, human bone progenitor cells and two mechanical loading conditions. The choice of the scaffold was motivated by its reinforced porous structure and enhanced bioactivity, whereas, for the choice of cells, we were driven by their low immunogenicity and high capacity for osteogenic differentiation. This capacity allowed us to evaluate two different bone cell fates originating from the same cell type. We then used the same mechanical loading parameters as in previous studies on scaffolds without cells. When loading was applied a few days post-implantation (early loading) and a few weeks post-implantation (delayed loading), moderate and advantageous effects for bone repair could respectively be observed. We focused our work on (1) the investigation of a potential immune reaction triggered by xenograft cells at an early stage of implantation in immuno-competent rats and (2) the evaluation of early and delayed mechanical loadings on bone formation when combined with cell therapy. Three scaffold conditions were used: human bone progenitor cell-seeded, osteogenic human bone progenitor cell-seeded and cell-free scaffolds. Each scaffold condition was implanted bilaterally in both femoral condyles of rats. In the first part of this thesis, early immune reaction was evaluated on implanted scaffolds based on histology. The results indicated that, unlike cell-free scaffolds, both cell-seeded types of scaffolds affected the surrounding tissue by forming fibrous tissue but without triggering particular specific immune reaction. In the second part, we followed static and dynamic bone parameters inside scaffolds based on microCT scans. We showed that, independently of mechanical loading conditions, a significantly higher amount of bone was formed within cell-free scaffolds than within the two cell-seeded ones. Depending on the cell-seeded scaffold conditions, early mechanical loading had different effects on bone formation. We concluded that the timing of mechanical loading and the cell types, as well as specific combinations thereof, are crucial for a beneficial bone repair. Overall, however, cell-free scaffolds used in this study could be considered as the best solution when combined with delayed mechanical loading, as it is simple and safe from a clinical point of view without increasing regulatory restriction due to the use of cells.

Keywords: Bone tissue engineering, scaffold, cell therapy, human bone progenitor cells, osteogenic human bone progenitor cells, early and delayed mechanical loading, histology, micro-computed tomography.

Résumé

Les lésions osseuses génèrent une forte demande de reconstruction d'os dans le monde entier. Notre société étant vieillissante, les besoins cliniques de reconstruction de ces lésions va augmenter dans les prochaines décennies. Par conséquent, le développement de tissus osseux de substitution comme alternatives aux auto- et allogreffes, liés à une offre de greffe limitée, se révèle être un véritable défi pour les chercheurs en ingénierie tissulaire de l'os. Pour relever ce défi, plusieurs biomatériaux ont été combinés avec l'enrichissement de différentes biomolécules, la thérapie cellulaire ou l'application de charges mécaniques. Dans cette thèse, nous avons évalué l'effet de la charge mécanique combinée à la thérapie cellulaire dans une matrice tissulaire. Nous avons utilisé une matrice composée de PLA/TCP, des cellules progénitrices d'os humaines et deux conditions de charge mécanique. Cette matrice a été choisie pour sa structure poreuse renforcée et sa bioactivité, tandis que les cellules ont été utilisées pour leur faible immunogénicité et leur grande capacité de différentiation ostéogénique. Cette capacité nous a permis d'évaluer deux différents destins de cellules osseuses provenant du même type cellulaire. Nous avons utilisé les mêmes paramètres de charge mécanique que ceux décrits dans des études précédentes démontrant un effet modéré et avantageux sur la repousse osseuse après l'application d'une charge précoce ou retardée. Notre travail s'est focalisé sur (1) l'étude de la réaction immunitaire provoquée par les cellules xénogreffées peu après l'implantation dans des rats immunocompétents et sur (2) l'évaluation de la thérapie cellulaire combinée à des charges mécaniques précoces et tardives sur la formation osseuse. Dans les deux cas, trois types de matrices ont été implantées bilatéralement dans des condyles fémoraux de rats: des matrices sans cellules ou ensemencées avec des cellules progénitrices d'os humaines ostéogéniques ou non différenciées. Dans la première partie, la réaction immunitaire précoce des matrices a été évaluée par histologie. Les résultats ont indiqués que les deux types de matrices ensemencées ont affecté le tissu environnant en formant du tissu fibreux contrairement aux matrices sans cellules, sans pour autant déclencher une réaction immunitaire spécifique. Dans la deuxième partie, nous avons quantifié les paramètres statiques et dynamiques osseux dans les matrices par l'analyse d'images obtenues via microCT. Nous avons montré qu'indépendamment des conditions de charges mécaniques, une quantité d'os significativement plus élevée a été formée dans les matrices sans cellules que dans les deux autres types. Selon le type de matrice ensemencée, la charge mécanique précoce a eu des effets différents sur la formation osseuse. Dans l'ensemble, nous pouvons conclure que le moment de l'application de la charge mécanique et le matériel biologique sont essentiels pour une reconstruction osseuse bénéfique. Notamment, les matrices sans cellules utilisées dans cette étude pourraient être considérées comme la meilleure solution lorsqu'elles sont combinées avec une charge mécanique tardive, car c'est une solution simple et sûre en clinique, qui n'augmente pas la contrainte règlementaire due à l'utilisation de cellules.

Keywords: Ingénierie tissulaire de l'os, matrice, thérapie cellulaire, cellules humaines progénitrices d'os, cellules humaines progénitrices d'os ostéogéniques, charge mécanique précoce et tardive, histologie, microCT.

Table of contents

Abbreviations

ALP: Alkaline phosphatase

Alu-ISH: Alu *in situ* hybridization

BF: Bone formation

BR: Bone resorption

BTE: Bone tissue engineering

BV/TV: Bone volume density

CF: Cell-free

CS: Cell-seeded

dH_2O: Distilled water

GAMM: General additive mixed model

GFP hBPCs: Green fluorescent protein transduced human progenitor cells

hBPCs: Human bone progenitor cells

hOBPCs: Osteogenic human bone progenitor cells

MSCs: Mesenchymal stem cells

microCT: Micro-computed tomography

OCS: Osteogenic cell-seeded

PLA: Poly(L-lactic acid)

RT: Room temperature

Tb.N: Trabecular number

Tb.Sp: Trabecular separation

Tb.Th: Trabecular thickness:

TCP: Tricalcium phosphate

VOI: Volume of interest

Chapter 1

Introduction

1.1 Motivation and Thesis Aims

Skeletal defects, caused by non-union fractures or resections of bone tumors, generate a high demand of bone repair and reconstruction which creates accordingly a great challenge in the actual field of bone regeneration (Al-Sayyad & Abdulmajeed 2006; Klenke et al. 2008; Muramatsu et al. 2009; Costa-Pinto et al. 2011). For instance, in the United States, the annual costs dedicated to bone repair has been estimated to be higher than $2.5 billion for the treatment of more than half a million patients (Baroli 2009; Amini et al. 2012). In addition, the incidence of bone disorders is expected to increase worldwide in the next decades, due to an aging society and the incidence of other diseases such as obesity (Amini et al. 2012).

As the current clinical use of bone auto- and allografts is related to restrictions, such as limited supply, donor site morbidity, scarring, surgical risk, risk of infections or cost issues (Klenke et al. 2008; Das & Botchwey 2011; Amini et al. 2012; Rechenberg et al. 2013), a growing interest in the field of bone tissue engineering (BTE) started to emerge 30 years ago. Nowadays, BTE deals with the pentaconcept in which cells, growth factors, scaffold (biomaterials), vascularization and mechanical stimuli should adequately be combined (Loi et al. 2016). The general aim is to heal bone in the shortest time frame, with the best possible functional recovery for the patient, without complications and post-surgery failures as stated by Gomez-Barrena et al. (Gomez-Barrena et al. 2015). Once implanted, the prime function of these bone substitutes, named scaffolds, is to replace the missing bone by giving a mechanical support and reinforcement to the surrounding bone tissue (Bose et al. 2012; Amini et al. 2012). This temporary support prevents from long-term deformity and gives the cells the time for scaffold colonization and formation of new mineralized tissue (Black, Goriainov, Gibbs, Kanczler, Tare & Oreffo 2015b), which structure is defined by the shape of the scaffold. Beside the mechanical support function and biocompatibility, the scaffold is often tuned by enhancing osteo-conductive and -inductive properties for better bone formation (Vaccaro 2002; Khan et al. 2012). It should also be adapted to the bone tissue structure and mechanical strength, which vary by distinct and dynamic conditions, as well as location in the body (Amini et al. 2012). The current main limitation of the developed BTE scaffolds is a localized bone formation at the periphery of the scaffold, mostly because of an insufficient and unsuited vascularization once implanted (Amini et al. 2012). Therefore different strategies have been combined and tested to improve scaffold integration and bone formation. Particularly, approaches based on cell therapy, surface treatment with growth factors and therapy using mechanical loading have been either combined or used separately within scaffolds (Robling et al. 2002; Duty et al. 2007; Roshan-Ghias et al. 2011; Boerckel, Kolambkar, et al. 2011; Boerckel et al. 2012; Black, Goriainov, Gibbs, Kanczler, Tare & Oreffo 2015a). Although many of these strategies have been investigated, only a few have been approved for clinical use. The application of these strategies in clinics are prevented by regulatory approval, by specific market needs and obtention of private investment do develop products with specific clinical indications (Hollister & Murphy 2011).

In that context, our project was motivated by the need to find an adequate scaffold for bone regeneration of a load-bearing site that would be friendly-to-use for surgeons, safe, with minimal regulatory constraints and with minimal surgical and rehabilitation costs for the patient. In particular, a scaffold that would allow an early and fast mobilization of the patient would not only decrease the rehabilitation costs, but would help him to load the operated site rapidly and quickly regain a good life quality.

To develop such scaffolds, our study takes basis on three previously *in vivo* studies completed in our laboratory, which showed that (1) human bone progenitor cells (hBPCs) seeded in poly(L-lactic acid) (PLA)/5% ß – tricalcium phosphate (ß–TCP) scaffolds promote bone repair (Montjovent et al. 2008), (2) early mechanical loading increases modestly bone formation inside PLA/5% ß–TCP scaffolds (Roshan-Ghias et al. 2010) and (3) delayed mechanical loading accelerates bone formation and decelerates bone resorption inside PLA/5% ß–TCP scaffolds (Roshan-Ghias et al. 2011), when applied in drilled defects in femoral condyles of rats.

The attractiveness of hBPCs arises from their multipotency and capacity for osteogenic differentiation, their proliferative ability and therefore facility of upscaling. Their low immunogenicity has been hypothesized (Montjovent et al. 2004; Montjovent et al. 2008; Krattinger et al. 2011; Hirt-Burri et al. 2011) and their scareless wound healing potential is assumed considering the one of skin and tendon progenitor cells (Applegate et al. 2009; M. S.-M. Hu et al. 2014; Fang et al. 2014). Furthermore, they have also been reported as good candidates for easy cell banking and its associated safety (Montjovent et al. 2008).

The choice of PLA/5% ß–TCP composited for this study was motivated by its advantages of providing reinforced porous structures with enhanced bioactivity and controlled resorption rate. Initially, scaffolds were either composed of either polymer (*e.g.* PLA) or ceramic (*e.g.* ß–TCP), which tended to be too flexible or too brittle, respectively (Mathieu et al. 2006). By combining them, mechanical properties were improved with a better structural integrity and flexibility than neat polymer and brittle ceramic, subsequently (Mathieu et al. 2006).

Therefore, in this thesis, we investigate the effect of the combination between mechanical loading application and cell therapy in a tissue engineering scaffold, possibly combining the benefits of both therapies to improve bone regeneration. Accordingly, this work stands at the intersection of two main functions of the bone, namely the biological function and the mechanical function. More precisely, we respectively explored (1) the addition of two different types of cells, being hBPC and osteogenic hBPC (hOBPCs) to the tissue engineering PLA/5% ß–TCP scaffold and (2) the effect of temporal mechanical loading onsets on the different scaffold conditions. To our knowledge, the combination of cell-seeded bone scaffold and mechanical loading in bone regeneration has been investigated for the first time in this thesis, which we believe would bring unique insights to understand and develop an integrated therapy, embracing both biological and mechanical features of bone healing.

The aims of the thesis are structured as follows:

Aim 1: Investigation of immune reaction triggered by xenograft of human fetal cells

In a first aim, we assessed the potential immune reaction triggered by xenograft of human fetal cells at an early stage post-implantation in immuno-competent rats. The human fetal cells used in this study were hBPCs and hOBPCs; both were seeded inside PLA/TCP scaffolds. After having characterized hBPCs-seeded (CS) scaffolds and hOBPCs-seeded (OCS) *in vitro*, we implanted them in drilled defects in femoral condyles and analyzed both locally and systemically the cellular immune response at 3, 7 and 14 days post-implantation.

Aim 2: Evaluation of temporal onset of mechanical loading on bone formation inside a tissue engineering scaffold combined with cell therapy *in vivo*

In our second aim, we evaluated the impact of temporal onsets of mechanical loading over 12 weeks in rats. We chose first to further investigate the effect of the combination between hBPCs or hOBPCs seeded within scaffolds and the early mechanical loading, starting 2 days post-implantation, as described by Roshan-Ghias et al. (Roshan-Ghias et al. 2010). We hypothesized that the sensitivity of the used cells to mechanical loading would improve the bone formation inside the cell-seeded implanted scaffolds than in cell-free (CF) scaffolds, which is of advantage for the patient as it translates to fast mobilization. In a second step, we then evaluated the effect of delayed mechanical loading, starting 14 days post-implantation, on bone formation in CF and CS scaffolds. In both early and delayed cases, the mechanical loading parameters were kept the same, but were implemented on scaffolds in which the bone formation was in different maturation states.

The Chapter 2 of this thesis covers aim 1 while Chapter 3 comprises aim 2. An overview scheme of the aims, their study conditions and the specific tasks are presented in Fig. 1.1.
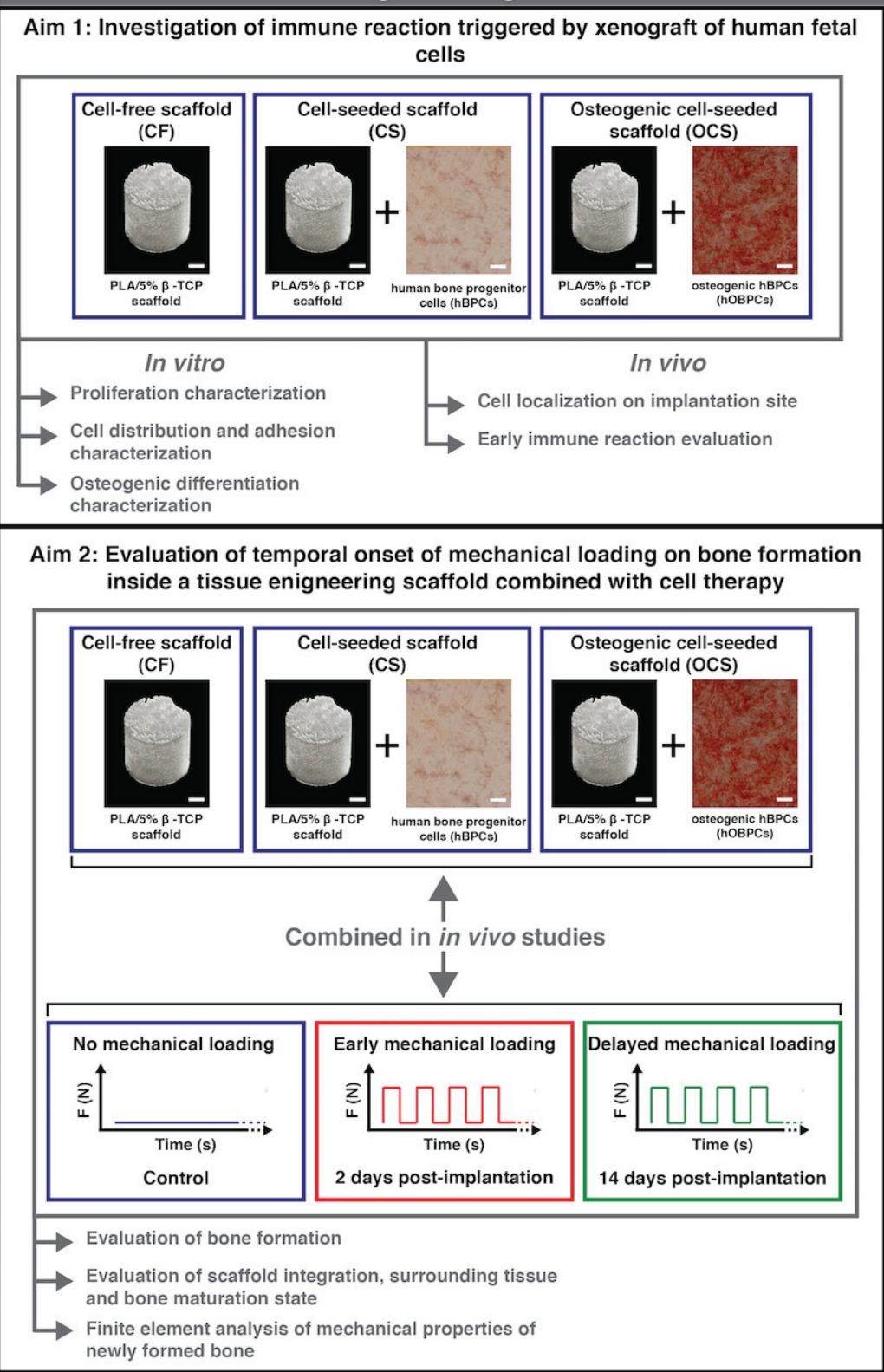
Figure 1.1 Overall objective and specific aims of this thesis.

1.2 Background

1.2.1 Bone

The commonly known function of bone for the human body is the mechanical protection for internal organs such as the brain, the heart, the spinal cord and pelvic organs. The 206 bones, which constitute an adult human skeleton, also play an important function in the direct motion and the locomotion process thanks to the muscles attachment to the bone either by a tendon, aponeurosis or by direct attachment. Furthermore, the bone is a protective housing for essential pluripotent precursor cells for the living organism such as hematopoietic stem cells and mesenchymal stem cells (MSCs). The first source of cells is involved in the renewing of the blood cells (monocytes, macrophages, neutrophils, eosinophils, erythroblasts, erythrocytes and platelets) and the second one contributes to the regeneration of tissues such as bone, cartilage, muscle, adipose, tendon, ligament and stroma (Gurkan & Akkus 2008). The bone is also a reservoir for mineral ions, such as calcium and phosphorus for the maintenance of a constant ionic environment in the extracellular fluid (Rodan 1998). Phosphorus is one of the main ionic components complexes with calcium required for the hydroxyapatite formation during the mineralization of the extracellular matrix (Moe et al. 2005; Penido & Alon 2012).

1.2.1.1 Bone Structure

Bone structures can vary depending on the function of the particular bone and its position in the body. Even if the structure of the bones can be different, they all present two histologically defined bone types: the cortical bone (dense bone) and the trabecular bone (spongy or cancellous bone) (Seibel et al. 2006). The cortical bone accounts for 80% of the skeleton mass (Seeman et al. 2010). It is a stiff bone with a porosity between 5-10%, while the trabecular bone has a porosity between 50-90%. It carries a considerable share of the total load of the skeleton (Augat & Schorlemmer 2006). It forms the outer layer of the bone and in between lays the trabecular bone as shown in Fig. 1.2.
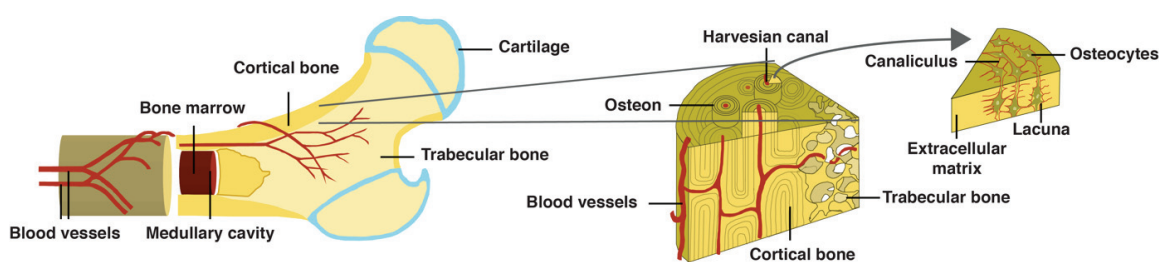
Figure 1.2 Structure of a typical long bone and the different units composing it (adapted from Copyright © 2004 Pearson Education, Inc., publishing as Benjamin Cummings Human Anatomy & Physiology, Sixth Edition).

The cortical bone is mainly composed of multiple osteons; each one composed of multiple layers of osteoblasts and osteocytes with in the middle a Haversian canal as depicted in Fig. 1.2 Those osteons lay longitudinally to the bone axis. Thanks to the Haversian canal, blood vessels, nerves or lymphatic vessels can travel through the bone. Furthermore, concentrically arranged layers called lamellae

form the canal. Between these lamellae, small spaces are situated, which are called lacunae. Each of these lacunae contains one single osteocyte (mature osteoblast) and small canals called canaliculi that interconnect them all. The outer layer of the cortical bone is covered by a periosteal surface whereas the inner layer is covered by an endosteal surface. The periosteal surface activity is important for positional growth and fracture repair, whereas the endosteal surface has higher remodeling activity than the periosteal surface (Clarke 2008). The periosteal surface also enables a boundary between the cortical and the trabecular bone (Eriksen et al. 1994). The trabecular bone represents 20% of the overall bone and is built of plates and rods averaging from 50 to 400 μm in thickness (Eriksen et al. 1994). As for the cortical bone, trabecular bone is constituted of osteons, which are semilunar in shape and composed of concentric lamellae.

Furthermore, cortical and trabecular bone are normally present in lamellar bone. The lamellar bone is mainly composed of collagen fibrils with alternating orientations, which are deposited by osteoblasts. This alternating composition results in a significant strength (Clarke 2008; Eriksen et al. 1994). A weaker and less organized bone structure than lamellar bone is found during the formation of primary bone, in fracture calli and in certain bone diseases. The difference in the organization of collagen fibrils between woven and lamellar bone is reflected in their different mechanical properties (Clarke 2008).

1.2.1.2   Bone Cells

Bone is a mineralized connective tissue composed of 50-70% of mineral, 20-40% of organic matrix and 5-10% of water (Clarke 2008). The inorganic matrix is composed of mineral salts, mostly hydroxyapatite, with small amount of carbonate, magnesium and acid phosphate. This inorganic matrix provides the mechanical rigidity and load-bearing strength to bone (Clarke 2008). The organic matrix, the so-called extracellular matrix (ECM), is similar to ECM found in other connective tissues. It consists mainly of 85-90% of collagenous proteins and the remaining non-collagenous protein are composed of growth factors and other molecules involved in bone activity (Clarke 2008). The extracellular matrix is responsible for the elasticity and the flexibility of the bone.

Four major cell types, namely osteoclasts, osteoprogenitor cells, osteoblasts and osteocytes compose the bone tissue as presented in Fig. 1.3. They all have the same cellular origin, namely human MSCs, except for osteoclasts. This later cell types are a differentiated multinucleated cells derived from hematopoietic stem cells lineage (Florencio-Silva et al. 2015). They are the unique cells having the capacity of resorbing bone, which depends on the osteoclast secretion of hydrogen ions and cathepsin K enzyme. The hydrogen ions one dissolves the mineral component of bone matrix, whereas the cathepsin K enzyme one digests the proteinaceous matrix (Clarke 2008). The second group of bone, the osteoprogenitor cells, is composed of self-renewing and pluripotent cells, derived from MSCs. They give rise to osteoblasts that play an important role in bone formation. Osteoblasts are located along the bone surface during bone formation (Florencio-Silva et al. 2015). They are called bone lining cells when they are in a quiescent state. This bone lining cells therefore cover the bone surface where neither resorption nor bone formation takes place (Miller et al. 1989; Florencio-Silva et al. 2015). The exact function of these cells is quite unknown, but they have been shown to prevent a direct interaction between osteoclasts and bone matrix especially when bone resorption should not occur (Mosley 2000). The last type of bone cells consists in osteocytes, which are differentiated osteoblasts. They also function within syncytial networks to support bone structure

and metabolism. They are the main instigator of bone remodeling process; they act as mechanosensors (Franz-Odendaal et al. 2005) and transduce stress signals from bending or stretching into biological activity (Clarke 2008).

1.2.1.3 Bone Modeling and Remodeling

Throughout life, bone undergoes a highly dynamic and complex process involving two important mechanisms, bone modeling and remodeling (Clarke 2008; Florencio-Silva et al. 2015). Bone modeling is crucial for growth and adaptation of the skeleton to mechanical forces and stresses. During bone modeling, bone formation and resorption occur independently at distinct anatomical sites (Clarke 2008). It is a process that takes place less often in adults than bone remodeling (Kobayashi et al. 2003). Bone remodeling is the process by which old and damaged bone is removed and repaired (Seeman 2009); it plays an important role in maintaining bone strength and mineral homeostasis (Clarke 2008). This process undergoes four sequential steps in a well-organized cycle as depicted in Fig. 1.3: (1) Activation which initiates the recruitment and activation of mononuclear osteoclast precursors, (2) resorption through osteoclasts activation, (3) reversal in which resorption transits to formation and (4) formation of bone through osteoblast activation (Clarke 2008; Florencio-Silva et al. 2015). The temporary anatomical structure, which results of the coordination between osteoclast, osteoblasts, osteocytes and bone lining cells, is called the basic multicellular unit (BMU) (Florencio-Silva et al. 2015).
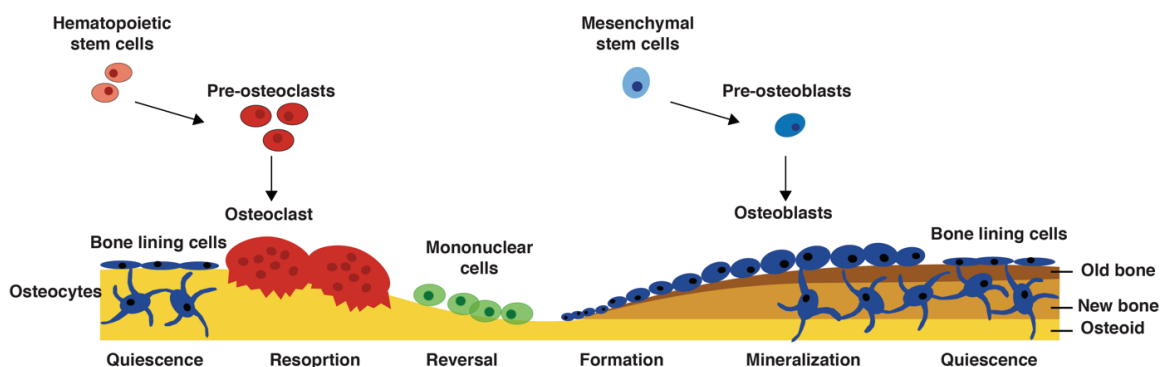
Figure 1.3 Bone remodeling process (adapted from Kapinas K. et al. 2011 and Biomedical Tissue Research, University of York).

1.2.2 Bone Damages and Current Available Clinical Therapies

Non-union after bone fracture, congenital abnormalities, aging, infections and bone tumor removal often result in long-term deformity due to a reduced bone structure and function (Black, Goriainov, Gibbs, Kanczler, Tare & Oreffo 2015a). Those impairments can lead to activity limitations as well as pain, and substantially affect the life quality of the patient. To overcome those serious issues of reconstructive surgery, different clinical available therapies exist. They rely on bone graft transplants, bone transport methods and implants based on various types of materials (Costa-Pinto et al. 2011). The gold standard of bone repair in reconstructive surgery, is the treatment of bone loss with cancellous bone autograft transplant derived from the iliac crest (Klenke et al. 2008; Das & Botchwey 2011). It's a reliable technique, which ensures a good biocompatibility. It stimulates new bone

formation and integration through osteogenesis and osteoconduction. One downside of this technique is that the harvesting of the autograft from the iliac crest involves an additional trauma to the patient (see Fig. 1.4). This additional intervention can cause some complications and also result in a significant morbidity of the graft site. As bone autograft has a limited supply, it is often combined with allografts or synthetic bone substitutes (Muramatsu et al. 2009; Al-Sayyad & Abdulmajeed 2006; Costa-Pinto et al. 2011) which are presented in Fig. 1.4. These two autograft extenders are considered as the main alternative solution to bone-grafting technique. Concerning bone allograft, a typically non-vital bone is harvested from cadaveric donors and is processed using the freeze-drying method. It is then stored under various forms, such as demineralized bone matrix, morcellised and cancellous chips, cortical and whole-bone segments (Amini et al. 2012; Costa-Pinto et al. 2011). It gives a structure in which bone growth is enabled and avoids donor-site morbidity like in bone autografts (Costa-Pinto et al. 2011). The main disadvantage of allografts is its slow incorporation rate and the potential risk of immune rejection and pathogen transfer from cadaver to the patient (Amini et al. 2012; Costa-Pinto et al. 2011).
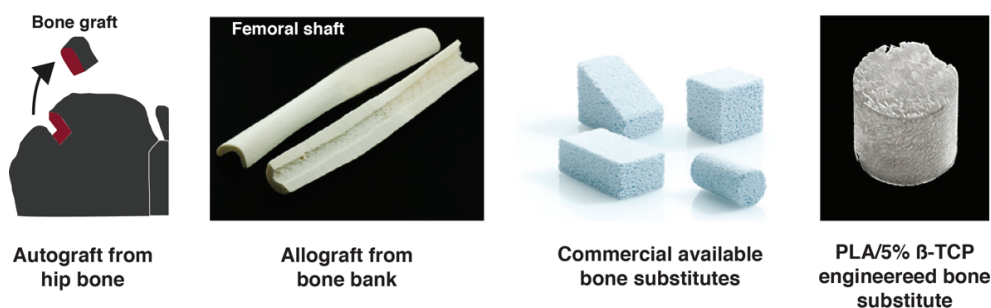
Figure 1.4 Clinical solutions for bone replacement. Autograft harvested from the iliac crest, femoral shaft used as bone allograft, commercially available bone substitutes and a tissue-engineered scaffold for research purposes (images either adapted from A.D.AM. Editorial Time or taken from ReproBone[TM] and SteriGraft[TM] or from A. Roshan-Ghias thesis).

Consequently, a growing interest in the development of synthetic bone substitutes, often called scaffolds, started three decades ago. The main advantages of this engineered scaffold are their biocompatibility, their capacity to integrate within the existing bone and to be filled by new-formed osseous tissue (Klenke et al. 2008). Furthermore, another advantages of synthetic bone substitutes over bone auto- and allografts are their unlimited availability as well as their controlled production process. As an illustration of their use, two clinical cases are shown in Fig. 1.5 and 1.6.
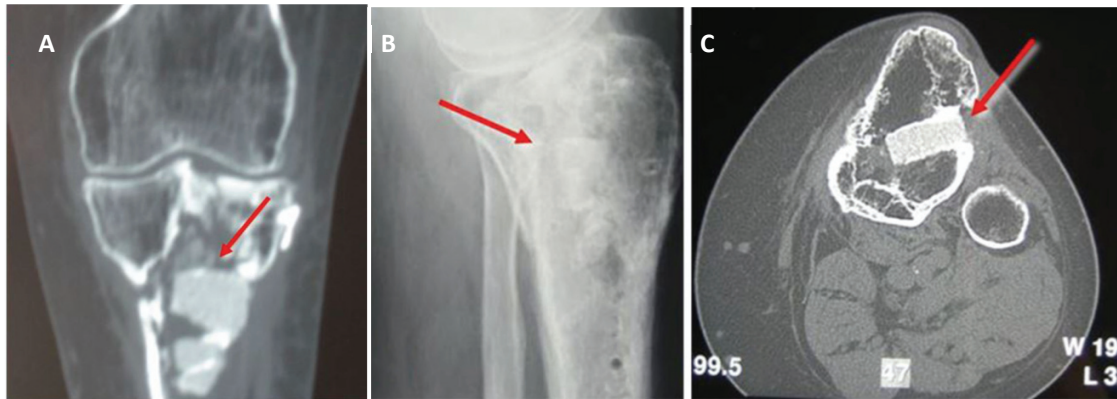
Figure 1.5 HA-TCP bone substitute in proximal tibia traumatic bone loss. X-rays (A and B) and CT scan (C) at 3-year follow-up in the proximal tibia without resorption of bone substitute. The red arrow is pointing out the implanted scaffold (adapted from Campana et al. 2014).

In the first example, a hydroxyapatite (HA) TCP bone substitute was used in a traumatic bone loss in the proximal tibia as described by Campana et al. (Campana et al. 2014). In this case, X-rays images were taken 3 years after the implantation. The scaffold osteo-integrated well, but without any sign of resorption or bone substitution. In the second example, shown in Fig 1.6, an X-ray follow-up of an aneurysmal bone cyst in the metacarpal bone is illustrated. X-rays before and just after grafting of calcium sulfate-based bone substitutes (Osteoset®) as well as 4 weeks and 5 months after surgery are shown. In this case, the bone substitutes were totally resorbed and replaced by healthy bone as described by Jung et al. (Jung et al. 2007).
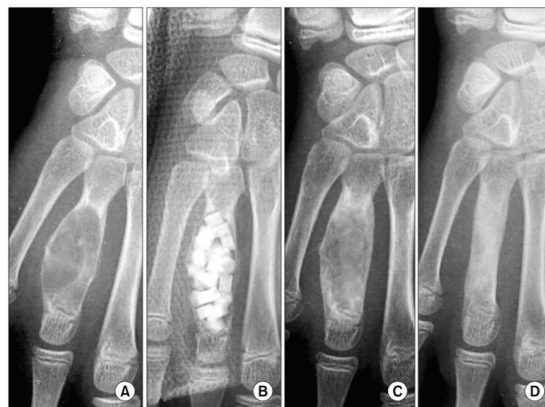
Figure 1.6 Follow-up of an aneurysmal bone cyst located in the metacarpal bone from pre-operation to 5 months post-surgery. Plain X-rays before implantation (A), after the curettage and grafting of bone substitutes (Osteoset®) (B), 4 weeks (C) and 5 months (D) after the surgery with resorption of bone substitutes and complete bone healing (adapted from Jung et al. 2014).

11

1.2.3 Bone Tissue Engineering

BTE is an interdisciplinary, complex and dynamic field of research, which focuses on alternative clinical options for bone replacement, thus ideally eliminating issues of the current clinical treatments (Amini et al. 2012; Motamedian et al. 2015). For this purpose, it applies the principles of biology and engineering for the development of functional substitutes that restore, maintain or improve damaged tissue (Langer & Vacanti 1993). Regarding the biological principles in bone healing, one can distinguish between three sequential main phases: inflammatory, reparative and remodeling phases (Marsell & Einhorn 2011). In a first phase, the injury initiates an acute inflammatory reaction necessary for the healing progress, followed by the recruitment of stromal MSCs, which differentiate into osteogenic cells. Simultaneously, the immune system clear the injured site from tissue and cell debris. As fracture healing requires oxygen and nutriment supply, neoangiogenesis and revascularization take place, which is essential for successful bone healing. Finally, bone regeneration progresses and is finalized by bone mineralization and bone remodeling processes (Marsell & Einhorn 2011). Therefore, BTE implemented and mimicked successively the different biological mechanisms and the main factors involved in bone healing as depicted in Fig. 1.7.
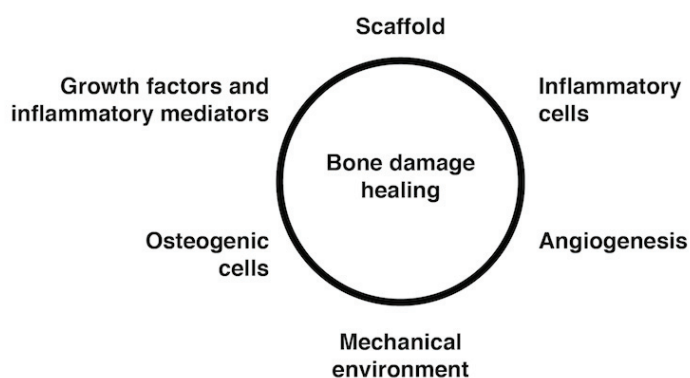
Figure 1.7 Main factors influencing bone healing in the field of bone tissue engineering (adapted from Loi et al. 2016).

Initially, biomaterials scaffolds were selected in BTE as first solution due to their mechanical properties and temporary structure restoration in which bone formation was enabled (Bose et al. 2012; Amini et al. 2012; Black, Goriainov, Gibbs, Kanczler, Tare & Oreffo 2015b). The scaffold properties, such as pore size, distribution and shape, surface roughness, scaffold structure and presence of cell attachment sites are important to consider for successful bone formation (Marolt et al. 2010). Secondly, to promote and increase bone growth inside these scaffolds, osteoconductive and osteoinductive properties were as well considered for their design (Bose et al. 2012). Among those biomaterials, ceramic (*e.g.* β-TCP or HA) are typically found. They are often used for their similar mineral composition than bone, their biocompatible and osteoconductive properties (Vaccaro 2002). As ceramic tends to brittle, its mechanical properties are often enhanced when combined with polymers, such as PLA. The porous structure in these biocomposites is therefore reinforced with an enhanced bioactivity and controlled resorption rate (Mathieu et al. 2006). Additionally, the enhancement of bone healing in BTE was completed by addition of growth factors, such as BMP (Cao

& Chen 2005; Boerckel, Kolambkar, et al. 2011), TGF-ß (Buijs et al. 2012) and/or VEGF (Grellier et al. 2009). These factors play either a role in osteogenesis, bone tissue regeneration, angiogenesis or ECM formation (Bose et al. 2012). Finally, two other approaches in BTE were combined separately in the scaffolds, namely (1) cell therapy with osteogenic cells (Srouji & Livne 2005; Jäger et al. 2007; Montjovent et al. 2008; Dupont et al. 2010; Xu et al. 2010; Y. Liu et al. 2013), such as MSCs, bone progenitor cells or osteoblast-like cells, or (2) the application of *in vivo* cyclic mechanical loading (Robling et al. 2002; Duty et al. 2007; Roshan-Ghias et al. 2011; Boerckel et al. 2012; Amini et al. 2012). Recently, more complex interactions among cells involved in bone remodeling and inflammatory cells have been shown to be essential for repair and bone healing. This new approach seems to be promising, although the implicated mechanisms are still largely unknown (Lassus et al. 1998; Mountziaris et al. 2011; Miron & Bosshardt 2016; Loi et al. 2016).

1.2.3.1 Therapeutic Cell Sources

The choice of cell source used for BTE in clinics is an ongoing debate, in which several basic considerations should be taken into account and secured (Marolt et al. 2010; Amini et al. 2012). It is of importance to take into account the listed parameters: Cell type (autologous or allogeneic adult cells, stem cells), cell isolation efficiency, cell yield, potential of proliferation (limited or self-renewing), controllable osteogenic phenotype and stability, long-term safety and automation, and quality control after implantation while respecting regulatory and administration affairs (Marolt et al. 2010). Until now, studies have investigated several cell types for their abilities to favor bone repair and regeneration within bone defects (Amini et al. 2012). Among these cell types, adult cells from bone marrow (Connolly 1995; Corre et al. 2015; Hempel et al. 2016) and periosteum (Marolt et al. 2010), MSCs, genetically engineered cells (Lu et al. 2013; Y.-C. Hu 2014; X. Liu et al. 2016; Bonadio et al. 1999), embryonic stem cells (Marolt et al. 2010) or fetal bone progenitor cells (Montjovent et al. 2004; Pioletti et al. 2006; Montjovent et al. 2008; Tamer & Reis 2009) have been investigated. This variety of possible candidates for BTE can be explained by the healing and regeneration mechanisms in which different and various cell fates are involved, from undifferentiated progenitor to mature bone cells. Thus far, only adult stem cells from bone marrow, adipose tissue and aspirated platelet rich plasma bone marrow are in clinical use (Amini et al. 2012). The remaining cell types have not been used yet. Their future translation would need further assessment on their safety and their regulatory approval.

1.2.3.2 Mechanical Loading

Already in 1892, Wolff described in "*The law of bone remodeling",* the adaptation of bone architecture to mechanical loading (Wolff 1892). Mechanical forces have been shown to be essential for proper morphogenesis and maintenance of normal bone structure and function (Kini & Nandeesh 2012). In the case of disuse, bone will become fragile and thin due to a rapid loss of bone mass as observed in astronauts (Robling et al. 2006; Robling & Turner 2009). On the other hand, in the case of overuse, the bone tissue is damaged which needs to be remodeled. If the damage accumulates faster than the remodeling and regeneration processes, microcracks may develop (Robling et al. 2006). If not stopped in time, they may result in stress fracture. It has been shown that effects of loading on bone remodeling follow a U-shaped curve. The sudden increase of bone remodeling under disused or overused is called turnover. The bone remodeling range in between these extreme loading conditions is called the physiological range.

As mechanical loading in a physiological range induces osteogenesis, mechanical loading plays an essential role in healing of bone damages such as fractures (Ulstrup 2008). To date, different *in vivo* studies in rodent models have shown the beneficial impact of mechanical loading on bone growth for BTE (Roshan-Ghias et al. 2010; Roshan-Ghias et al. 2011; Boerckel, Kolambkar, et al. 2011; Boerckel, Uhrig, et al. 2011; Boerckel et al. 2012). For example, a study has been made on the bone growth at the level of a large bone defect (6 mm) (Boerckel et al. 2012) while another study discusses the bone regeneration around a titanium implant at different loading frequencies (Zhang et al. 2012).

Furthermore, the onset of the mechanical loading, early or delayed, also has a strong impact on bone formation and angiogenesis. For instance in critical size defect (8 mm height) *in vivo*, Boerckel et al. have showed that early loading (immediate) disrupted neovascular ingrowth and prevented bone formation. When delayed loading (4 weeks onset) was applied, the vascular network remodeling was stimulated and bone regeneration was increased (Boerckel, Uhrig, et al. 2011). Similar observations have been done concerning the effect of early (3 days onset) and delayed loading (2 weeks onset) on bone formation inside implanted scaffolds (3 mm height and 3 mm diameter) in femoral condyles of rats (Roshan-Ghias et al. 2010; Roshan-Ghias et al. 2011). In the first study, they showed that early mechanical loading increased moderately the amount of formed bone inside implanted scaffolds after 13 weeks of implantation (Roshan-Ghias et al. 2010). In the second study, they have demonstrated that delayed mechanical loading has significantly increased the amount of formed bone after already 7 weeks of implantation (Roshan-Ghias et al. 2011). All three studies have determined the delayed mechanical loading was more beneficial for bone volume increase inside implanted scaffolds than early mechanical loading.

1.3 References

Al-Sayyad, M.J. & Abdulmajeed, T.M., 2006. Fracture of the anterior iliac crest following autogenous bone grafting. *Saudi Medical Journal*, 27(2), pp.254–258.

Amini, A.R., Laurencin, C.T. & Nukavarapu, S.P., 2012. Bone tissue engineering: recent advances and challenges. *Critical Reviews in Biomedical Engineering*, 40(5), pp.363–408.

Applegate, L.A. et al., 2009. Whole-cell bioprocessing of human fetal cells for tissue engineering of skin. *Skin Pharmacology and Physiology*, 22(2), pp.63–73.

Augat, P. & Schorlemmer, S., 2006. The role of cortical bone and its microstructure in bone strength. *Age and Ageing*, 35(suppl 2), pp.ii27–ii31.

Baroli, B., 2009. From natural bone grafts to tissue engineering therapeutics: Brainstorming on pharmaceutical formulative requirements and challenges. *Journal of pharmaceutical sciences*, 98(4), pp.1317–1375.

Black, C.R.M., Goriainov, V., Gibbs, D., Kanczler, J., Tare, R.S. & Oreffo, R.O.C., 2015a. Bone tissue engineering. *Current Molecular Biology Reports*, 1(3), pp.132–140.

Black, C.R.M., Goriainov, V., Gibbs, D., Kanczler, J., Tare, R.S. & Oreffo, R.O.C., 2015b. Bone tissue engineering. *Current Molecular Biology Reports*, 1(3), pp.132–140.

Boerckel, J.D. et al., 2012. Effects of *in vivo* mechanical loading on large bone defect regeneration. *Journal of Orthopaedic Research*, 30(7), pp.1067–1075.

Boerckel, J.D., Kolambkar, Y.M., et al., 2011. Effects of protein dose and delivery system on BMP-mediated bone regeneration. *Biomaterials*, 32(22), pp.5241–5251.

Boerckel, J.D., Uhrig, B.A., et al., 2011. Mechanical regulation of vascular growth and tissue regeneration in vivo. *Proceedings of the National Academy of Sciences of the United States of America*, 108(37), pp.E674–E680.

Bonadio, J. et al., 1999. Localized, direct plasmid gene delivery in vivo: prolonged therapy results in reproducible tissue regeneration. *Nature Medicine*, 5(7), pp.753–759.

Bose, S., Roy, M. & Bandyopadhyay, A., 2012. Recent advances in bone tissue engineering scaffolds. *Trends in Biotechnology*, 30(10), pp.546–554.

Buijs, J.T., Stayrook, K.R. & Guise, T.A., 2012. The role of TGF-β in bone metastasis: novel therapeutic perspectives. *BoneKEy reports*, 1(6), pp.1–10.

Campana, V. et al., 2014. Bone substitutes in orthopaedic surgery: from basic science to clinical practice. *Journal of Materials Science: Materials in Medicine*, 25(10), pp.2445–2461.

Cao, X. & Chen, D., 2005. The BMP signaling and *in vivo* bone formation. *Gene*, 357(1), pp.1–8.

Clarke, B., 2008. Normal bone anatomy and physiology. *Clinical Journal of the American Society of Nephrology*, 3 Suppl 3(Supplement 3), pp.S131–9.

Connolly, J.F., 1995. Injectable bone marrow preparations to stimulate osteogenic repair. *Clinical Orthopaedics and Related Research*, 313, pp.8–18.

Corre, P. et al., 2015. Direct comparison of current cell-based and cell-free approaches towards the repair of craniofacial bone defects – A preclinical study. *Acta Biomaterialia*, 26, pp.306–317.

Costa-Pinto, A.R., Reis, R.L. & Neves, N.M., 2011. Scaffolds based bone tissue engineering: The role of chitosan. *Tissue Engineering Part B: Reviews*, 17(5), pp.331–347.

Das, A. & Botchwey, E., 2011. Evaluation of angiogenesis and osteogenesis. *Tissue Engineering Part B: Reviews*, 17(6), pp.403–414.

Dupont, K.M. et al., 2010. Human stem cell delivery for treatment of large segmental bone defects. *Proceedings of the National Academy of Sciences*, 107(8), pp.3305–3310.

Duty, A.O., Oest, M.E. & Guldberg, R.E., 2007. Cyclic mechanical compression increases mineralization of cell-seeded polymer scaffolds in vivo. *Journal of Biomechanical Engineering*, 129(4), pp.531–539.

Eriksen, E.F., Axelrod, D.W. & Melsen, F., 1994. *Bone histomorphometry*, Lippincott Williams & Wilkins.

Fang, Z. et al., 2014. Transplantation of fetal instead of adult fibroblasts reduces the probability of ectopic ossification during tendon repair. *Tissue Engineering: Part A*, 20(13-14), pp.1815–1826.

Florencio-Silva, R. et al., 2015. Biology of bone tissue: Structure, function, and factors that influence bone cells. *Biomed Research International*, 2015, pp.1–17.

Franz-Odendaal, T.A., Hall, B.K. & Witten, P.E., 2005. Buried alive: How osteoblasts become osteocytes. *Developmental Dynamics*, 235(1), pp.176–190.

Gomez-Barrena, E. et al., 2015. Bone fracture healing: Cell therapy in delayed unions and nonunions. *Bone*, 70, pp.93–101.

Grellier, M. et al., 2009. Role of vascular endothelial growth factor in the communication between human osteoprogenitors and endothelial cells. *Journal of Cellular Biochemistry*, 106(3), pp.390–398.

Gurkan, U.A. & Akkus, O., 2008. The mechanical environment of bone marrow: a review. *Annals oBiomedical Engineering*, 36(12), pp.1978–1991.

Hempel, U. et al., 2016. Human bone marrow stromal cells: A reliable, challenging tool for *in vitro* osteogenesis and bone tissue engineering approaches. *Stem Cells International*, 2016(1-2), pp.–14.

Hirt-Burri, N. et al., 2011. Biologicals and fetal cell therapy for wound and scar management. *ISRN Dermatology*, 2011(1), pp.1–16.

Hollister, S.J. & Murphy, W.L., 2011. Scaffold translation: Barriers between concept and clinic. *Tissue Engineering Part B: Reviews*, 17(6), pp.459–474.

Hu, M.S.-M. et al., 2014. The Role of Stem Cells During Scarless Skin Wound Healing. *Advances in wound care*, 3(4), pp.304–314.

Hu, Y.-C., 2014. Gene Therapy for Bone Tissue Engineering. In *Gene therapy for cartilage and bone tissue engineering*. Berlin, Heidelberg: Springer Berlin Heidelberg, pp. 33–53.

Jäger, M. et al., 2007. Bone healing and migration of cord blood-derived stem cells into a critical size femoral defect after xenotransplantation. *Journal of Bone and Mineral Research : the Official Journal of the American Society for Bone and Mineral Research*, 22(8), pp.1224–1233.

Jung, S.T., Kim, M.S. & Jeong, K.C., 2007. The usefulness of calcium sulfate in treatment of benign bone Tumor. *Journal of the Korean*, 42(5), p.623.

Khan, W.S. et al., 2012. An Osteoconductive, Osteoinductive, and Osteogenic Tissue-Engineered Product for Trauma and Orthopaedic Surgery: How Far Are We? *Stem Cells International*, 2012(5110), pp.1–7.

Kini, U. & Nandeesh, B.N., 2012. Physiology of bone formation, remodeling, and metabolism. In *Radionuclide and Hybrid Bone Imaging*. Berlin, Heidelberg: Springer Berlin Heidelberg, pp. 29–57.

Klenke, F.M. et al., 2008. Impact of pore size on the vascularization and osseointegration of ceramic bone substitutes *in vivo*. *Journal of Biomedical Materials Research Part A*, 85A(3), pp.777–786.

Kobayashi, S. et al., 2003. Trabecular minimodeling in human iliac bone. *Bone*, 32(2), pp.163–169.

Krattinger, N. et al., 2011. Regulation of proliferation and differentiation of human fetal bone cells. *European Cells and Materials*, 21, pp.46–58.

Langer, R. & Vacanti, J.P., 1993. Tissue engineering. *Science*, 260(5110), pp.920–926.

Lassus, J. et al., 1998. Macrophage activation results in bone resorption. *Clinical Orthopaedics and Related Research*, (352), pp.7–15.

Liu, X. et al., 2016. Osteoprotegerin gene-modified BMSCs with hydroxyapatite scaffold for treating critical-sized mandibular defects in ovariectomized osteoporotic rats. *Acta Biomaterialia*.

Liu, Y. et al., 2013. Integration of a calcined bovine bone and BMSC-sheet 3D scaffold and the promotion of bone regeneration in large defects. *Biomaterials*, 34(38), pp.9998–10006.

Loi, F. et al., 2016. Inflammation, fracture and bone repair. *Bone*, 86, pp.119–130.

Lu, C.-H. et al., 2013. Recent progresses in gene delivery-based bone tissue engineering. *Biotechnology Advances*, 31(8), pp.1695–1706.

Marolt, D., Knezevic, M. & Novakovic, G.V., 2010. Bone tissue engineering with human stem cells. *Stem Cell Research & Therapy*, 1(2).

Marsell, R. & Einhorn, T.A., 2011. The biology of fracture healing. *Injury-International Journal of the Care of the Injured*, 42(6), pp.551–555.

Mathieu, L.M. et al., 2006. Architecture and properties of anisotropic polymer composite scaffolds for bone tissue engineering. *Biomaterials*, 27(6), pp.905–916.

Miller, S.C. et al., 1989. Bone lining cells: structure and function. *Scanning Microscopy*, 3(3), pp.953–60– discussion 960–1.

Miron, R.J. & Bosshardt, D.D., 2016. OsteoMacs: Key players around bone biomaterials. *Biomaterials*, 82, pp.1–19.

Moe, S.M., 2005. Disorders of calcium, phosphorus, and magnesium. *American Journal of Kidney Diseases*, 45(1), pp.213–218.

Montjovent, M.-O. et al., 2004. Fetal bone cells for tissue engineering. *Bone*, 35(6), pp.1323–1333.

Montjovent, M.-O. et al., 2008. Human fetal bone cells associated with ceramic reinforced PLA scaffolds for tissue engineering. *Bone*, 42(3), pp.554–564.

Mosley, J.R., 2000. Osteoporosis and bone functional adaptation: Mechanobiological regulation of bone architecture in growing and adult bone, a review. *Journal of Rehabilitation Research and Development*, 37(2), pp.189–199.

Motamedian, S.R. et al., 2015. Smart scaffolds in bone tissue engineering: A systematic review of literature. *World Journal of Stem Cells*, 7(3), pp.657–668.

Mountziaris, P.M. et al., 2011. Harnessing and modulating inflammation in strategies for bone regeneration. *Tissue Engineering Part B: Reviews*, 17(6), pp.393–402.

Muramatsu, K. et al., 2009. Recalcitrant posttraumatic nonunion of the humerus: 23 patients reconstructed with vascularized bone graft. *Acta Orthopaedica Scandinavica*, 74(1), pp.95–97.

Penido, M.G.M.G. & Alon, U.S., 2012. Phosphate homeostasis and its role in bone health. *Pediatric Nephrology*, 27(11), pp.2039–2048.

Pioletti, D.P. et al., 2006. Bone tissue engineering using fetal cell therapy. *Swiss Medical Weekly*, 136, pp.557–560.

Rechenberg, von, B. et al., 2013. Evaluation of four biodegradable, injectable bone cements in an experimental drill hole model in sheep. *European Journal of Pharmaceutics and Biopharmaceutics*, 85(1), pp.130–138.

Robling, A.G. & Turner, C.H., 2009. Mechanical signaling for bone modeling and remodeling. *Critical Reviews in Eukaryotic Gene Expression*, 19(4), pp.319–338.

Robling, A.G. et al., 2002. Improved bone structure and strength after long-term mechanical loading is greatest if loading Is separated into short bouts. *Journal of Bone and Mineral Research*, 17(8), pp.1545–1554.

Robling, A.G., Castillo, A.B. & Turner, C.H., 2006. Biomechanical and molecular regulation of bone remodeling. *Annual Reveiw of Biomedical Engineering*, 8(1), pp.455–498.

Rodan, G.A., 1998. Bone homeostasis. *Proceedings of the National Academy of Sciences of the United States of America*, 95(23), pp.13361–13362.

Roshan-Ghias, A. et al., 2010. *In vivo* cycling loading as potent stimulatory signal for bone formation inside tissue engineereing scaffolds. *European Cells and Materials*, 19, pp.41–49.

Roshan-Ghias, A. et al., 2011. *In vivo* loading increases mechanical properties of scaffold by affecting bone formation and bone resorption rates. *Bone*, 49(6), pp.1357–1364.

Seeman, E., 2009. Bone modeling and remodeling. *Critical Reviews in Eukaryotic Gene Expression*, 19(3), pp.219–233.

Seeman, E. et al., 2010. Microarchitectural deterioration of cortical and trabecular bone: Differing effects of denosumab and alendronate. *Journal of Bone and Mineral Research*, 25(8), pp.1886–1894.

Seibel, M.J., Robins, S.P. & Bilezikian, J.P., 2006. *Dynamics of bone and cartilage metabolism*, Academic Press.

Srouji, S. & Livne, E., 2005. Bone marrow stem cells and biological scaffold for bone repair in aging and disease. *Mechanisms of Ageing and Development*, 126(2), pp.281–287.

Tamer, El, M.K. & Reis, R.L., 2009. Progenitor and stem cells for bone and cartilage regeneration. *Journal of Tissue Engineering and Regenerative Medicine*, 3(5), pp.327–337.

Ulstrup, A.K., 2008. Biomechanical concepts of fracture healing in weight-bearing long bones. *Acta Orthopaedica Belgica*.

Vaccaro, A.R., 2002. The role of the osteoconductive scaffold in synthetic bone graft. *Orthopedics*, 25(5), pp.S571–S578.

Wolff, J., 1892. The law of bone remodelling. *Berlin: August Hirschwald*.

Xu, C. et al., 2010. A novel biomimetic composite scaffold hybridized with mesenchymal stem cells in repair of rat bone defects models. *Journal of Biomedical Materials Research Part A*, 95(2), pp.495–503.

Zhang, X. et al., 2012. *In vivo* assessment of the effect of controlled high- and low-frequency mechanical loading on peri-implant bone healing. *Journal of The Royal Society Interface*, 9(72), pp.1697–1704.

Chapter 2

Human Bone Progenitor Cells for Clinical Application: What Kind of Immune Reaction Do Xenograft Cells Trigger in Rats?

Hausherr T.C., Nuss K., Thein E., Damo M., Applegate L.A., Pioletti D.P.

2.1 Abstract

The potential of human fetal bone cells for successful bone regeneration has been shown *in vivo.* In particular, it has been demonstrated that the seeding of these cells in porous poly(L-lactic acid)/ß-tricalcium phosphate scaffolds improved considerably the bone formation than in cell-free scaffolds. However, even if the outcome is an improvement of bone formation, a thorough analysis concerning any immune responses, due to the implantation of xenograft cells, is not known. As the immune response and skeletal system relationship may either contribute to success or failure of an implant, we were interested in evaluating the presence of any immune cells and specific reactions of human fetal cells, also called human bone progenitor cells, once implanted in femoral condyles of rats. For this purpose either (1) cell-free scaffolds, (2) human bone progenitor cells or (3) osteogenic human bone progenitor cells within scaffolds were implanted over 3, 7 and 14 days. The results indicated that human bone progenitor cells and osteogenic human bone progenitor cells affect the surrounding tissue by forming fibrous tissue than in cell-free scaffolds, but without triggering particular specific immune reaction.

Keywords: Bone tissue engineering, scaffold, cell therapy, human bone progenitor cells, osteogenic human bone progenitor cells, immune response.

2.2 Introduction

The high demand of bone repair due to bone trauma, non-unions or resection of tumors creates a great challenge to the actual field of bone regeneration (Muramatsu et al. 2009; Al-Sayyad & Abdulmajeed 2006; Costa-Pinto et al. 2011). Problems related to the use of auto- and allografts, such as limited supply, donor site morbidity, scarring, surgical risk, risk of infections, cost issues and logistical challenges in creating bone banks (Klenke et al. 2008; Das & Botchwey 2011; Amini et al. 2012; Rechenberg et al. 2013), led to a growing interest in the field of bone tissue engineering (BTE) in the last three decades (Amini et al. 2012). Therefore, the current aim of BTE, which matches the needs of the orthopedic medicine, is to obtain bone healing in the shortest time frame, with the best possible functional recovery associated with the least complications (Gomez-Barrena et al. 2015). To achieve this goal, different approaches have been used, in which synthetic bone substitutes, with similar mechanical properties than bone and allowing a sufficient vascularization, are either combined with osteogenic engineered cells, morphogenic signals or mechanical stimulations (Roshan-Ghias et al. 2011; Boerckel et al. 2011; Boerckel et al. 2012; Amini et al. 2012; Black et al. 2015).

Several approaches combining biomaterials with bone marrow preparations (Connolly 1995; Quarto et al. 2001), bone marrow-derived mesenchymal stem cells (Krebsbach et al. 1998; Serafini et al. 2014), or osteoblasts (Amini et al. 2012) were described to be promising for BTE. Furthermore, the potential of human fetal cells, for a successful engineered regeneration of adult skeletal tissue has been shown (Montjovent et al. 2004; Krattinger et al. 2011). In the *in vitro* studies, the investigators have demonstrated that these human fetal cells, also called human bone progenitor cells (hBPCs), could be of great interest for bone research due to their efficient cell isolation, rapid growth rate, advanced osteogenesis development and ability to differentiate into stable and mature osteoblasts. In the present study, those mature osteoblasts, derived from hBPCs, are referred to as osteogenic hBPCs (hOBPCs). In a later *in vivo* study, Montjovent et al. (Montjovent et al. 2008) evaluated the effect of hBPCs in combination with porous poly(L-lactic acid)/ß-tricalcium (PLA/ß-TCP) scaffolds. Cell-free and cell-seeded scaffolds were implanted in skulls of rats followed by a histological qualitative evaluation of bone repair after 12 days, 6 and 12 months after implantation. They analyzed the ossification along the dura and the porous ossification inside the different scaffold conditions. The investigators discovered that the cells improved the bone formation inside the scaffolds in this animal model.

Even though the final outcome was an improvement of bone formation, a thorough analysis concerning associated immune responses with the implantation of xenograft cells, is necessary. This kind of information is especially relevant to the envisioned clinical application of transplanting hBPCs into different patients, which will then represent an allograft. As the immune response and skeletal system relationship may either contribute to success or failure of an implant (Yin et al. 2016), we therefore investigated what kind of immune response would be potentially triggered in an early stage of implantation of scaffolds seeded with hBPCs or without any cells as the control. Furthermore, hOBPCs seeded scaffolds were as well studied as an extra control. This control allowed us to get more information on the behavior of the differentiated and mineralized state of hBPCs *in vivo*. Because hBPCs cells may mature into hOBPCs, they may as well trigger a different immunological reaction in the host. As little information is available concerning the difference in behavior between hBPCs and hOBPCs *in vivo*, we wanted to evaluate if these different cell fates

influenced the immune reaction of the host. For this purpose, each scaffold group was implanted in both femoral condyles of female Wistar rats. A tissue analysis was performed after 3, 7 and 14 days of implantation. In addition to the interest in potential immune reaction, the localization and eventual migration of the cells was of interest. By analyzing differential leukocyte counts and evaluating cellular events histologically, we have shown that both hBPCs and hOBPCs affect the surrounding tissue by inducing the formation of a fibrous tissue, but without triggering particular specific immune reaction.

2.3   Materials and Methods

2.3.1   Cell Culture

In this work, all *in vitro* and *in vivo* studies were done using hBPCs. These were obtained from a Biobank developed at the Unit of Regenerative Therapy at the CHUV under the supervision of Prof. L.A. Applegate (CHUV, Switzerland). The cell bank development was approved by the Ethics committee of the CHUV (Ethical Protocols 51/10). The bone cells were harvested from a tissue donation under the registered Transplantation Program (fetal bone tissue of 15 weeks gestational age following a voluntary interruption of pregnancy) and treated as described elsewhere (Montjovent et al. 2008). For cell expansion, the cells were cultured in T75 flasks (TPP, Sigma-Aldrich, ST Louis, USA) in a standard culture medium composed of Dulbecco's Modified Eagle Medium (DMEM, Invitrogen, Life Technologies Ltd, Thermo Fisher Scientific, Waltham, USA, Waltham, USA), supplemented with 10% (v/v) fetal bovine serum (FBS, Thermo Fisher Scientific), 1% (v/v) L-Glutamine (200 mM, Invitrogen). They were maintained in culture at 37 °C in 5% CO_2 atmosphere with culture media changed twice weekly and were passaged when they reached 80% confluency.

When hOBPCs were used for *in vitro* and *in vivo* experiments, the following osteogenic differentiation medium was prepared: α-MEM (Gibco), 10% (v/v) FBS (Thermo Fisher Scientific), 1% (v/v) L-Glutamine (200 mM, Invitrogen), 1% (v/v) Vitamin C (5 mg/mL, Sigma-Aldrich), 1% (w/v) β-glycerophosphate (500 mM, Sigma-Aldrich) and 1% (w/v) dexamethasone (1mM, Sigma-Aldrich). The cells were first plated in a standard culture medium and then exposed to the osteogenic differentiation medium at the third day of culture. The medium was renewed 3 times a week over two or three weeks, depending on the experiment.

2.3.2   Scaffold Seeding and Cellular Characterization

2.3.2.1   Scaffold Fabrication

The scaffolds used in this work were developed in collaboration with Laboratory of Polymer and Composite Technology (LTC, EPFL). The robust processing and properties analysis of the scaffolds were carried out as described elsewhere (Mathieu et al. 2006). In short, the scaffolds were made of poly(L-lactic acid) pellets (PLA, Boehringher Ingelheim, Germany) and ß-tricalcium phosphate (β-TCP) ceramic powder (Fluka, Sigma-Aldrich, ST Louis, USA), which were mixed (5% (w/w)) and melt-extruded using a micro-compounder (Xplore, Geleen The Netherlands) (Mathieu et al. 2006). Afterwards, the melt-extruded product was foamed with supercritical CO_2 in a custom made high-pressure chamber. Once the CO_2 was dissolved in PLA, foaming was achieved by sudden gas release,

which induces bubble nucleation and their formation. The uprising porous structured was then fixed by simultaneously cooling down and depressurize the high-pressure chamber (Montjovent et al. 2008); the distribution of TCP particles was controlled to be homogeneously distributed in pore walls (Mathieu et al. 2006). The final volume of synthetic composite PLA/5% β-TCP used for *in vitro* and *in vivo* studies was machined into cylinders of 3 mm height and 3 mm of diameter.

2.3.2.2 Scaffold Preparation and Seeding

The PLA/5% β-TCP scaffolds were sterilized by ethylene oxide at the CHUV (Lausanne, Switzerland). Prior to cell seeding, the scaffolds were wet and sonicated (Ultrasonik, Ismatec SA, Werheim, Germany) during 20 min in order to avoid micro-air bubbles. For *in vitro* studies, the experiments were performed with cells between passages 4 and 7, whereas for *in vivo* studies the cells were at passage 4. In both cases, the cells were seeded at a concentration of 0.5×10^6 cells/scaffold in PLA/5% β-TCP scaffolds using a pressure-driven technique (see section 2.7 Supporting Information, sub-section 2.7.1 Scaffold Seeding). The cell concentration was based on Montjovent's *in vivo* studies (Montjovent et al. 2008). Once seeded, the scaffolds were placed on a rotating platform allowing a homogeneous cell distribution inside the scaffold.

For several *in and in vivo* studies, we distinguished between three different types of scaffolds: cell-free (CF), cell-seeded (CS) and osteogenic cell-seeded (OCS) scaffolds (shown in Fig. 2.1). In the case of CF scaffold, the scaffolds were wet with 0.9% NaCl solution (B. Braun, Melsungen, Germany) for the sonication and then left in 200 μL 0.9% NaCl solution for 72 h in the incubator before implantation or any *in vitro* experiments. The CS scaffolds were wet with standard culture medium and were seeded with hBPCs three days before implantation whereas the OCS scaffolds were seeded with hBPCs two weeks before implantation for *in vivo* experimentation. The medium of the OCS scaffolds was changed three times a week with osteogenic differentiation medium to obtain OCS scaffolds. Just before implantation, every scaffold was washed three times with sterile 0.9% NaCl solution (B. Braun).
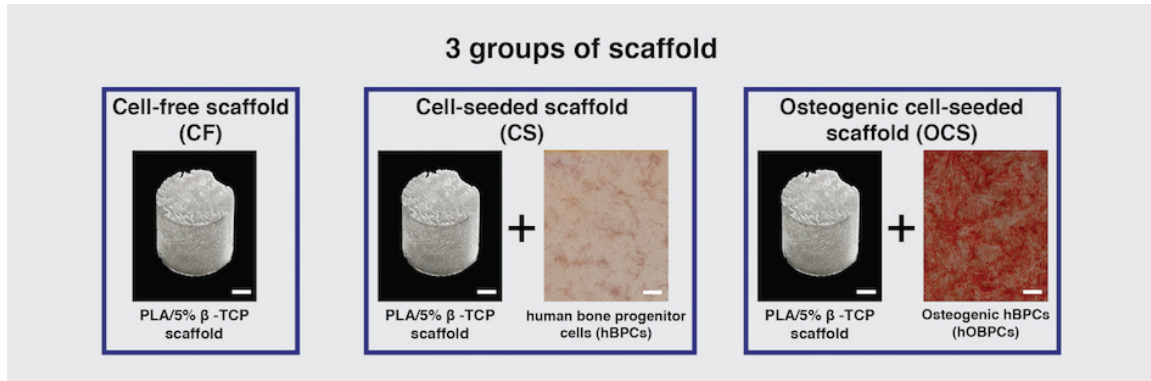
Figure 2.1 Experimental conditions of scaffolds. Cell-free (CF), cell-seeded (CS) and osteogenic cell-seeded (OCS) poly(L-lactic acid)/5% ß-tricalcium (PLA/5% β-TCP) scaffolds were prepared for this study. For CS scaffolds, human bone progenitor cells (hBPCs) were cultured in standard medium and seeded in PLA/5% β-TCP scaffolds 3 days before implantation. In the case of OCS scaffolds, hBPCs were seeded in PLA/5% β-TCP scaffolds and cultured in differentiation osteogenic medium for 2 weeks before implantation to obtain osteogenic hBPCs (hOBPCs). On the photographs, hBPCs and hOBPCs are stained with Alizarin Red S to reveal the mineralization in red. The detection of the presence of extracellular matrix mineralization shows the differentiation capacity of hBPC into hOBPCs (scale bars: 1 mm, picture of the scaffold adapted from A. Roshan-Ghias thesis).

2.3.2.3 Cell Viability in 2D Culture and in Scaffold

The hBPCs were seeded either in 96-well plates (2D sample, 10 000 cells/cm^2 per well) or in PLA/5% β-TCP scaffolds (3D sample) as described in section 2.3.2.2. The cells were either cultured in standard medium for hBPCS or in osteogenic differentiation medium for hOBPCs as described in section 2.3.1. The cell viability was measured after 0, 3, 7 and 14 days of culture and for each time point, standard medium without cells was as well prepared as a negative control. The Cell-Titer-Glo 3D viability kit (Promega, Fitchburg, WI, USA) was used for 2D and 3D samples analysis. This assay is a homogeneous method to determine the number of viable cells in a 3D cultures based, which can as well be used for 2D cultures, and it is based on the amount of present ATP. The cells are lysed and the released ATP reacts with a thermo stable luciferase, which emits a luminescence. This obtained luminescence intensity is directly proportional to the cells quantity. According to the manufacturer's instructions, the ready-to-use reagent was added 1:1 (v/v) to each sample. After 5 min of plate shaking and 25 min of rest at room temperature (RT) in a light free environment, 100 µL of the obtained solution was deposited in a black flat bottom 96-well plate (Greiner bio-one, Germany). The luminescence intensity was then quantified with a Victor Wallac multiplate reader 1420 (PerkinElmer, Waltham, MA, USA). A t-test was performed to examine the statistical difference between hBPCs and hOBPCs at each time point (n=3). A p-value of less than 0.05 was considered as significant.

2.3.2.4 Quantitative Cell Adhesion Assay on Scaffold

As CS and OCS scaffolds have different duration of cell culture before implantation (3 days and 14 days respectively), an assay was set up to compare the cell adhesion to the PLA/5% β-TCP scaffold. In this assay, the adhesion was quantified by comparing the number of cells, which detached after 0, 1,

2 or 3 washings of the scaffold with 0.9% NaCl using the Cell-Titer-Glo 3D viability kit. One washing step equaled to 5 min in 0.9% NaCl solution. The number of cells contained in the culture medium, the 0.9% NaCl solution after each washing as well as the scaffold itself after washing were analyzed using the Cell-Titer-Glo 3D viability kit as described in section 2.3.2.3. The following conditions were used: the hBPCs and hOBPCs were seeded on scaffolds as described in section 2.3.2.2 and analyzed at day 0, 3 and 14. As the osteogenic differentiation starts at day 3 of culture, the results for day 0 and 3 were only performed on CS scaffolds, whereas the adherence quantification was done on CS and OCS scaffolds at day 14. For each time point (day 0, 3, and 14) and for each scaffold condition (CS and OCS), triplicates (for each washing condition) were prepared. As a control, cells were seeded in 96-well plates (10 000 cells/cm^2 per well) for each time point and a negative control of 0.9% NaCl was plated. A t-test was carried out to define the significance of the difference between two data groups (n=3). A p-value of less than 0.05 was considered as significant.

2.3.3 Cell Distribution and Immunofluorescent Staining

2.3.3.1 Cell Distribution

To have an overview of the cell distribution within the scaffold, hBPCs were seeded in the scaffold as described in section 2.3.2.1. The seeded scaffolds were either exposed to standard or to osteogenic media as described in section 2.3.1. After 3 days or 14 days of culture, they were stained using the 3-(4, 5-dimethylthiazolyl-2)-2,5-diphenyltetrazolium bromide (MTT) viability assay kit (Cell Proliferation Kit I, Roche, Basel, Switzerland) according to the manufacturer's instructions. When MTT is added to a cell culture, the cells metabolize the MTT and produced purple formazan. The stained and seeded scaffolds were then fixed with 4% PFA and imaged with a Leica stereomicroscope using different magnifications (Leica Microsystems, Wetzlar, Germany). The MTT assay is complementary to the cell viability assay described under section 2.3.2.3.

2.3.3.2 Immunofluorescent Staining of Cells in 2D and in Scaffold

For this experiment, hBPCs and hOBPCs were used and imaged after 3 and 14 days of culture. For each condition and time points, triplicates were prepared. Each cell type was either seeded in 96-well plates (2D sample) or on thin PLA/5% β-TCP scaffolds (3D sample), which had a thickness of 0.5 mm and a diameter of 3 mm. The reason why we used smaller scaffold was given by an imaging limitation of the confocal microscope. In order to have precise images, the maximum height of a sample should not exceed 0.5 mm. After an ethanol oxide sterilization, the scaffolds were sonicated during 20 min before adding 20 µL of a cell suspension containing 5 000 cells. Each seeded scaffold was put in a 96-well and left for 10 min at 37°C. A volume of 200 µL of standard medium was then added. In the case of 2D samples, the cells were seeded at 10 000 cells/cm^2 per well and cultured in 200 µL of standard culture medium. For the 2D and 3D samples, the medium was changed accordingly to the protocol described in section 2.3.1.

Before staining, CS and OCS scaffolds were washed three times during 5 min in phosphate-buffered saline 1x (PBS, Invitrogen Life Technologies Ltd Thermo Fisher Scientific) and fixed with 4% paraformaldehyde (PFA, Sigma-Aldrich) in PBS for 1 h at room temperature (RT). They were then rinsed three times for 5 min in PBS. 0.2% (v/v) Triton X-100 (AppliChem, Darmstadt, Germany) in PBS was added for 5 min on each sample and were washed once for 5 min with 0.02% (v/v) Triton X-100 in PBS. The primary and secondary antibodies as well as the immunofluorescent labels were all

diluted in 0.02% (v/v) Triton X-100. The primary antibody, containing rabbit anti-fibronectin (1:400, Sigma-Aldrich), was incubated for 1 h and then washed three times in PBS. In parallel to the secondary antibody (goat anti-rabbit, 1:100, Sigma-Aldrich) which stains fibronectin, 4', 6-Diamino-2-phenylindole dihydrochloride (DAPI, 1:50, Merck Millipore Corporation, Darmstadt, Germany) and Alexa Fluor 488® conjugated Phalloidin (1:1000, Invitrogen) were incubated for 45 min to stain the cell nuclei and actin fibers respectively. The samples were all washed three times for 20 min in PBS before imaging. The images of the fluorescent-labeled 2D and the 3D samples were all visualized using the Zeiss LSM 700 inverted confocal microscope with a 10x magnification objective (Carl Zeiss, Jena, Germany).

2.3.4 Characterization of GFP-Transgenic Human Bone Progenitor Cells

2.3.4.1 GFP-Lentiviral Transfection and GFP Vector Transduction in Cells

The GFP-lentiviral vectors used for the transduction of hBPCs were a kind gift of Prof. Hubbell and were produced by Dr. Martina Damo from Laboratory for Regenerative Medicine and Pharmacobiology (LMRP, EPFL). Large-scale preparation of the plasmid DNA of enhanced green fluorescent protein (eGFP, sequence: pRRLSIN.cPPT.PGK-GFP.WPRE from Addgene, England) was carried out using the Macherey-Nagel (Düren, Germany) endotoxin-free high purity plasmid maxi-prep kit, according to the manufacturer's instructions.

VSV-G-pseudotyped third-generation lentiviruses were produced by Ca_3PO_4 transient transfection into HEK-293T cells, as previous described (Follenzi & Naldini 2002a; Follenzi & Naldini 2002b). Before the transfection of the cells of interest, the lentivirus were aliquoted at a concentration of 10^9 TU/mL (Transducing Units/mL) and stored at -80°C.

For the characterization of GFP transduced hBPCs (GFP hBPCs), cells were transduced at passage 5, whereas cells used for *in vivo* experiments, were transfected at passage 3. For this purpose, hBPCs were seeded at 10^5 cells per well in a 12 well plate in a standard culture medium for at least 8 h allowing the cells to adhere to the plate. Four µL of virus solution was diluted in 400 µL of fresh culture medium and was added in each well. The cells and the virus were incubated for 3 days at 37°C in 5% CO_2 atmosphere and were then washed thoroughly with PBS to rinse off the viruses. The transduced cells were then plated in T75 culture flask for extension. Once extended and tested negative to any lentivirus using a HIV-1 p24 Antigen ELISA kit (ZeptoMetrix Corporation, Buffalo, NY, USA), the cells were either directly used for *in vitro* experiments or stored at -80°C.

2.3.4.2 Genomic DNA Isolation and GFP Transduction Efficiency

GFP hBPCs and hBPCs were cultured for 3 and 14 days. Each cell type was cultured in standard culture medium as well as in osteogenic differentiation medium as described in section 2.3.1. For each condition, total DNA of 10^6 cells was extracted using NucleoSpin® Tissue XS kit (Macherey Nagel, Düren, Germany) according to the manufacturer's instructions. The DNA was quantified using Nanodrop ND-100 Spectrophotometer (Witec AG, Switzerland). Quantitative PCR was performed using the Fast SYBR Green Master Mix (Applied Biosystem, Life Technologies Ltd Thermo Fisher Scientific, Waltham, USA) as well as primers synthesized by Microsynth (Balgach, Switzerland) for eGFP, human Alu elements and human GAPDH housekeeping gene. The primer sequences of the eGFP gene were designed by pasting the eGFP sequence of the plasmid (pRRLSIN.cPPT.PGK-

GFP.WPRE from Addgene, England) in the Primer Blast machine of Pubmed (NCBI, USA). Concerning the design of the human Alu elements sequences, it was taken from a study done by van der Horst et al. 2005 (van der Horst et al. 2004). The sequences of the GAPDH housekeeping gene were selected thanks to the GenBack accession N° NG_007073.2. Ten ng of the extracted DNA were added with 250 nM of primers to each well of reaction plate (Microamp Fast Optical 96-well, Applied Biosystem). The StepOne^{TM} Real-Time PCR system (Applied Biosystem) was used to perform the quantitative PCR. The design of the primers for each gene is shown in Table 2.1.

Table 2.1. qRT-PCR primer sequences.

Sequence Symbol	GenBank Accession N°	Sequence
GAPDH	NG_007073.2	F: 5'- GGAGGTAGAGGGGTGATGT -3' R: 5'- ATGGCATGGACTGTGGTCTG -3'
ALU	Design taken from van der Horst, 2004 (van der Horst et al. 2004)	YB8-ALU-S69: 5' GTCAGGAGATCGAGACCATCCT-3' YB8-ALU-AS244: 5'- AGTGGCGCAATCTCGGC-3'
GFP	Provisional RefSeq, eGFP sequence was pasted in Primer Blast	F: 5'- CTCGTGACCACCCTGACCTA -3' R: 5'- AGTCGTGCTGCTTCATGTGG -3'

The gene data processing was done following the comparative Ct model described elsewhere (Pfaffl 2001), where the gene expression levels are normalized by the housekeeping gene. In our case, we chose the Alu elements as the reference gene, because those Alu elements are highly concentrated around housekeeping genes (Eller et al. 2007). The housekeeping gene GAPDH (Barber et al. 2005) and eGFP gene were used to quantify the transduction efficiency of the GFP cells compared to non-transfected GFP cells (hBPCs). For this purpose, the ratio between GFP and the GAPDH genes were both normalized by the ALU gene. A t-test was used to examine the differences in GFP transduction efficiency (n=3). A p-value of less than 0.05 was considered as significant.

2.3.4.3   Proliferation Assay

GFP hBPCs and hBPCs were plated separately in 96-well plates for the proliferation assay for different time points (Day 0, 3, 7, 10, 14, 17 and 21). The cells used for the experiments were between passages 4 and 7. The proliferation quantification assay was performed with CellTiter 96 *Aqueous* One Solution reagent (Promega). As described by the supplier's protocol, 20 µL of CellTiter 96 *Aqueous* One Solution was added to each well, which was containing freshly changed 100 µL of standard culture medium. The wells were then left at 37°C in 5% CO_2 atmosphere for 1.5 h. 100 µL of each well was then transferred into a new well of another 96-well plate for absorbance recording. The wells were read at 490 nm using a Victor Wallac multiplate reader 1420 (PerkinElmer). A t-test was performed at each time point to analyze whether there is a significant difference between hBCPs and GFP hBCPs (n=3). A p-value of less than 0.05 was considered as significant.

2.3.4.4   Alkaline Phosphatase Activity Assay and Mineralization

In order to characterize the alkaline phosphatase (ALP) activity and the mineralization of GFP hBPCs and hBPCs after osteogenic differentiation (GFP hOBPCs), ALP staining and Alizarin Red S staining were used respectively. The cells were seeded at 10 000 cells/cm^2 in 35 mm plates and incubated for 4 h, 3 and 14 days in a humidified, 5% CO_2 atmosphere. For GFP hBPCs and hBPCs, cells were cultured in standard and osteogenic culture media as described in section 2.3.1. The qualification and quantification of Alizarin Red S were both performed using the same samples, whereas the ALP qualification and quantification were assessed on two separate samples.

GFP hBPCs and hBPCs cultures for ALP staining for both standard and osteogenic culture media were washed 3 times with freshly, sterile, pre-warmed distilled water (dH_2O). One mL of fixative solution (60% (v/v) acetone (pure, Sigma-Aldrich) and 40% (v/v) citrate (1.5 M, Sigma-Aldrich)) was added in each plate and incubated for 30 sec. After rinsing the plates once with dH_2O, 1 mL of revelation solution (0.25 mg Fast Violet (Sigma-Aldrich) in 1 mL dH_2O and 0.04 μL Naphtol (Sigma-Aldrich)) was added for 30 min. After this step was completed, images of the samples were taken using a Leica stereomicroscope (Leica Microsystems).

In order to measure ALP activity, cell culture media were removed and the cultures kept at -80°C for at least 15 min. The cells were scraped and collected using dH_2O in 1.5 mL Eppendorf tubes. After 30 sec of sonication (Ultrasonik) for cell disruption, the tubes were centrifuged at 5 000 RPM at 4°C during 5 min as described elsewhere (Krattinger et al. 2011). The supernatant was transferred into new 1.5 mL Eppendorf tubes and heated in a water bath at 37°C for 5 min. The ALP activity was determined in the supernatant using 10 mM *p*-nitrophenyl phosphate (pNPP). The ALP activity by pNPP dosage was carried out using the QuantiChrom^{TM} Alkaline Phosphatase Assay kit (Socochim SA, Bioassay Systems, Lausanne, Switzerland), according to the manufacturers' instructions. The ALP activity was normalized to the total protein content determined by a Micro BCA protein assay reagent kit (Life Technologies Ltd Thermo Fisher Scientific). Aliquots (100 μL) of the supernatants were read with a Victor Wallace multiplate reader 1420 (PerkinElmer) at 405 nm and 590 nm in 96-well plates for the obtained ALP activity and the protein solutions respectively.

Monolayers in 35 mm plates were washed with PBS and fixed with 70% ethanol for 1 h at -20°C for mineralization measurements. The monolayer was then washed with excess dH_2O prior to the addition of 0.5% (w/v) Alizarin Red S (342.26 M, Sigma-Aldrich) working solution. The samples were incubated at RT for 15 min with a gentle shaking. After aspiration and rinsing the plates with dH_2O, images of the stained monolayers were taken using a Leica stereomicroscope (Leica Microsystems). The dye extraction protocol was adapted from C. A. Gregory, 2004 (Gregory et al. 2004). After rinsing the plate once with dH_2O, 800 μL of 10% (v/v) acetic acid (pure, diluted in PBS, Fluka) was added to each sample. They were incubated for 30 min at RT. Afterwards the plates were scraped in order to recover the stained cells, which were transferred in 1.5 mL Eppendorf tubes. Each tube was vortexed during 30 sec and 500 μL of glycerin (Sigma-Aldrich) was then added. The tubes were left for 5 min and subsequently centrifuged at 5 000 RPM for 15 min. The pH of the samples was neutralized with 200 μL of 10% (v/v) ammonium hydroxide (28-30%, Sigma-Aldrich) to ensure that it was between 4.1 and 4.5. An Alizarin standard curve was prepared using 0.5% (w/v) Alizarin Red S Aliquots (Sigma-Aldrich) and 10% (v/v) ammonium hydroxide at different dilutions. Sample aliquots of the supernatants along with the sample of the standard curve (100 μL) were read with a Victor Wallace

multiplate reader 1420 (PerkinElmer) at 405 nm in 96-well plates. A t-test was used to examine the statistical differences on the readings (n=3). A p-value of less than 0.05 was considered as significant.

2.3.5   *In Vivo* Study

2.3.5.1   Study Design

The study included three experimental groups defined by the implanted PLA/5% β-TCP scaffold conditions (CF, CS and OCS) as described in section 2.3.2.2. Each type of scaffold was implanted in a pre-drilled hole in both femoral condyles of rats. The cells used for this *in vivo* study were GFP hBPCs cells, which were seeded as described in section 2.3.2.2. In each experimental group, 10 rats were operated. Three to four of the rats were euthanized either at 3, 7 or 14 days after implantation in order to detect any immune reaction possibly due to the use of hBPCs. The purpose of the labeled GFP hBPCs was to determine if and where the hBPCs migrated. Blood samples were collected before the surgical intervention and before the euthanasia to make a white blood cell count analysis. The study design is shown in Fig. 2.2.
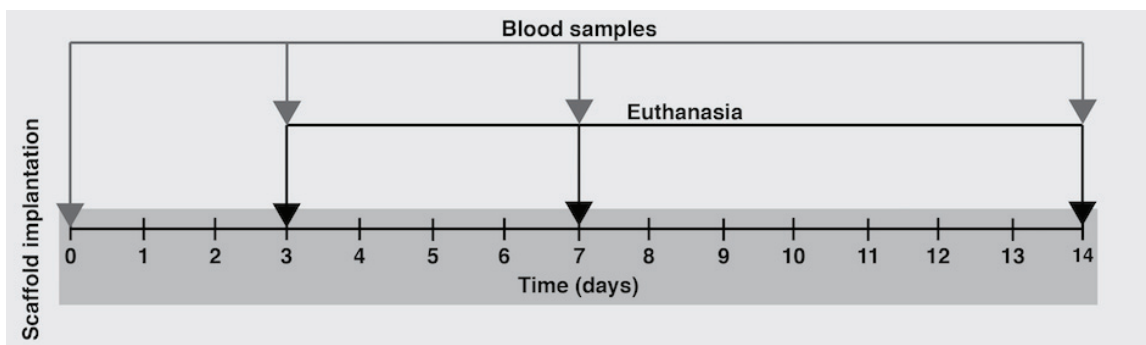
Figure 2.2 *In vivo* study design over 14 days. Each experimental group of rats was implanted on both femoral condyles with one type of scaffold (CF, CS or OCS). Blood samples were collected from each rat before the surgery (day 0), and just before euthanasia. Three to four rats of each group were euthanized either at 3, 7 or 14 days after implantation.

2.3.5.2   Animal Model

All animal procedures were performed with the approval of the local animal care and use committee (license N° 2631.0, EXPANIM, SCAV, Epalinges, Switzerland). Female Wistar rats, weighing between 280 g and 300 g at the time of surgery (12-13 weeks of age), were purchased from Janvier Labs (Saint-Berthevin, France). The animals were housed in groups of three in standard plastic cages with white poplar sawdust, tissue and nesting materials. Strictly controlled housing conditions were used, namely 12 h light to 12 h dark cycles, relative humidity of 55% and temperature at 22°C. They had access *ad libitum* to a balanced solid diet (KLIBA NAFAG 3436, Provimi Kliba AG, Switzerland) and sterilized acidified tap water. Rats were allowed to acclimate to the new surrounding for 2 weeks before initiation of any experimental procedure.

2.3.5.3 Surgical Procedure

For implanting scaffolds in femoral condyles of rats, they were anesthetized with Isoflurane (Piramal Enterprise Ltd., Bombay, India). For the induction, 5% Isoflurane in oxygen was used at a flow rate of 2.0 L/min and during the surgery, 2.5% Isoflurane was maintained at a flow rate of 0.8 mL/min. After the anesthesia, blood was taken from the tail of the rat using an Insulin syringe (Becton Dickinson and Company, Franklin Lakes, NJ, USA). The legs of the animals were then shaved and Buprenorphine (0.03 mg/kg/day, Temgesic®, Reckitt Benckiser AG, Wallisellen, Switzerland) was injected subcutaneously as analgesic to avoid pain during the surgical intervention. The surgery was performed in an aseptic environment and all instruments were sterilized before use. During the surgical intervention, the rat was situated on a custom made table on the opposite side of the operated leg as shown in Fig 2.3. During the entire intervention, the surgery table was deposited on a heating mat to avoid a decrease in the rat's body temperature and the rat's eyes were covered with substitutes for tear fluid (Visoctears®, Alcon, Fort Worth, TX, USA) to avoid eye drying. The knee of the rat was in a flexed position in order to fix and to stabilize the leg. After the skin incision of 1-2 cm on the lateral side of the distal femoral end, the muscle fascia was carefully removed and the muscles were blunt dissected as described elsewhere (Kettenberger et al. 2014). The condyle was exposed and a hole with a diameter of 3 mm and 3 mm of height was drilled in the condyle using a motorized dentist's drill (DEC 100, Nobelcare, Sweden).
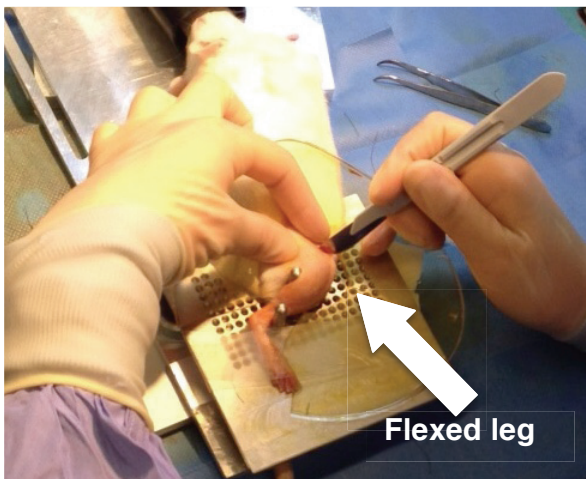
Figure 2.3 Rat position during the operation. On the photograph, the rat is positioned on his left side while the right leg is flexed on the custom made table. The skin of the rat is incised with a scalpel from 1 to 2 cm.

Before and after the drilling, the site of implantation was cooled and rinsed with 0.9% NaCl (B Braun, Melsungen, Germany). The bone and blood remaining were removed out from the site with a surgical vacuum. Afterwards PLA/5% β-TCP scaffold (CF, CS or OCS) was implanted by press-fitting it inside the drilled hole (shown in Fig. 2.4). The scaffolds were placed on a heating mat before the implantation to allow the cells to be at an appropriate temperature before being implanted. After the scaffold implantation, the muscles were closed with synthetic absorbable sterile surgical sutures (coated VICRYL®(polygalctin 910), 5-0, Ethicon Inc., Somerville, USA), followed by the closing of the skin with interrupted subcutaneous sutures (coated VICRYL®(polygalctin 910), 5-0). The animal was then prepared to make the same surgical intervention on the contralateral femur. After the surgery was completed, the rat was placed in a heated chamber for post-surgical recovery.
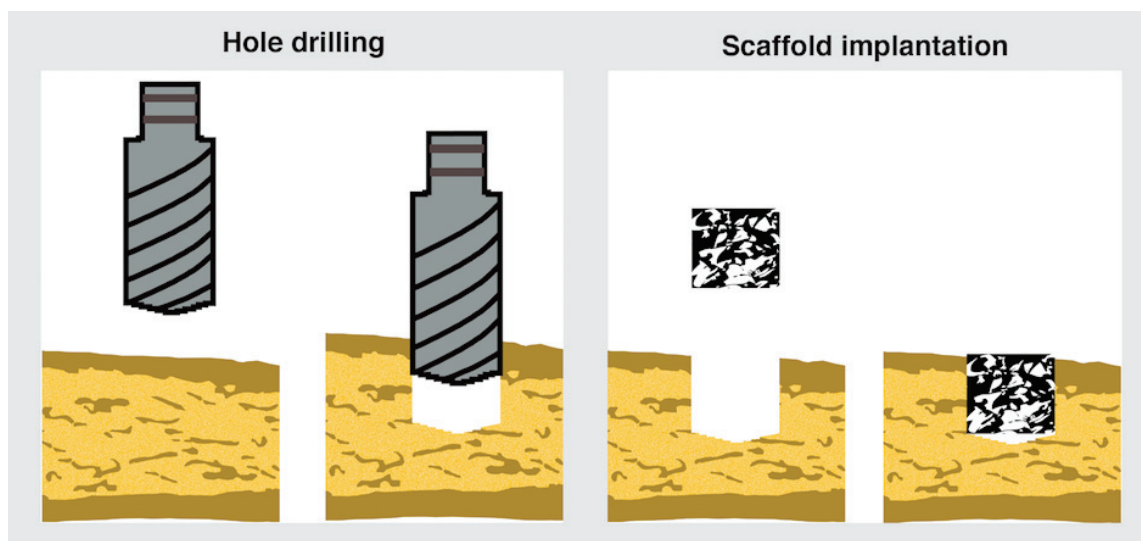
Figure 2.4 Scaffold implantation in the femoral condyle of the rat. The hole is drilled with a dentist drill before the press-fit insertion of the scaffold inside the bone (coronal view).

The post-operative care consisted in injecting buprenorphine subcutaneously every 8 h for the first 48 h after the surgery for pain relief. Paracetamol (Dafalgan 500 mg effervescent tablet, UPSA Bristol-Myers Squibb SA, Barr, Switzerland) was added to the drinking water of the rats for 1 week. In case the rats opened their wounds one day after surgery, Ibuprofen (15 mg/kg/day, Algifor®, Vifor SA, Villars-sur-Glâne, Switzerland) was administrated in the drinking water for 1 week instead of Paracetamol. Furthermore, those rats were injected subcutaneously with antibiotic (150 mg/mL, CLAMOXYL L.A, Pfizer, Brookline, NY, USA) for 1 week. Intracardiac blood samples were collected before the rats were euthanatized with an intracardiac Pentobarbital (< 200 mg/kg, Esconarkon, Streuli Pharma SA, Uznach) injection at 3, 7 and 14 days after the scaffold implantation.

2.3.6   Histology

2.3.6.1   Blood Smear Staining and Leukocyte Count

After the blood was collected from the rat, a drop of blood was smeared on a glass slide (Polysciences Inc., Warrington, PA, USA). The samples were then stained with Hemacolor® Rapid staining (Merck Millipore Corporation) according to manufacturer's instructions. This staining is based on the Pappenheim staining technique, which enables the differential counts of white blood cells including lymphocytes, monocytes, non-segmented neutrophils, juvenile neutrophils, segmented neutrophils, eosinophils and basophils based on their morphology. All samples were counted twice by two separate investigators for 100 cells and results were averaged. A t-test was performed at each time point to analyze whether there is a significant difference between the different scaffolds (n=3 to 4). A p-value of less than 0.05 was considered as significant.

2.3.6.2   Resin Embedding and Sample Mounting

After the blood sample collection, the animals were directly euthanized and their distal parts of the femur were dissected and fixed in 4% PFA solution for approximately 1 day. The samples were

dehydrated by immersing them in a series of ethanol (EtOH, VWR, Dietikon, Switzerland) solutions with ascending concentration (70%, 80%, 90%, 96%, 100%) as described elsewhere (Kettenberger et al. 2014). Each immersion lasted for 24 h. After clearing the sample in toluene (VWR), 1 x 24 h followed by 1 x 48 h of immersion, 2/3 of the femur samples were embedded by infiltration with methylmethacrylate (MMA, 100 mL, Sigma-Aldrich) and 0.5% bis(tert-butylcyclohexyl) peroxydicarbonate (Perkadox 16, Dr Grogg Chemie AG, Deisswil, Switzerland) at 4°C during 5 days. For the polymerization, 100 mL of MMA, 20-25 mL of dibutylphtalate (DBP, Sigma-Aldrich) and 1% of Perkadox 16 (Dr Grogg Chemie AG) were prepared and the samples were polymerized at RT over 3 weeks. The left 1/3 of the samples was embedded in Technovit 9100 (Heraeus Kulzer GmbH, Hanau, Germany) according the manufacturer's instructions. The Technovit 9100 has a polymerization temperature between -4°C and 0°C, which allows the preservation of DNA and RNA.

After polymerization, MMA and Technovit 9100 embedded samples (referred to as resin blocks) were cut with a diamond-coated inner diameter saw (Leica SP 1600, Leica Microsystems) into slices of around 180 µm thickness (referred to as thick slice). Four to five of these preparations were cut and attached to custom-made opaque OMMA microscope slides (Semadeni, Ostermundingen, Switzerland) with acrylic glue (Loctite, 401, Henkel, Düsseldorf, Germany). They were then ground to around 80-100 µm thicknesses with a grinding machine (Pedemax-2, Sturers, Willich, Germany) before staining.

The rest of the Technovit 9100 resin blocks were cut with a microtome (HM325, Microm International GmbH, Walldorf, Germany) into slices of around 10 µm (referred to as thin slide). They were attached on silane glass slides (Polysciences) with 90% EtOH. Finally, the slides were clamped at 37°C over 48 h and released for at least 2 h at RT before staining.

2.3.6.3 Histology Stains

The surface of thick slides was etched with 1% formic acid (AppliChem) before being stained with 0.1% toluidine blue (VWR). For the thin slides, the resin was deplastified with a series of different bathes. First the slides were immersed three times for 20 min in toluene (VWR), followed by hydration of 1 x 10 min of immersion in a series of EtOH with descending concentration (100%, 90%, 80% and 70%). The slides were finally put in dH_2O before specific human – Alu *in situ* hybridization (Alu-ISH) for the detection of hBPCs. Positive controls, provided by the histology facility, were simultaneously run with our samples. The positive controls were human tissue (heart, skin or demineralized bone) embedded in paraffin. The Alu-ISH was performed using a FITC labeled human specific Alu probe (Roche Diagnostics, Rotkreuz, Switzerland). The Alu-ISH on rat femur resin sections was done using the fully automated instrument Ventana Discovery xT (Roche Diagnostics). All steps, except of the deplastification described previously, were performed on the machine with Ventana solutions (Roche Diagnostics), as described elsewhere (Sflomos et al. 2016; Schormann et al. 2008). Briefly, deplastified and rehydrated resin sections were pretreated with the RiboMap kit and with the protease 1 for 8 min at 37°C. The human specific Alu probe was hybridized for 1 h at 47°C. Sections were then washed three times with Ribowash (2x saline sodium citrate (SSC) buffer with 0.1% sodium dodecyl sulphate (SDS)) for 8 min at 45°C. After incubation with an anti-FITC biotin (1:300, Jackson ImmunoResearch Laboratories, West Grove, PA, USA), chromogenic revelation was performed with BlueMap kit for 2 h. Counterstain using Nuclear Fast Red (Carl Roth GmbH & Co. KG, Karlsruhe, Germany) was performed on a Tissue-Tek® Prisma® automate (Sakura Finetek, Alphen aan

den Rijn, The Netherlands) for 5 min. Slides were mounted with a xylene-based glue (Sakura Fineteks). Images were taken with an upright light microscope with different magnifications (DM 5500, Leica Microsystems). Based on the stained sections, a qualitative evaluation was performed, where cellular events were interpreted. The osteoblast activation, the osteoblast shape and the presence of inflammatory cells (neutrophils, macrophages, lymphocytes, plasma cells and multinuclear giant cells as well as fibrous capsule) were observed and commented. The percentage of fibrous tissues and the number of blood vessels were evaluated inside the scaffolds.

2.4   Results

2.4.1   Cell Growth and Distribution

In 2D culture and PLA/5% β-TCP scaffolds, hBPCs exhibited an equivalent growth kinetic after a period of 14 days of culture (Fig. 2.5). The shift in the luminescence curves between the 2D and the 3D conditions is mainly due to the fact that the initial seeded cell concentration was 50 times less in the 2D condition than in the scaffold.
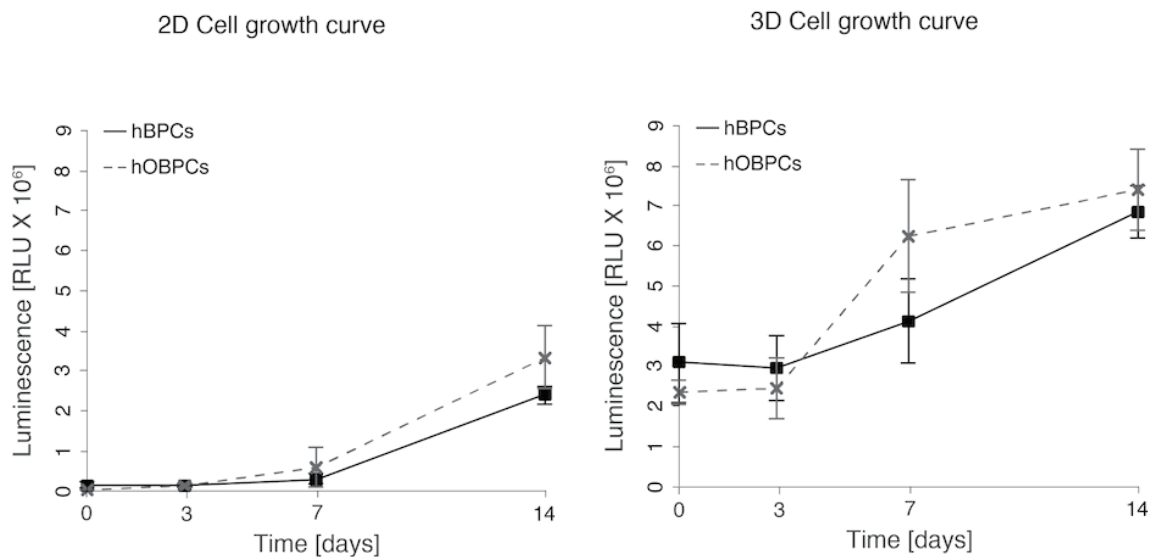
Figure 2.5 Cell proliferation of hBPCs and hOBPCs seeded over 14 days. The cells were cultured over 14 days and were seeded at an initial concentration of 10 000 cells per cm^2 and 0.5 x 10^6 cells per well in 96-well plates (2D) and in PLA/5% β-TCP scaffold (3D) respectively (with n=3, repeated 2-3-times). No statistical significant difference was found between hBPCs and hOBPCs over the entire duration of the experiment.

Cell adhesion on 2D plates and in thin scaffolds was verified by immunohistochemistry. The actin fibers of hBPCs and hOBPCs, their deposed fibronectin and cell nuclei were stained after 3 days and 14 days of culture. The osteogenic differentiation of hBPCs started after the third day of culture. Therefore the osteogenic condition is only shown after 14 days of culture, as we can observe in Fig. 2.6 and 2.7. As expected, the cell density increased after 14 days of culture than after 3 days, but no difference was visible between hBPCs and hOBPCs after 14 days of culture.
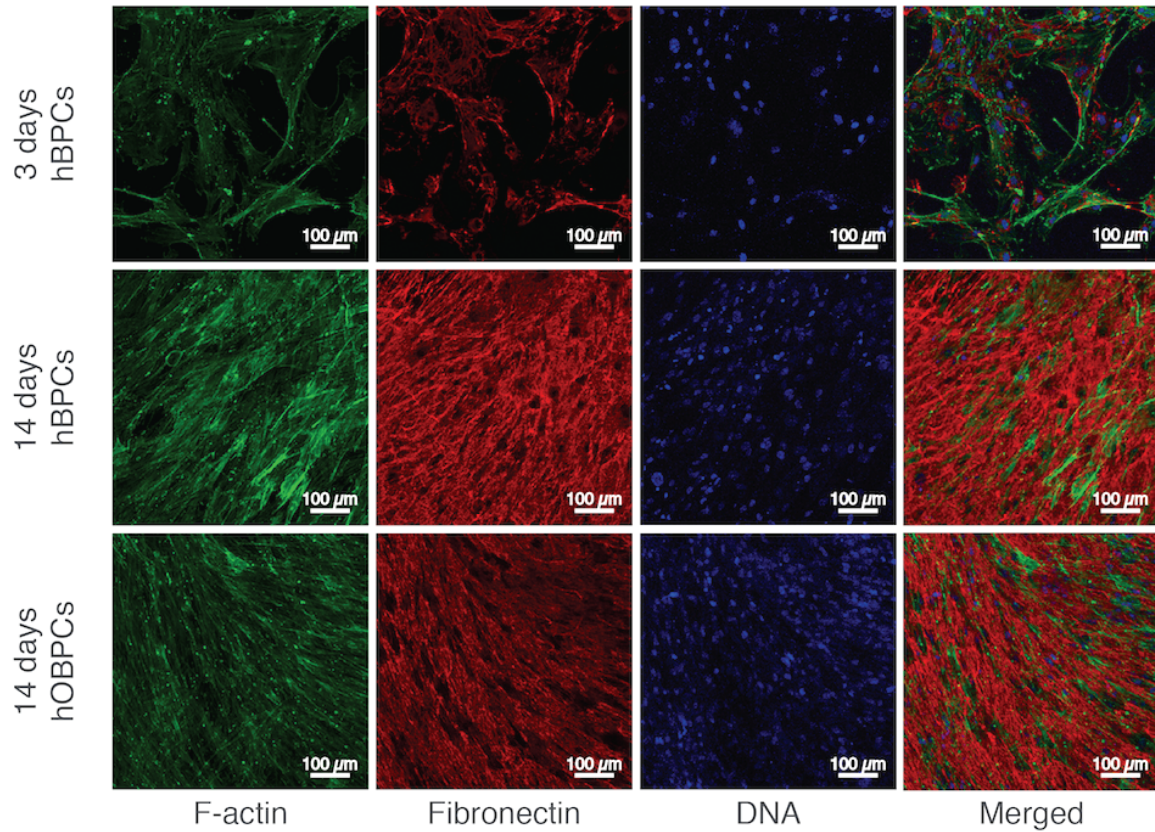
Figure 2.6 Immunohistochemistry of primary and osteogenic hBPCs seeded in 96-well plates after 3 days and 14 days of culture. The actin fibers are shown in green, the fibronectin is in red and the nuclei are stained in blue. The cells were seeded at an initial concentration of 10 000 cells per cm^2.

Using immunohistochemistry, one can distinguish the pores of the scaffolds around which the cells grew (Fig. 2.7). The staining also showed a homogeneous distribution of the fibronectin all over the surface of the scaffold.
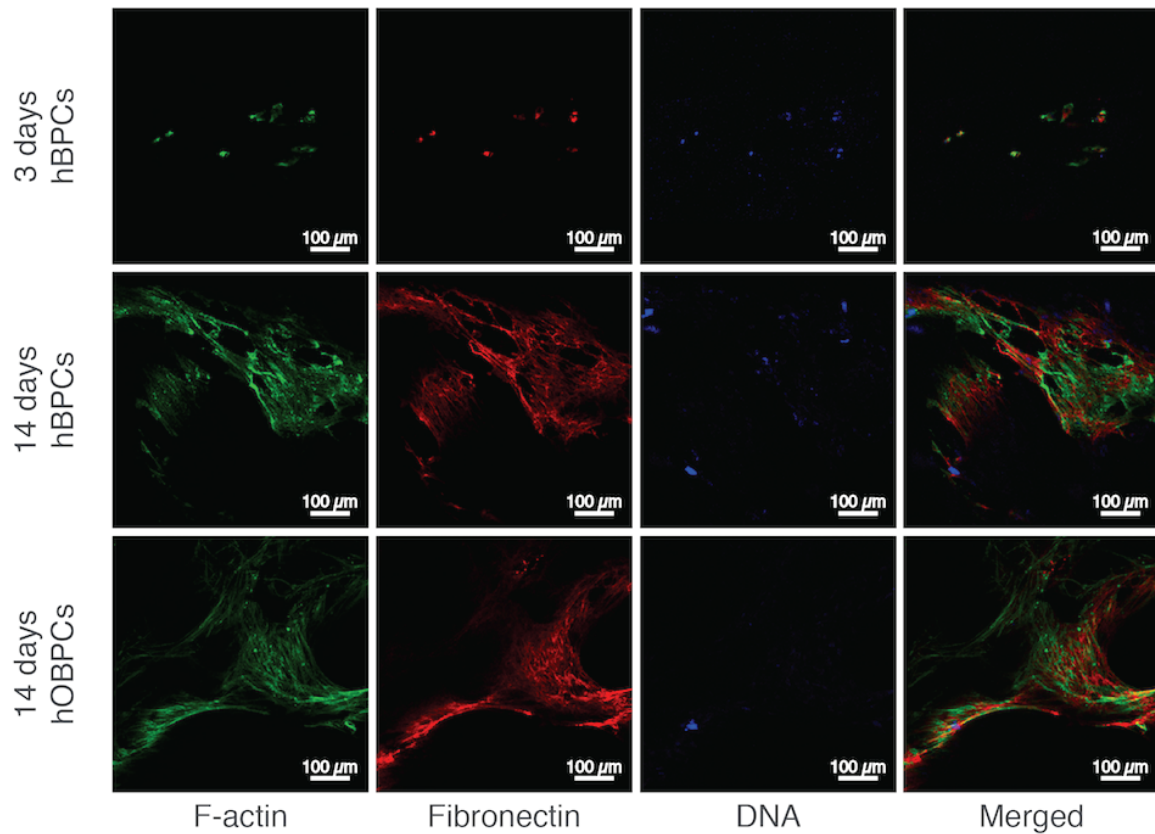
Figure 2.7 Immunohistochemistry of hBPCs and hOBPCs seeded in PLA/5% β-TCP scaffolds after 3 days and 14 days of culture. The actin fibers are shown in green, the fibronectin is in red and the nuclei are stained in blue. The cells were seeded at an initial concentration of 0.5 x 10^6 cells per scaffold. In this figure, the scaffold is not visible.

As the immunohistochemistry was performed on thin scaffolds (~0.5 mm high), it was of importance to have a macroscopic visualization of the cell distribution in the scaffold. We therefore stained the scaffold using the MTT assay after 3 and 14 days for hBPCs and hOBPCs. The staining revealed (Fig 2.8), that the cells were mainly on the border of the scaffold after 3 days of culture and migrated inside the scaffold after 14 days of culture. This observation was seen for both hBPCs and hOBPCs-seeded scaffolds.
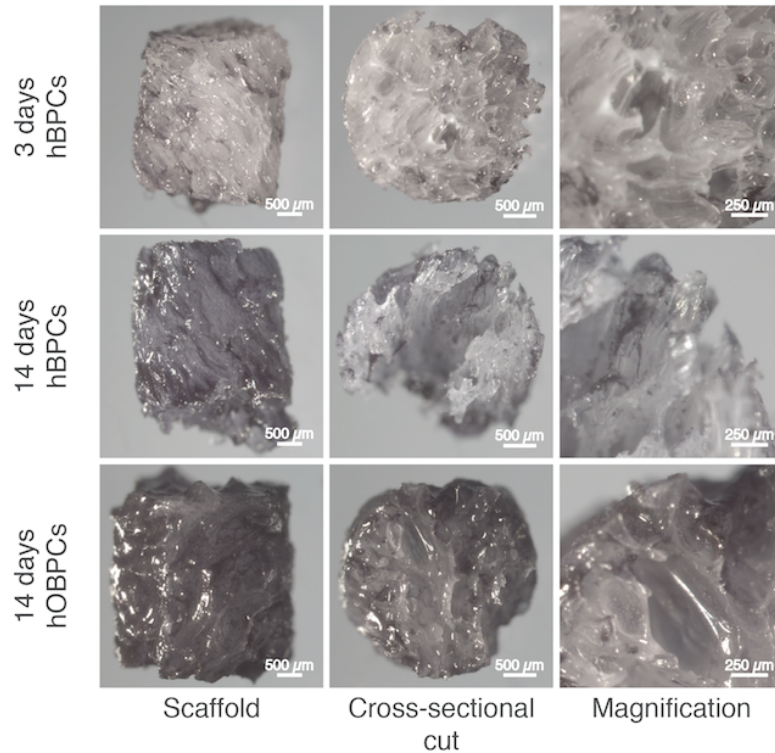
Figure 2.8 Distribution of hBPCs and hOBPCs cultured in PLA/5% β-TCP scaffolds after 3 and 14 days. The cells on the scaffolds were stained using an MTT assay (dark purple stain) and were imaged using a stereomicroscope. Darker the stained scaffolds are, higher the amount of cells inside the scaffolds. Different views of the scaffolds are shown.

2.4.2 Cell Adherence

As cell-seeded scaffolds implanted in femoral condyles of rats contained cells with different pre-implantation seeding periods, namely 3 days and 14 days, we were interested in evaluating the different adherence of hBPCs and hOBPCs on the scaffolds after 3 and 14 days of culture. In Fig. 2.9, the luminescence of the hBPCs and hOBPCs is shown after having washed the scaffold once, twice and three times as well as without any wash. The results show that after 3 washing steps, 50% of the cell detached after 3 days of culture, whereas there is no difference between the scaffolds seeded with hBPCs or hOBPCs after 14 days of culture. The luminescence therefore demonstrated that the longer cells were seeded on the scaffold, less cells detachment was noticed. Furthermore, we can observe that the luminescence obtained with hOBPCs was significantly higher in the condition of no wash and one wash than in the luminescence obtained with hBPCs. This phenomenon was no longer observed after the second and third washes.
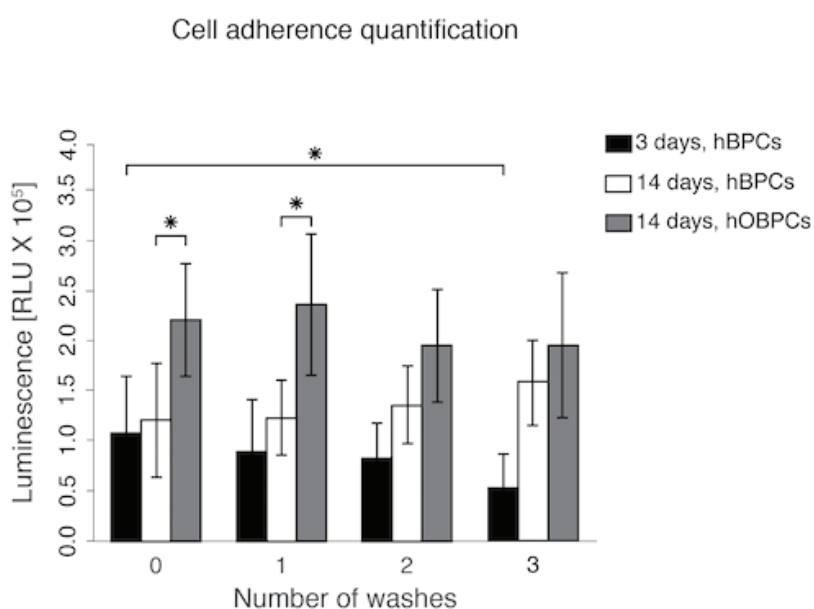
Figure 2.9 Cell adherence of hBPCs and hOBPCs cultured in PLA/5% β-TCP scaffolds after different washing steps at day 3 and day 14 quantified by luminescence. The scaffolds were washed several times (0 -3 times) and the luminescence of the remaining cells was quantified after each washing step (with n=3, repeated 2-3-times). Significant *P*-values *$P<0.05$.

2.4.3 Characterization of GFP-Transgenic Human Bone Progenitor Cells

As we wanted to visualize hBPCs inside the scaffolds by histology, we transduced the cells with a GFP-lentivirus. Before using the GFP cells for *in vivo* experiments, we characterized them *in vitro*. We started first with the evaluation of GFP transduction efficiency of hBPCs after 3 and 14 days of culture in both standard and osteogenic culture medium as presented in Fig. 2.10 (left side). After 3 days, 44.75 ± 17.13% and 50.78± 3.54% of GFP hBPCs and GFP hOBPCs cells were observed respectively. In the case of 14 days of culture, 52.58± 4.55% and 41.47±7.37% of GFP hBPCs and GFP hOBPCs cells were observed respectively. In general, no significant difference was observed within the groups. Therefore, the osteogenic differentiation had no effect on the GFP-transduction efficiency. On the right side of the Fig. 2.10, images of GFP hBPCs are shown after 3 and 7 days of culture in a standard culture medium.
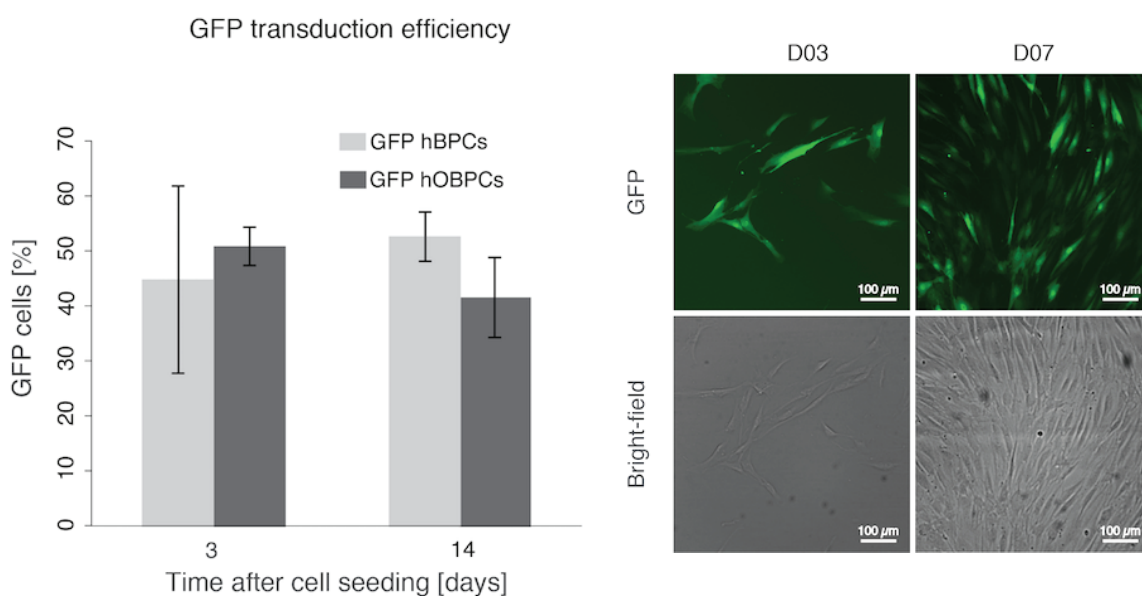
Figure 2.10 GFP transduction efficiency and fluorescent images. Percentage of GFP hBPCs and GFP hOBPCs after 3 and 14 days of culture. The ratio between GFP and GAPDH genes of GFP hBPCs and hBPCs, which were both normalized by the ALU gene, was used to quantify the transduction efficiency. The same was done for GPF hOBPCs and hOBPCs. The analyzed genes were extracted for each sample from 10^6 cells (with n=3, repeated 2-3-times). On the right, the GFP transfected hBPCs after 3 and 7 days of culture with their corresponding bright-field images. Significant *P*-values *$P<0.05$.

In Fig. 2.11, the cell growth kinetics of hBPCs and GFP hBPCs are presented. In both cases, the cells proliferated over 21 days without any difference between both groups.

Cell growth curve
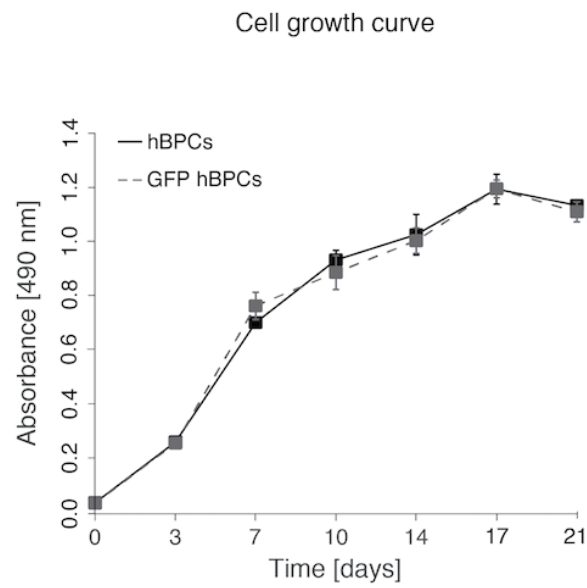
Figure 2.11 Cell growth of hBPCs and GFP hBPCs cultured in 96-well plates over 21 days measured by absorbance. GFP hBPCs and hBPCs were cultured over 21 day in a standard culture medium and were seeded at an initial concentration of 10 000 cells per cm^2 (with n=3, repeated 2-3-times). No statistical significant difference was found between hBPCs and GFP hBPCs over the entire duration of the experiment.

2.4.4 Alkaline Phosphatase Activity

Qualitative and semi-quantitative analysis of the ALP enzymatic activity in hBPCs, GFP hBPCs, hOBPCs and GFP hOBPCs over 14 days are shown in Fig. 2.12 and 2.13, respectively. On day 0, only the ALP staining of hBPCs is shown, as the osteogenic differentiation was induced only 3 days after cell seeding. As expected, ALP activity was visible in hOBPCs after 14 days of culture (Fig. 2.12). This activity was missing in hBPCs and GFP hBPCs cultured in standard medium over 14 days (Fig. 2.12).

Figure 2.12 ALP stain of hBPCs and GFP hBPCs, hOBPCs and GFP hOBPCs after 4 h and 14 days of culture. The hBPCs and GFP hBPCs were cultured either in standard culture medium or in an osteogenic differentiation medium to obtain hOBPCs and GFP hOBPCs. The cells were seeded at an initial concentration of 10 000 cells per cm^2 in 35 mm plates.

An increase in the ALP concentration was observed for GFP hBPCs and GFP hOBPCs, especially from day 7 until the end of experiment (Fig. 2.13, on the left). The concentration was lower in the GFP cell types than in hBPCs and hOBPCs. It was relevant to investigate the activity of ALP, as the production of an enzyme does not necessarily means it is active. The results presented in Fig 2.13 on the right, show no difference between all cell conditions on day 0. After 7 and 14 days the ALP activity of hBPCs and GFP hBPCs remained significantly low while the ALP activity of hOBPCs and GFP hOBPCs increased significantly. Therefore, based on those results, the GFP transduction of hBPCs did not affect the ALP activity when GFP hBPCs were cultured in an osteogenic differentiation medium.
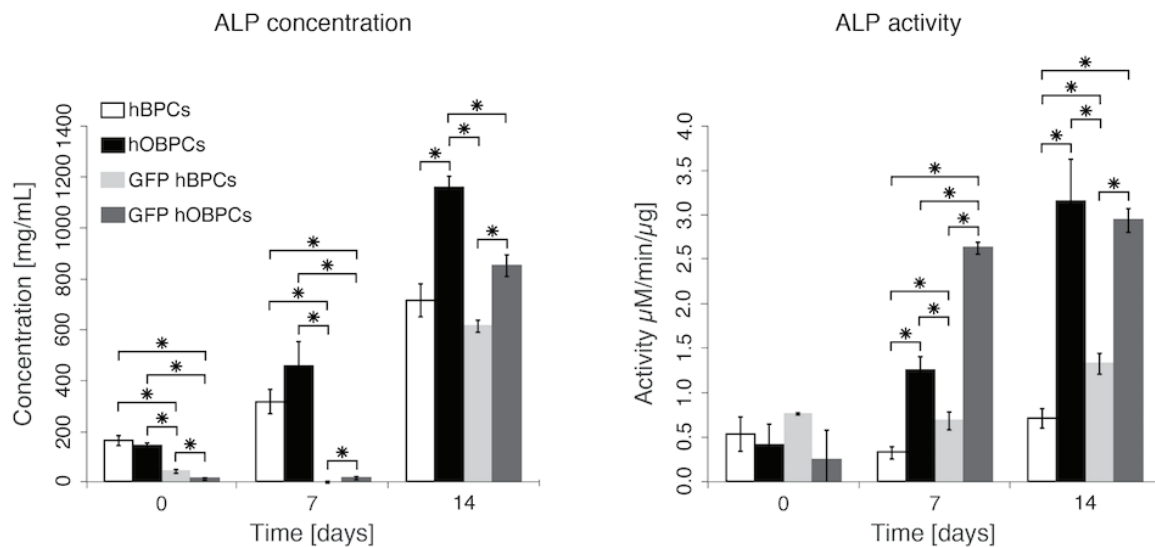
Figure 2.13 ALP concentration and activity hBPCs, GFP hBPCs, hOBPCs and GFP hOBPCs after 4 h and 14 days of culture. The hBPCs and GFP hBPCs were cultured either in standard culture medium or in an osteogenic differentiation medium to obtain hOBPCs and GFP hOBPCs. The cells were seeded at an initial concentration of 10 000 cells per cm^2 in 35 mm plates (with n=3, repeated 2-3-times). The ALP concentration and activity was evaluated by ALP staining. Significant *P*-values *$P<0.05$.

2.4.5 Mineralization

Qualitative and semi-quantitative analysis of extracellular matrix mineralization by Alizarin Red staining in hBPCs, GFP hBPCs, hOBPCs and GFP hOBPCs over 14 days are shown in Fig. 2.14 and 2.15, respectively. As for ALP staining, only the mineralization of hBPCs at day 0 is shown, as the osteogenic differentiation was induced only 3 days after cell seeding. As expected, for hBPCs and GFP hBPCs, the amount of mineralization in the extracellular matrix increased over time when cultured in an osteogenic differentiation medium than in the cells in standard culture medium.
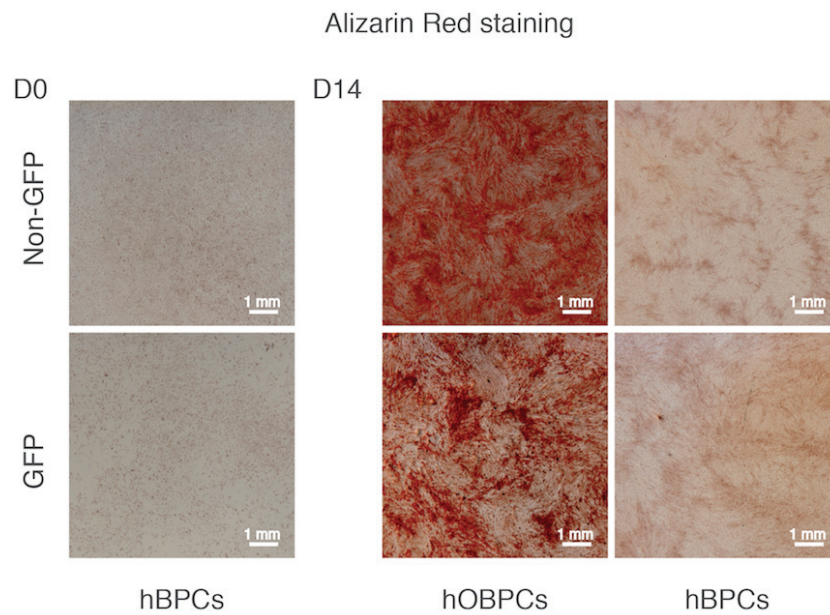
Figure 2.14 Extracellular matrix mineralization of hBPCs, GFP hBPCs, hOBPCs and GFP hOBPCs after 4 h and 14 days of culture. The hBPCs and GFP hBPCs were cultured either in standard culture medium or in an osteogenic differentiation medium to obtain hOBPCs and stained with Alizarin Red. The cells were seeded at an initial concentration of 10 000 cells per cm^2 in 35 mm.

The results in Fig. 2.15 show that the concentration of the extracellular matrix mineralization of hOBPCs and GFP hOBPCs increased significantly after 14 days in osteogenic culture medium. Furthermore, hOBPCs presented almost a three times higher mineralization concentration than in hBPCs. In the case of GFP cells, the mineralization was approximately one and a half times higher in GFP hOBPCs than in GFP hBPCs. This difference in mineralization concentration increase between hOBPCs and GFP hOBPCs could be affected by technical issues, such as different cell detachment behaviors during the washing phases. Still the mineralization concentration was significantly higher in both hOBPCs and GFP hOBPCs than in hBPCs and GFP hBPCs. Thus, the GFP transduction of hBPCs did slightly affect the mineralization of the extracellular matrix after osteogenic differentiation.
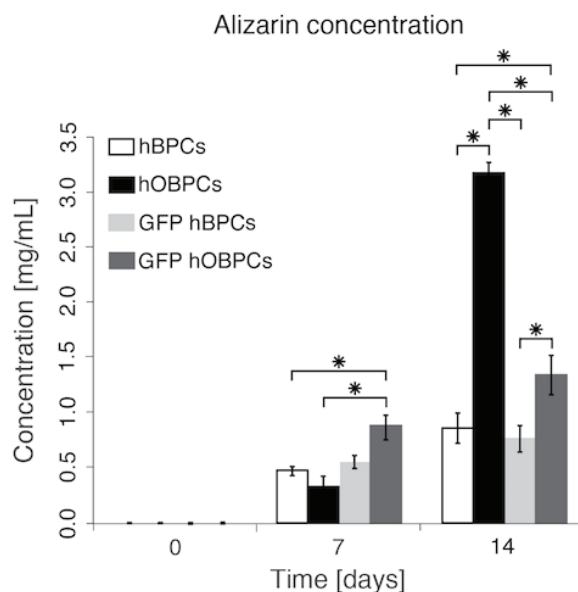
Figure 2.15 Extracellular matrix mineralization evaluation of hBPCs, GFP hBPCs, hOBPCs and GFP hOBPCs after 4 h and 14 days of culture. hBPCs and GFP hBPCs were cultured ei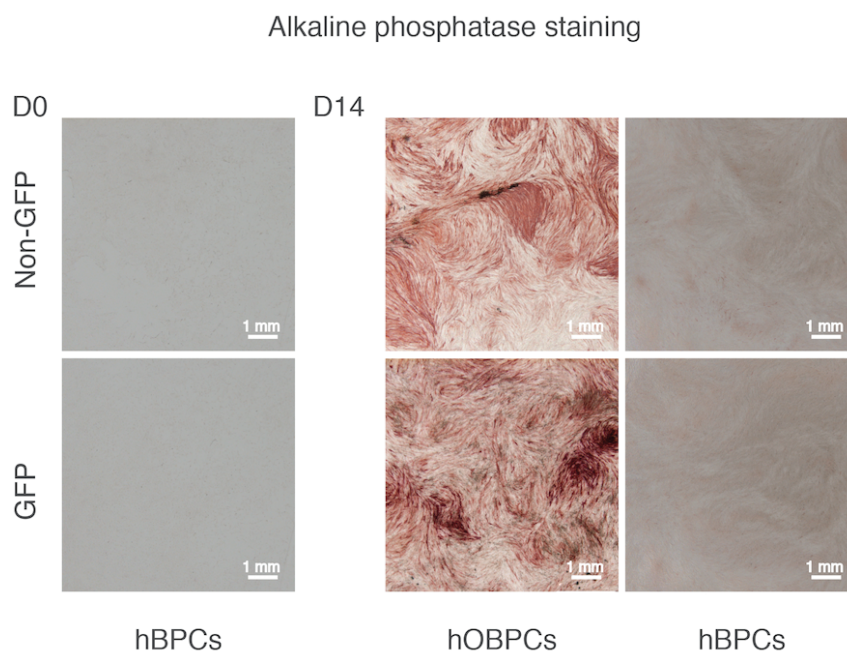ther in standard culture medium or in an osteogenic differentiation medium to obtain hOBPCs and GFP hOBPCs. The cells were seeded at an initial concentration of 10 000 cells per cm^2 in 35 mm plates (with n=3, repeated 2-3-times). The mineralization concentration was evaluated by Alizarin Red staining. Significant *P*-values *P<0.05.

2.4.6   Cell Visualization and Localization

For the localization of hBPCs inside and around the scaffold with an eventual observation of a migration pattern outside the scaffold over time, two different staining methods were investigated in parallel. The first one was the GFP-transduction of hBPCs in order to detect their fluorescent expression on the histological section visualized using fluorescent imaging. Unfortunately, no result can be presented due to the scaffold autofluorescence, which weakened the already feeble GFP signal of hBPCs.

The second technique consisted in using human specific Alu elements with *in situ* hybridization of thin deplastified resin slides. For this application, we chose a specific resin with a polymerization temperature around 0°C in order to avoid the DNA and RNA denaturalization due to temperature. The obtained results are shown in Fig. 2.16. Two samples out of 20 did polymerize correctly, where

one of them was our first test sample (CS condition, after 4 days of implantation) and the second one was an OCS scaffold after 14 days of implantation.

On both stained samples, hBPCs and hOBPCs were detected inside the scaffold. In the case of the CS scaffold, which was implanted for 4 days, the cells were visible in different regions inside and at the border of the scaffold (black arrows). They were localized inside the pores and at their surface. On the right top image, we can observe a cluster of cells. On the images from the OCS scaffold, implanted for 14 days, few cells were detected and localized in pores near the border. In this case, the cells seem not to adhere at the surface of the pores, but are seen inside the pores, surrounded by extracellular matrix and other cell types. The low amount of hOBPCs inside the scaffold after 14 days of implantation could be explained either by cell migration or cell death. Furthermore, no inflammatory cells were evaluated.
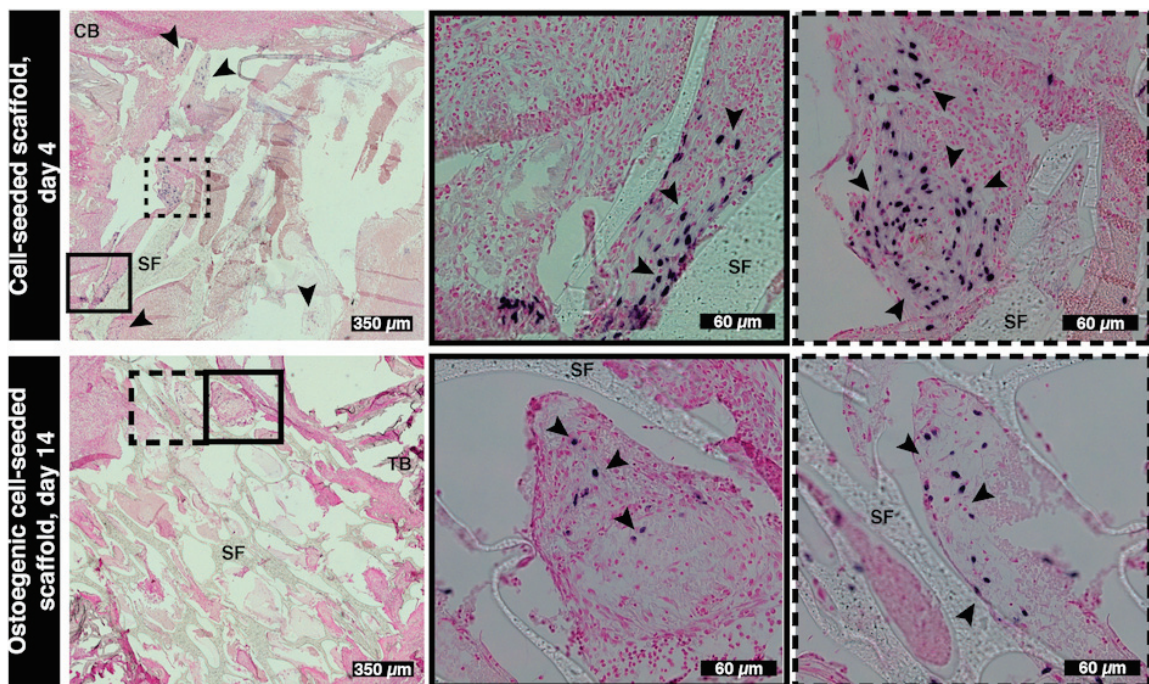
Figure 2.16 Alu-ISH with a counter nuclear Fast Red stain on sections of CS scaffolds after 4 days and of OCS scaffold after 14 days of implantation. The black arrows indicate hBPCs and hOBPCs (in blue) inside the scaffolds. The different abbreviations stand for: Trabecular bone (TB), cortical bone (CB) and scaffold (SF).

2.4.7   Hematology

The results of the normalized differential leukocyte count are shown in Fig. 2.17, 2.18 and 2.19. The leukocyte count of day 3, 7 and 14 days were all normalized to the leukocyte count of day 0. The absolute values after 0, 3, 7 and 14 days of implantation are summarized in Tab. S2.1 under Supporting Information (sub-section 2.7.2). After 3 days of implantation, no significant difference was observed in the percentage of different white blood cells in between the scaffold conditions as presented in Fig. 2.17.
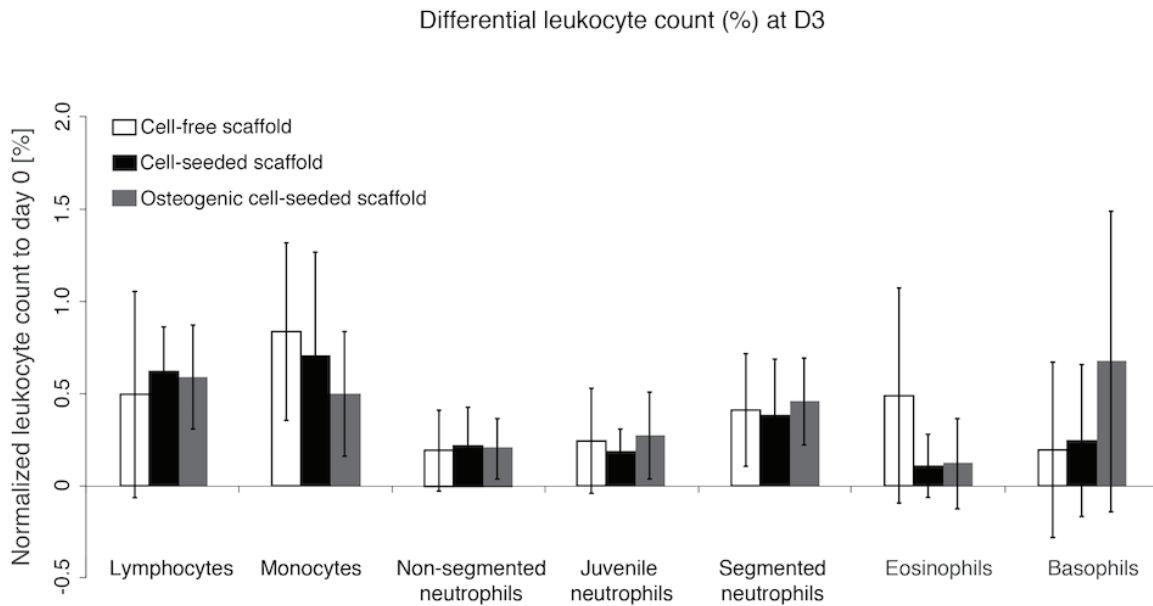
Figure 2.17 Normalized leukocyte count in blood taken after 3 days of CF, CS and OCS scaffolds implantation in femoral condyles of rats respectively. Blood smears (with n=3-4) were analyzed using the Pappenheim method. The lymphocytes, monocytes, non-segmented, juvenile and segmented neutrophils, eosinophils and basophils after 3 days of implantation were normalized to the one just before implantation (day 0). Significant *P*-values *$P<0.05$.

In Fig 2.18 results at day 7 are presented. Lymphocytes increased significantly for OCS scaffolds than in CF and CS scaffolds. Furthermore monocytes, non-segmented and juvenile neutrophils decreased for OCS scaffolds. The segmented neutrophils, however, augmented for CF scaffolds. The number of eosinophils and basophils stayed quite similar in all three scaffold conditions.
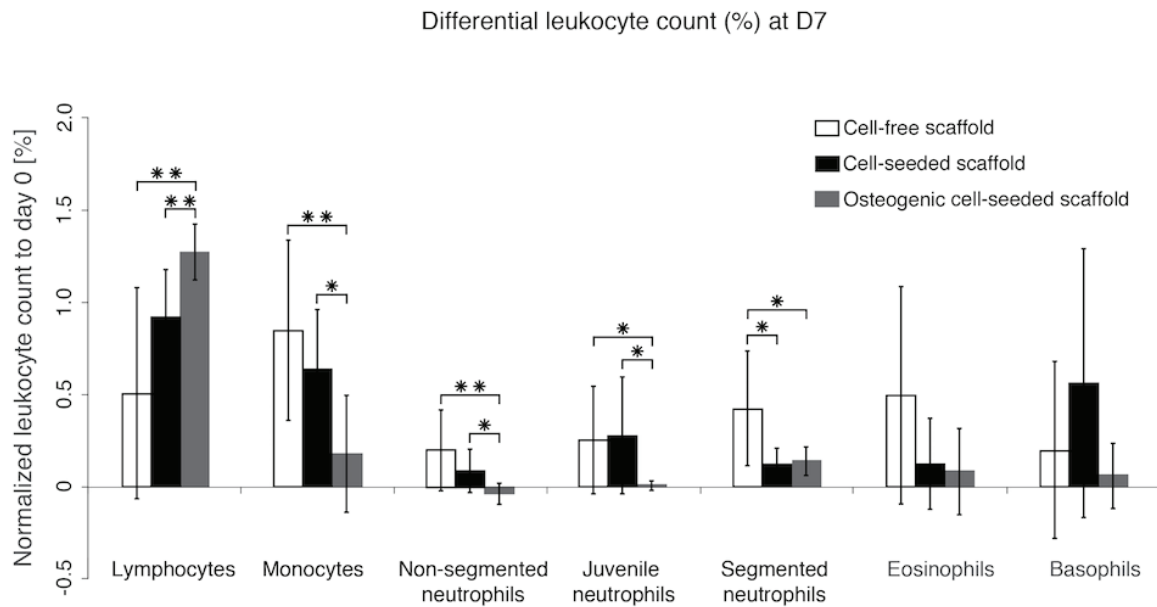
Figure 2.18 Normalized leukocyte count in blood taken after 7 days of CF, CS and OCS scaffolds implantation in femoral condyles of rats respectively. Blood smears (with n=3-4) were analyzed using the Pappenheim method. The lymphocytes, monocytes, non-segmented, juvenile and segmented neutrophils, eosinophils and basophils after 7 days of implantation were normalized to the one just before implantation (day 0). Significant *P*-values *$P<0.05$.

After 14 days of implantation, the monocyte levels increased between CF and CS scaffolds as well as between CF and OCS scaffolds (Fig. 2.19).

Differential leukocyte count (%) at D14
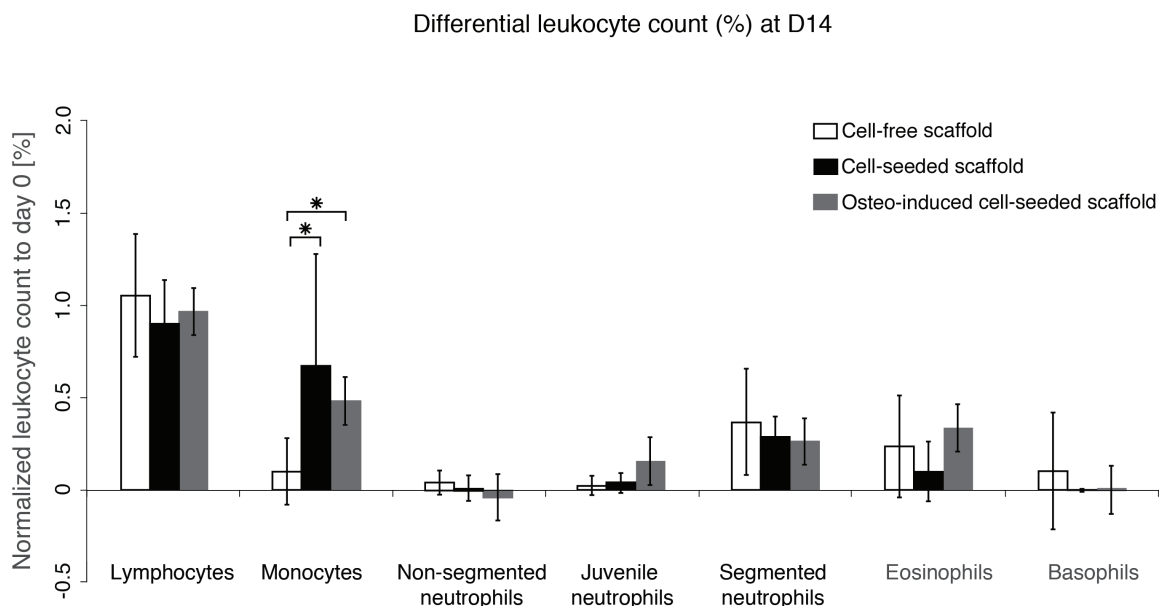
Figure 2.19 Normalized leukocyte count in blood taken after 14 days of CF, CS and OCS scaffolds implantation in femoral condyles of rats respectively. Blood smears (with n=3-4) were analyzed using the Pappenheim method. The lymphocytes, monocytes, non-segmented, juvenile and segmented neutrophils, eosinophils and basophils after 14 days of implantation were normalized to the one just before implantation (day 0). Significant *P*-values *$P<0.05$.

In general, the level of lymphocytes increased for all three scaffold conditions over the 14 days, whereas the juvenile, non-segmented and segmented neutrophil levels tended to decrease. The monocytes levels decreased after 7 days of implantation for CS and OCS scaffolds and stayed quite stable for CF scaffolds. After 14 days of implantation, the monocytes levels increased for CS and OCS and decreased for CF scaffolds.

2.4.8   Histology

The choice of making the histological expertise with toluidine blue, was based on two factors: (1) The distinction of tissue information and cell morphology were more obvious on thick slides than on thin slides (partial tissue or scaffold detachment), which limitedthe choice of the stains and (2) the evaluation was done externally in the laboratory of Prof. von Rechenberg (Rechenberg et al. 2013; Mathieu et al. 2006). In this laboratory, they are experts in toluidine blue staining within resins. Furthermore, no algorithm or automatized system was used as they can not recognize the different cell morphology as good as a human.

However, the qualitative evaluations of this study are summarized in Tab. S2.2, and Tab. S2.3, under Supporting Information (sub-section 2.7.3). The corresponding images of histological slides of OCS, CS and CF scaffolds after 3, 7 and 14 days of implantation are shown in Fig 2.20, 2.21 and 2.22,

respectively. In the case of OCS and CS scaffolds, 10-95% and 5-50% of fibrous tissue was present inside the scaffold, respectively. In both conditions, it was partially forming at the top and around the scaffold without encapsulating the scaffold. In the case of CF scaffolds, 5-20% of fibrous tissue was mainly observed at the top of the scaffolds. The CF scaffolds were in direct contact with the surrounding bone. In all three conditions, osteoblast activation toward the scaffolds as well as newly formed bone at the bottom of the scaffold were observed. Many red blood cells were visible inside all three scaffolds, mainly after 3 and 7 days of implantation. The neutrophils, macrophages, lymphocytes, plasma cells and multinuclear giant cells were qualitatively observed from rare to some in the three scaffold conditions. A slight higher amount of those cells were observed inside CF scaffolds than inside CS and OCS scaffolds. For all scaffold conditions and time points, the amount of observed immune cells were in a normal range. Inside OCS and CS scaffolds, the extracellular matrix of the implanted cells was visible, which was totally absent inside CF scaffolds. Immature bone started to grow inside OCS, CS and CF scaffolds after 7 days and started to mineralize after 14 days of implantation. In CF scaffolds, the mineralization process was more pronounced and evolved than in CS and OCS scaffolds.
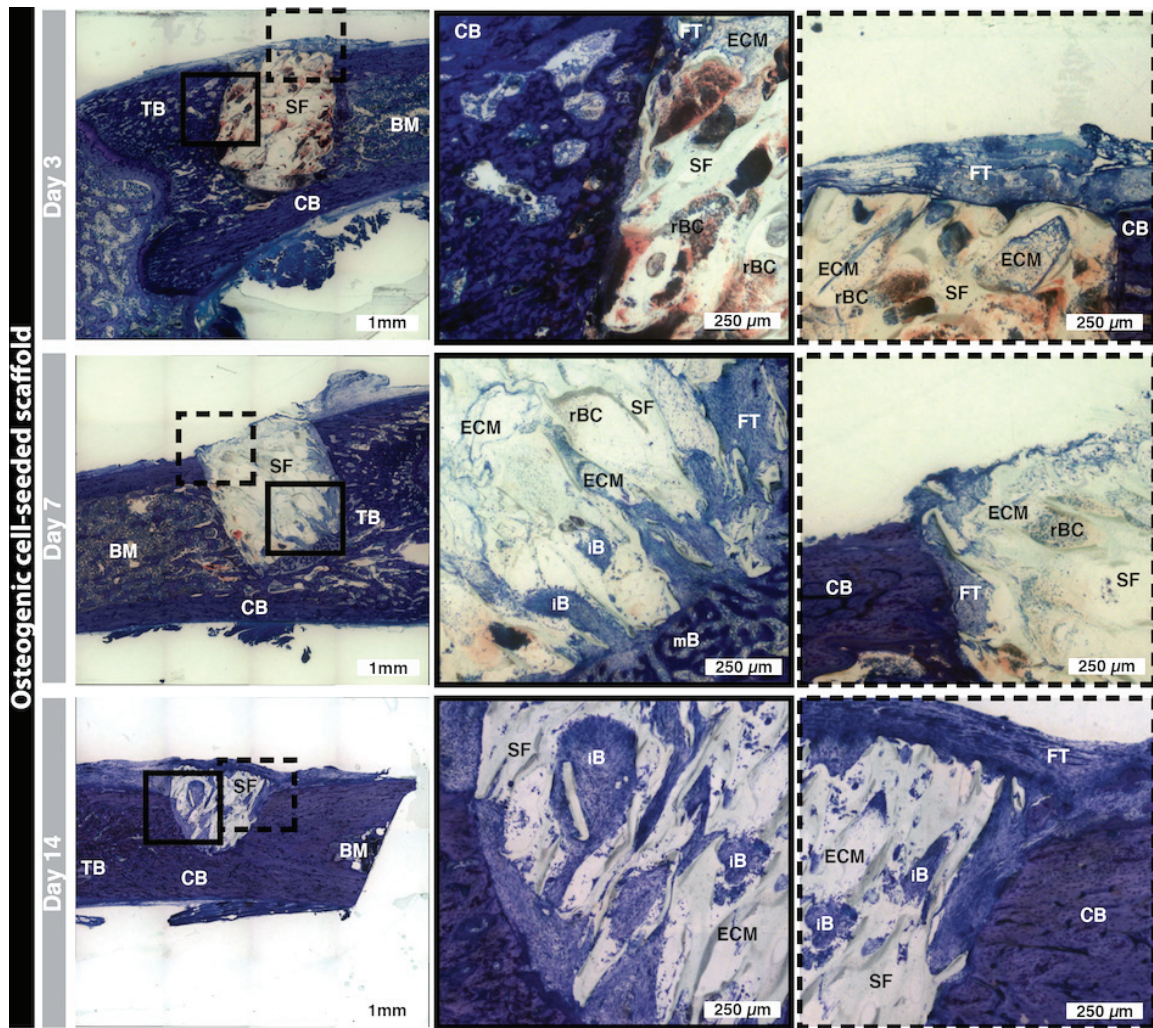
Figure 2.20 Toluidine blue stained sections of OCS scaffolds after 3, 7 and 14 days of implantation. The different tissues and scaffolds are shown using the following abbreviations: Trabecular bone (TB), cortical bone (CB), bone marrow (BM), scaffold (SF), red blood cells (rBC), fibrous tissue (FT), extracellular matrix (ECM), immature bone (iB), mature bone remodeling (mB). The sections were cut in the coronal plane.
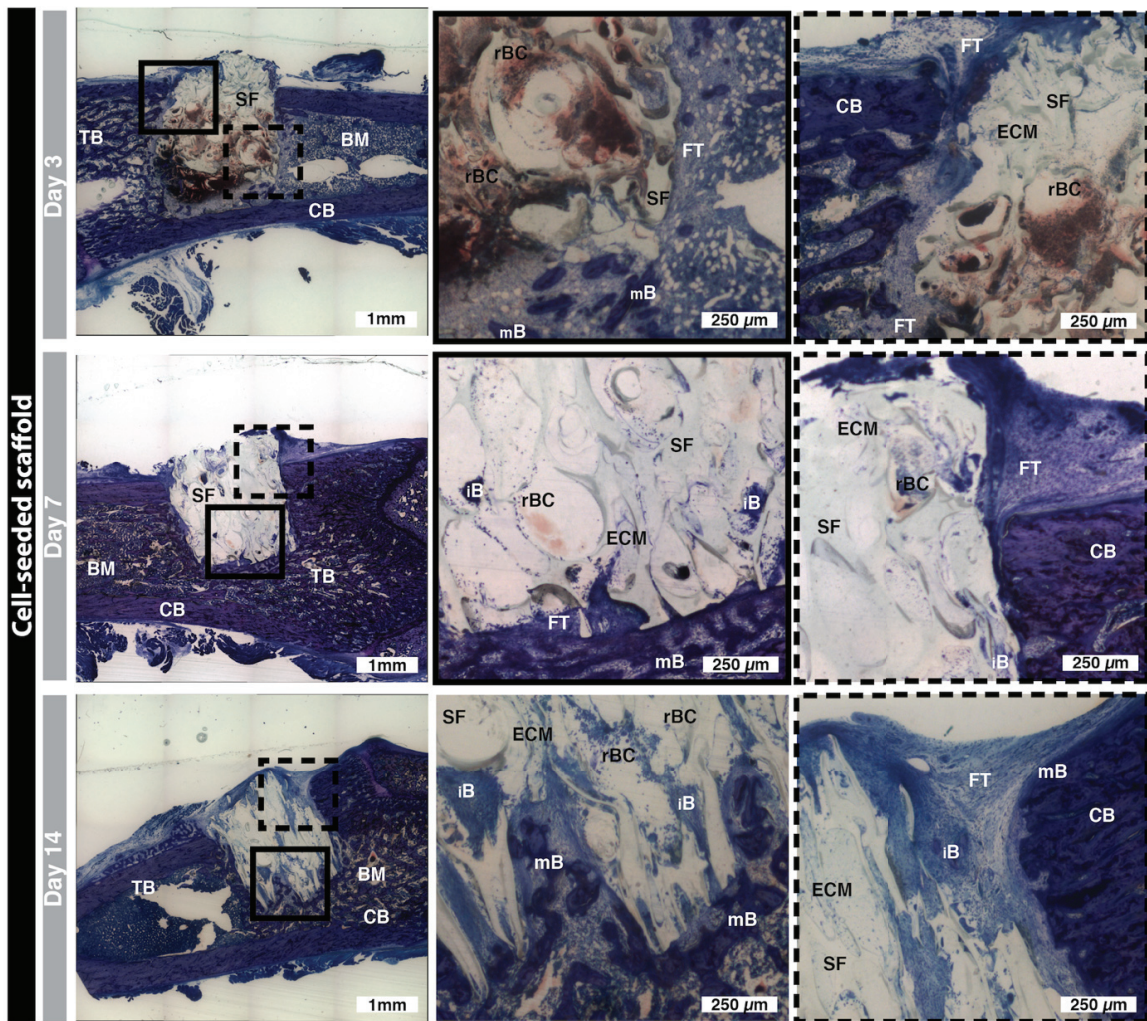
Figure 2.21 Toluidine blue stained sections of CS scaffolds after 3, 7 and 14 days of implantation. The different tissues and scaffolds are shown using the following abbreviations: Trabecular bone (TB), cortical bone (CB), bone marrow (BM), scaffold (SF), red blood cells (rBC), fibrous tissue (FT), extracellular matrix (ECM), immature bone (iB), mature bone remodeling (mB). The sections were cut in the coronal plane.
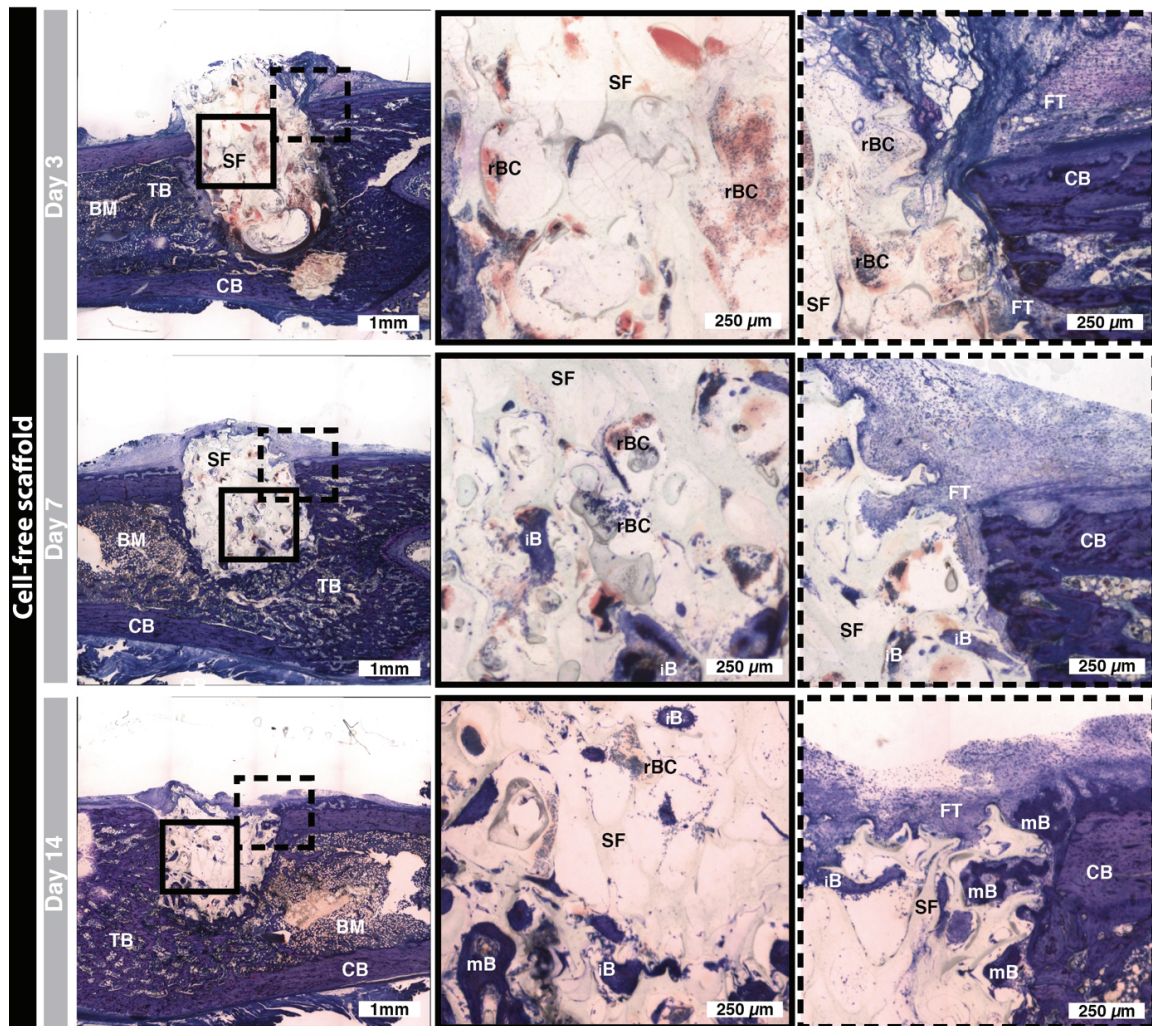
Figure 2.22 Toluidine blue stained sections of CF scaffolds after 3, 7 and 14 days of implantation. The different tissues and scaffolds are shown using the following abbreviations: Trabecular bone (TB), cortical bone (CB), bone marrow (BM), scaffold (SF), red blood cells (rBC), fibrous tissue (FT), extracellular matrix (ECM), immature bone (iB), mature bone remodeling (mB). The sections were cut in the coronal plane.

2.5 Discussion

The use of hBPCs for BTE has been demonstrated to be promising *in vivo* after several weeks of implantation in rats (Montjovent et al. 2004; Montjovent et al. 2008). However, a more extensive evaluation of the host's body reaction at an early stage of implantation of these xenograft cells was missing. In the optic to use hBPCs in clinical application as allograft cells, we preferred to further deepen the investigation on hBPCs rather than using rat bone progenitor cells. These later cells would have been more consistent in terms of immunological compatibility, but we wanted to ensure their capacity to be an accurate xenograft cell therapy model for future investigations in rat models. Therefore, the aim of this study was to evaluate a potential immune reaction triggered by hBPCs and

hOBPCs several days after implantation in a bone site. We chose to implant hBPCs- and hOBPCs-seeded scaffolds in a homotopic site instead of an ectopic site (*e.g.* skin) as we were interested by the host's immune response in the complex environment of bone. The xenograft cells would have been surrounded by more connective tissues in skin instead of osteoblasts, osteoclasts and bone marrow. The secreted cytokines and biomolecules would have been different and would have influenced the final outcome of the study. We therefore implanted the scaffolds in femoral condyles of rats and analyzed them after 3, 7 and 14 days of implantation.

In a first step, the presented data of *in vitro* studies indicated that hBPCs, isolated from 15-week-old human fetal femur, were able to differentiate in osteoblasts when cultured in osteogenic differentiation medium. They were also found to have a similar growth kinetic to those of hBPCs described elsewhere (Montjovent et al. 2004). Furthermore, the adhesion of hBPCs and hOBPCs on PLA/5% β-TCP scaffold presented no difference after 14 days of culture, but increased between 3 and 14 days of culture. The difference of adhesion between day 3 and 14, is mainly due to the synthesis of extracellular matrix, which we showed by immunofluorescent staining of fibronectin.

In a second step, we demonstrated that the osteogenic differentiation and the culture duration did not change the percentage of GFP-positive hBPCs. Furthermore, we showed that once hBPCs were transduced with a GFP lentivirus, their proliferation, ALP enzymatic activity and extracellular matrix synthesis were similar than for hBPCs. The two latter characteristics have been demonstrated to be crucial for the calcification mechanism of bone by osteoblast (van Straalen et al. 1991; Catelas et al. 2006). Alizarin and ALP staining showed that induction of osteogenesis was indispensable in order to activate *in vitro* a proper mineralization. Indeed, we observed that without induction, there was no trace of mineralization or ALP enzymatic activity as previously described (Montjovent et al. 2004; Krattinger et al. 2011). These findings were confirmed with the semi-quantitative and qualitative analysis of the enzymatic activity and the extracellular mineralization synthesis. Although the mineralization concentration was higher for hOBPCs than for GFP hOBPCs, both showed a significant higher mineralization compared to hBPCs and GFP hBPCs. A similar difference between hOBPCs and GFP hOBPCs was also observed for the ALP enzymatic activity after 7 days of culture, but it vanished after 14 days of culture. Based on these results, we concluded that the GFP-transduction did not affect the osteogenic differentiation of hBPCs and they can be used for *in vivo* experiments. Similar results were found with GFP lentiviral transfection of adipose stem cell (Wang et al. 2009) and lentiviral transduction of fetal monkey bone marrow derived mesenchymal stem cells (C. I. Lee et al. 2004).

In a third step, we localized and visualized hBPCs and hOBPCs with the use of an Alu-ISH on resin slides. We observed that both hBPCs and hOBPCs were still on site after 4 and 14 days of implantation *in vivo*, respectively. Only two unique samples out of 20 embedded samples were obtained, as the specific MMA resin (Technovit 9100) we used portrayed an unstable polymerization behavior. On the majority of these 20 samples, the Technovit resin either did not polymerize homogeneously, infiltrated poorly or dried out the bone. Therefore, the bone samples were brittle inside the resin and broke during slicing. Furthermore, even if the bone was not brittle during slicing, the Alu-ISH did not work out for the remaining samples, except for the two ones showed in the results section. In parallel to this technique, we examined the thin deplastified histology slides to visualize the GFP hBPCs using a fluorescent microscope. The GFP signal was too weak to correctly image the cells. While imaging the slides for the detection of GFP hBPCs, we changed the wavelength

filter within red fluorophore and noticed no autofluorescence of the scaffold. Therefore, we performed an immunofluorescent staining of F-actin using a red fluorophore after thin slide deplastification, which did not work either. For future work, either a non-autofluorescent scaffold should be chosen or red fluorescent protein transgenic hBPCs could be produced. The red fluorescent protein has widely been used for transgenic animals (Vintersten et al. 2005; Matsunari et al. 2008; Hong et al. 2009). However, further experimental data would be needed to see how often and where the cells tend to remain after 14 days in the scaffold. Furthermore, it would also be interesting to evaluate the difference between hBPCs and hOBPCs in terms of localization in the scaffolds and their different migration kinetics or death rate.

Finally, a differential leukocyte counts and histological evaluations were performed on samples obtained from the *in vivo* study. We showed that the implantation of GFP hOBPCs in immuno-competent rats did not trigger any specific immune response, even if they initiated a temporal formation of fibrous tissue.

For the hematological analysis, significant differences were observed between the different scaffold conditions after 7 days and 14 days of implantation. The percentage of lymphocytes was statistically significantly increased in OCS scaffolds compared to CS and CF scaffolds, whereas the percentage of monocytes, non-segmented and juvenile neutrophils showed the inverse behavior after 7 days of implantation. At the same time point, the segmented neutrophils showed a higher percentage for CF scaffolds than for CS and OCS scaffolds. After 14 days of implantation, the monocyte percentage was significantly lower for CF scaffolds than for the two others types of scaffolds. Comparing the absolute values of the different types of white blood cells with other publications (Montjovent et al. 2007; Dyer & Cervasio 2008; Gupta et al. 2015), we found that they were within the normal range for Wistar and Sprague-Dawley rats, except for the monocyte values (see sub-section 2.7.2 under Supporting Information). The absolute monocytes values were much higher in our study than in the published one, even before the surgical intervention. The normalized monocytes values were in the same range after 3 days of implantation, decreased for OCS scaffolds after 7 days of implantation and were significantly higher in CS and OCS scaffolds after 14 days of implantation. As some hBPCs and hOBPCs surely died after 14 days of implantation, the monocytes were more active. They might have phagocyted hBPCs and hOBPCs debris and were therefore present in a higher range than for CF scaffolds. However, we considered that there was no acute hematological effect due to implantation of CF, CS and OCS scaffolds. To confirm and giving more substance to those results, 3-5 more blood samples per condition would be needed to increase the power of the statistical analysis.

The histological evaluation clearly showed, that the presence of the immune cells, such as neutrophils, macrophages, lymphocytes, plasma cells and multinuclear giant cells was rarely observed in all three conditions from 3 days to 14 days of implantation, while fibrous tissue was seen within CS and OCS scaffolds. We observed as well a higher fibrous tissue formation in OCS scaffolds than in CS scaffolds. At this early stage of implantation, the observed higher amount of fibrous tissue in CS and OCS scaffolds is not necessarily related to a foreign body reaction. As the immune response and the skeletal system work closely together, the immune cells play a pivotal role in determining the *in vivo* fate of the implanted material. It contributes either to its success by facilitating new bone formation or to its failure with the creation of an inflammatory fibrous tissue capsule (Miron & Bosshardt 2016; Yin et al. 2016). The combination of these results with the one published by Montjovent et al. (Montjovent et al. 2008), in which bone formation was observed after 6 and 12

months of implantation, indicates that the host's body overcame the fibrous tissue formation, instead of encapsulating the xenograft cell-seeded engineering scaffolds. Therefore, the fibrous tissue formation in CS and OCS conditions could be favored by another cellular mechanism or cellular secretion, which arose certainly from the implanted hBPCs themselves. As cell fate is a temporal, spatial and mechanical interplay between cells, cytokines and growth factors (Amini et al. 2012), it is merely impossible to describe the interaction of the implanted hBPCs and the surrounding tissue of the rat. A possible cue could be given in a study published by Safadi et al. (Safadi et al. 2003). They demonstrated that connective tissue growth factor (CTGF) was expressed in normal bone during active growth or modeling and that its expression increased during the matrix mineralization and proliferation of primary osteoblasts from neonatal rats. This CTGF expression increase could be a plausible explanation for the higher increase of fibrous tissue in OCS scaffolds than in CS scaffolds. Other publications described that this growth factor was important in osteogenesis, but played rather a more relevant role in fibrogenesis (Moussad & Brigstock 2000; C. H. Lee et al. 2010). Therefore, the temporal effect of secreted CTGF from hBPCs and hOBPCs could cause the presence of formed fibrous tissue.

In order to demonstrate this hypothesis, further *in vitro* and *in vivo* studies would be needed. In the case of *in vitro* studies, CTGF secretion of hBPCs and hOBPCs could be compared to those of rat BPC (rBPCs) and endothelial cells, first observed and described to secrete CTGF (Bradham 1991). Furthermore, additional *in vivo* experiments should give proof that the insertion of BPCs influences the formation of fibrous tissue, by analyzing the effect of implanted scaffolds seeded with either rBPCs or osteogenic rBPCs in rats. Furthermore, CF implanted scaffolds could be loaded with different concentrations of CTGF and other growth factors or cytokines to modulate the immune systems of the host in order to understand exactly what signaling hBPCs and hOBPCs give to the surrounding tissue.

2.6 Conclusion

Inflammatory reactions in bone after the insertion of a biocomposite scaffold depend on several factors such as the extent of defect, size, shape, polymer degradation rate as well as the physical, chemical and mechanical properties of the implanted material (Little & Parkhouse 1962; Homsy 1970; Wood et al. 1970; Gupta et al. 2015). To complete the study by Montjovent et al. (Montjovent et al. 2007), in which they analyzed only the inflammatory response of PLA/5% β-TCP scaffold without cells, we evaluated the different effects of CF, CS and OCS scaffolds on the immune system after a few days of implantation in femoral condyles of rats. For cell localization purposes, we worked with GFP hBPCs in this project, which were characterized *in vitro* in a first step. Therefore, we showed that GFP transduced hBPCs had a similar growth kinetic than hBPCs and, that they kept their capacity to differentiate in osteoblasts when put in an osteogenic environment. In a second step, our preliminary *in vivo* data showed that hBPCs and hOBPCs were still present after 4 and 14 days of implantation. Then, the histological evaluation indicated that a similar amount of immune cells was observed in all three types of scaffolds without any formation of fibrous tissue capsule around the xenograft scaffolds. The presence of hBPCs and hOBPCs, however, increased the formation of fibrous tissue compared to CF scaffolds, which could be explained by the temporal secretion of signaling factors, such as CTGF, by hBPCs and hOBPCs. Though more studies would be needed to confirm the

last hypothesis, the results of this study demonstrated that hBPCs and hOBPCs affect the surrounding tissue by forming a temporary fibrous tissue, but without triggering any particular specific immune reaction.

2.7   Supporting Information

2.7.1   Scaffold Seeding

Prior to sterilization, each scaffold was introduced in a 1 cm long plastic tube (Prolongeur Heidelberger, B. Braun). Once sterilized using ethanol oxide (CHUV, Lausanne), a 0.5 mL syringe (B. Braun) was added at one end of the Heidelberger tube. Afterwards, 20 µL of either 0.9% NaCl or standard culture medium (depending on the scaffold condition, see sub-section 2.3.2.2) was deposited on the top of the scaffold. The solution was then pushed-pulled several times through the scaffold thanks to the syringe. The syringe was taken away and the scaffold within the Heidelberger tube was then placed in a 0.5 mL Eppendorf tube for sonication. After 20 min of sonication (Ultrasonik), a new 0.5 mL syringe was added to one end of the tubing in order to aspirate the solution.

At this step, the CF scaffolds were taken out of the tubes and directly immersed in 200 µL of 0.9% NaCl contained in a 0.5 mL Eppendorf tube. For CS scaffold and OCS scaffolds, 20 µL of cell suspension ($0.5 *10^6$ cells/20 µL) was dropped onto each scaffold and pushed-pulled gently through the scaffold until it was entirely covered with cell suspension. The seeded scaffolds within the Heidelberger tubing were then put in a 0.5 mL Eppendorf tube, which was fixed on a rotating platform for 1 h. The scaffolds were then taken out of the tube and immersed in 200 µL of standard cell culture medium contained in a 0.5 mL Eppendorf tube. The cap of the 0.5 mL Eppendorf tubes were punctured with a 25G needle (B. Braun) and put in the incubator. The times of culture as well as the medium types were depended on the experiment and the scaffold condition.

2.7.2 Hematology: Table

Table S2.1 Differential leukocyte counts before and after 3, 7 and 14 days of implantation of CF, CS and OCS scaffolds.

Duration of implantation (days)	Reference values for rats (Adapted from S. M Dyer and E. L. Cervasio, 2008)	Before surgery 0	Cell-free scaffold 3	Cell-free scaffold 7	Cell-free scaffold 14	Cell-seeded scaffold 3	Cell-seeded scaffold 7	Cell-seeded scaffold 14	Osteo-induced cell-seeded scaffold 3	Osteo-induced cell-seeded scaffold 7	Osteo-induced cell-seeded scaffold 14
Differential leukocyte counts (%)											
Lymphocytes (%)	72.2 (± 31.9)	63.5 (± 17.8)	67.9 (± 11.4)	57.8 (± 21.1)	77.9 (± 12.3)	62.5 (± 9.1)	73.1 (± 9.5)	72.3 (± 8.6)	61.8 (± 10.6)	98.4 (± 5.6)	74.7 (± 10.3)
Monocytes (%)	0.3 (± 0.2)	12.2 (± 4.9)	10.6 (± 4.1)	18.6 (± 7.8)	6.6 (± 2.9)	16.5 (± 9.2)	15.0 (± 5.0)	16.0 (± 10.0)	13.1 (± 5.5)	9.0 (± 4.0)	13.0 (± 5.0)
Non segmented neutrophils (%)	26.8 (± 11.8)	5.4 (± 4.6)	2.8 (± 1.6)	3.6 (± 2.9)	1.5 (± 0.9)	4.0 (± 2.8)	2.1 (± 1.6)	1.1 (± 0.8)	3.8 (± 2.1)	0.6 (± 0.8)	0.5 (± 0.8)
Juvenile neutrophils (%)		4.6 (± 3.8)	0.9 (± 1.0)	3.3 (± 3.8)	0.3 (± 0.7)	2.5 (± 1.6)	4.0 (± 4.0)	1.0 (± 1.0)	3.6 (± 3.1)	0.0 (± 0.0)	2.0 (± 3.0)
Segmented neutrophils (%)		13.1 (± 11.6)	17.0 (± 8.1)	14.8 (± 11.0)	12.8 (± 10.1)	13.7 (± 10.9)	4.4 (± 3.0)	10.1 (± 3.8)	16.4 (± 8.4)	5.7 (± 2.7)	9.2 (+/-5.7)
Eosinophils (%)	0.5 (± 0.4)	0.5 (± 1.0)	0.7 (± 0.8)	1.5 (± 1.8)	0.7 (± 0.8)	0.3 (± 0.5)	0.4 (± 0.7)	0.3 (± 05)	0.4 (± 0.7)	0.3 (± 0.7)	1.0 (± 1.5)
Basophils (%)	0.2 (± 0.2)	0.6 (± 0.8)	0.1 (± 0.3)	0.4 (± 1.0)	0.2 (± 0.6)	0.5 (± 0.8)	1.0 (± 1.0)	0.0 (± 0.0)	1.4 (± 2.0)	0.0 (± 0.0)	0.0 (± 0.0)

In Tab. S2.1, the percentage of lymphocytes, monocytes, non-segmented, juvenile and segmented neutrophils, eosinophils and basophiles are described before and after implantation of CF, CS and OCS scaffolds. Furthermore, adapted values from Dyer and Cervasio. (Dyer & Cervasio 2008) are listed in the same table. The three neutrophil cell types were pooled together in the reference values. In comparison to the values of day 0, the values are in the same range, except for the monocytes.

59

2.7.3   Histological Evaluation

The percentage of fibrous tissue as well as osteoblast activation and number of vessels evaluated on histology slides are summarized in Tab. S2.2. Osteoblast activation and number of vessels were estimated to be the same for all scaffold conditions and time points. Concerning the percentage of fibrous tissue, an increase was observed between the different scaffold conditions. In the case of CF scaffold, 5-20% of fibrous tissue was estimated, whereas for CS scaffolds it was 5-50% and for OCS it was 10-95% of fibrous tissue. Furthermore, we saw a slight increase of fibrous tissue for all scaffold conditions from day 3 to day 7, and a slight decrease from day 7 to day 14.

Table S2.2 Qualitative evaluations of cellular events based on histology slides. The osteoblastic activation was evaluated as rare, few, some or many (n=3).

Scaffold	Time post-implantation (Day)	Osteoblast activation (rare, few, normal range)	Number of vessels approximation	Fibrous tissue approximation (%)
CF	3	Few	< 5	5-20%
	7	Few	< 5	10-20%
	14	Few	< 5	10-15
CS	3	Few	< 5	5-50%
	7	Few	< 5	25-50%
	14	Few	< 5	25-30%
OCS	3	Few	< 5	10-90%
	7	Few	< 5	30-95%
	14	Few	< 5	25-75%

The qualitative evaluation of the immune response is summarized in Tab. S2.3. The presence of immune cells (neutrophils, macrophages, lymphocytes, plasma cells and multinuclear giant cells) were quantified from rare to some in all scaffold conditions, where in general more immune cells were noticed after 7 and 14 days of implantation in CF scaffolds compared to CS and OCS scaffolds. For all scaffold conditions and time points, the amount of observed immune cells were in a normal range.

Table S2.3 Qualitative evaluations of the immune response based on the histology slides. The immune response was evaluated as rare, few, some or many (n=3).

Scaffold	Time post-implantation (Day)	Neutrophils	Macrophages	Lymphocytes	Plasma cells	Multinuclear giant cells
CF	3	Rare to some	Rare to some	Rare to some	Rare to some	Rare to some
	7	Some	Some	Some	Some	Rare to some
	14	Some	Some	Some	Some	Rare to some
CS	3	Few to some	Rare to some	Rare to some	Rare to some	Rare to some
	7	Rare to some	Rare to some	Rare to some	Rare to some	Rare to some
	14	Rare	Rare	Rare	Rare	Rare
OCS	3	Rare	Rare	Rare to some	Rare to some	Rare to few
	7	Rare to few	Rare to few	Rare to some	Rare to some	Rare to some
	14	Rare	Rare	Rare	Rare	Rare to some

2.8   Acknowledgements

2.9   References

Al-Sayyad, M.J. & Abdulmajeed, T.M., 2006. Fracture of the anterior iliac crest following autogenous bone grafting. *Saudi Medical Journal*, 27(2), pp.254–258.

Amini, A.R., Laurencin, C.T. & Nukavarapu, S.P., 2012. Bone tissue engineering: recent advances and challenges. *Critical Reviews in Biomedical Engineering*, 40(5), pp.363–408.

Barber, R.D. et al., 2005. GAPDH as a housekeeping gene: analysis of GAPDH mRNA expression in a panel of 72 human tissues. *Physiological Genomics*, 21(3), pp.389–395.

Black, C.R.M. et al., 2015. Bone tissue engineering. *Current Molecular Biology Reports*, 1(3), pp.132–140.

Boerckel, J.D. et al., 2011. Effects of protein dose and delivery system on BMP-mediated bone regeneration. *Biomaterials*, 32(22), pp.5241–5251.

Boerckel, J.D. et al., 2012. Effects of *in vivo* mechanical loading on large bone defect regeneration. *Journal of Orthopaedic Research*, 30(7), pp.1067–1075.

Bradham, D.M., 1991. Connective tissue growth factor: a cysteine-rich mitogen secreted by human vascular endothelial cells is related to the SRC-induced immediate early gene product CEF-10. *The Journal of Cell Biology*, 114(6), pp.1285–1294.

Catelas, I. et al., 2006. Human mesenchymal stem cell proliferation and osteogenic differentiation in fibrin gels *in vitro*. *Tissue Engineering*, 12(8), pp.2385–2396.

Connolly, J.F., 1995. Injectable bone marrow preparations to stimulate osteogenic repair. *Clinical Orthopaedics and Related Research*, 313, pp.8–18.

Costa-Pinto, A.R., Reis, R.L. & Neves, N.M., 2011. Scaffolds based bone tissue engineering: The role of chitosan. *Tissue Engineering Part B: Reviews*, 17(5), pp.331–347.

Das, A. & Botchwey, E., 2011. Evaluation of angiogenesis and osteogenesis. *Tissue Engineering Part B: Reviews*.

Dyer, S.M. & Cervasio, E.L., 2008. An overview of restraint and blood collection techniques in exotic pet practice. *The veterinary clinics of North America. Exotic animal practice*, 11(3), pp.423–443.

Eller, C.D. et al., 2007. Repetitive sequence environment distinguishes housekeeping genes. *Gene*, 390(1-2), pp.153–165.

Follenzi, A. & Naldini, L., 2002a. Generation of HIV-1 derived lentiviral vectors. In *Gene Therapy Methods*. Methods in Enzymology. Elsevier, pp. 454–465.

Follenzi, A. & Naldini, L., 2002b. HIV-based vectors: Preparation and use. *Methods in Molecular Medicine*, 69, pp.259–274.

Gomez-Barrena, E. et al., 2015. Bone fracture healing: Cell therapy in delayed unions and nonunions. *Bone*, 70, pp.93–101.

Gregory, C.A. et al., 2004. An Alizarin red-based assay of mineralization by adherent cells in culture: comparison with cetylpyridinium chloride extraction. *Analytical Biochemistry*, 329(1), pp.77–84.

Gupta, A. et al., 2015. Biocompatibility of single-walled carbon nanotube composites for bone regeneration. *Bone & Joint Research*, 4(5), pp.70–77.

Homsy, C.A., 1970. Bio-compatibility in selection of materials for implantation. *Journal of Biomedical Materials Research Part A*, 4(3), pp.341–356.

Hong, S.G. et al., 2009. Generation of red fluorescent protein transgenic dogs. *Genesis*, 47(5), pp.314–322.

Kettenberger, U. et al., 2014. Does locally delivered Zoledronate influence peri-implant bone formation? - Spatio-temporal monitoring of bone remodeling *in vivo*. *Biomaterials*, 35(37), pp.9995–10006.

Klenke, F.M. et al., 2008. Impact of pore size on the vascularization and osseointegration of ceramic bone substitutes *in vivo*. *Journal of Biomedical Materials Research Part A*, 85A(3), pp.777–786.

Krattinger, N. et al., 2011. Regulation of proliferation and differentiation of human fetal bone cells. *European Cells and Materials*, 21, pp.46–58.

Krebsbach, P.H. et al., 1998. Repair of craniotomy defects using bone marrow stromal cells. *Transplantation*, 66(10), pp.1272–1278.

Lee, C.H. et al., 2010. CTGF directs fibroblast differentiation from human mesenchymal stem/stromal cells and defines connective tissue healing in a rodent injury model. *The Journal of Clinical Investigation*, 120(9), pp.3340–3349.

Lee, C.I. et al., 2004. Morphological analysis and lentiviral transduction of fetal monkey bone marrow-derived mesenchymal stem cells. *Molecular Therapy*, 9(1), pp.112–123.

Little, K. & Parkhouse, J., 1962. Tissue reactions to polymers. *Lancet*, 2(7261), pp.857–861.

Mathieu, L.M. et al., 2006. Architecture and properties of anisotropic polymer composite scaffolds for bone tissue engineering. *Biomaterials*, 27(6), pp.905–916.

Matsunari, H. et al., 2008. Transgenic-cloned pigs systemically expressing red fluorescent protein, Kusabira-Orange. *Cloning and Stem Cells*, 10(3), pp.313–324.

Miron, R.J. & Bosshardt, D.D., 2016. OsteoMacs: Key players around bone biomaterials. *Biomaterials*, 82, pp.1–19.

Montjovent, M.-O. et al., 2004. Fetal bone cells for tissue engineering. *Bone*, 35(6), pp.1323–1333.

Montjovent, M.-O. et al., 2008. Human fetal bone cells associated with ceramic reinforced PLA scaffolds for tissue engineering. *Bone*, 42(3), pp.554–564.

Montjovent, M.-O. et al., 2007. Repair of critical size defects in the rat cranium using ceramic-reinforced PLA scaffolds obtained by supercritical gas foaming. *Journal of Biomedical Materials Research Part A*, 83A(1), pp.41–51.

Moussad, E.E. & Brigstock, D.R., 2000. Connective tissue growth factor: what's in a name? *Molecular Genetics and Metabolism*, 71(1-2), pp.276–292.

Muramatsu, K. et al., 2009. Recalcitrant posttraumatic nonunion of the humerus: 23 patients reconstructed with vascularized bone graft. *Acta Orthopaedica Scandinavica*, 74(1), pp.95–97.

Pfaffl, M.W., 2001. A new mathematical model for relative quantification in real-time RT-PCR. *Nucleic Acids Research*, 29(9), pp.E419–E423.

Quarto, R. et al., 2001. Repair of large bone defects with the use of autologous bone marrow stromal cells. *The New England Journal of Medicine*, 344(5), pp.385–386.

Rechenberg, von, B. et al., 2013. Evaluation of four biodegradable, injectable bone cements in an experimental drill hole model in sheep. *European Journal of Pharmaceutics and Biopharmaceutics*, 85(1), pp.130–138.

Roshan-Ghias, A. et al., 2011. In vivo assessment of local effects after application of bone screws delivering bisphosphonates into a compromised cancellous bone site. *Clinical Biomechanics*, 26(10), pp.1039–1043.

Safadi, F.F. et al., 2003. Expression of connective tissue growth factor in bone: Its role in osteoblast proliferation and differentiation in vitro and bone formation *in vivo*. *Journal of Cellular Physiology*, 196(1), pp.51–62.

Schormann, W. et al., 2008. Tracking of human cells in mice. *Histochemistry and Cell Biology*, 130(2), pp.329–338.

Serafini, M. et al., 2014. Establishment of bone marrow and hematopoietic niches in vivo by reversion of chondrocyte differentiation of human bone marrow stromal cells. *Stem Cell Research*, 12(3), pp.659–672.

Sflomos, G. et al., 2016. A preclinical model for ERα-positive breast cancer points to the epithelial microenvironment as determinant of luminal phenotype and hormone response. *Cancer Cell*, 29(3), pp.407–422.

van der Horst, E.H. et al., 2004. TaqMan-based quantification of invasive cells in the chick embryo metastasis assay. *BioTechniques*, 37(6), pp.940–945.

van der Pol, U. et al., 2010. Augmentation of bone defect healing using a new biocomposite scaffold: An *in vivo* study in sheep. *Acta Biomaterialia*, 6(9), pp.3755–3762.

van Straalen, J.P. et al., 1991. Bone-alkaline phosphatase as indicator of bone formation. *Clinica Chimica Acta*, 201(1-2), pp.27–34.

Vintersten, K. et al., 2005. Mouse in red-red fluorescent protein expression in mouse ES cells, embryos and adult animals. *Genesis*, 42(3), pp.218–218.

Wang, Q. et al., 2009. *In vitr*o osteogenic differentiation of adipose stem cells after lentiviral transduction with green fluorescent protein. *Journal of Craniofacial Surgery*, 20(6), pp.2193–2199.

Wood, N.K., Kaminski, E.J. & Oglesby, R.J., 1970. The significance of implant shape in experimental testing of biological materials: Disc vs. rod. *Journal of Biomedical Materials Research Part A*, 4(1), pp.1–12.

Yin, X. et al., 2016. Osteoimmunomodulation for the development of advanced bone biomaterials. *Frontiers in Bioengineering and Biotechnology*, 4.

CHAPTER 3

Effect of Temporal Onsets of Mechanical Loading on Bone Formation Inside a Tissue Engineering Scaffold Combined with Cell Therapy

Hausherr T.C., Nuss K.,Thein, E., Krähenbühl S., Stadelmann V., Applegate L.A., Pioletti D.P.

3.1 Abstract

Several approaches to combine bone substitutes with biomolecules, bone cells or mechanical loading have been explored as an alternative to the limitation- and risk-related bone auto- and allografts. In particular, human bone progenitor cells seeded in porous poly(L-lactic acid)/tricalcium phosphate scaffolds have shown promising results. Furthermore, the application of mechanical loading has long been known to be a key player in the regulation of bone architecture and mechanical properties. Several *in vivo* studies have pointed out the importance of its temporal offset: When an early mechanical loading was applied few days after scaffold implantation, it had an ineffective to a moderate effect on bone formation, whereas a delayed mechanical loading of several weeks was beneficial for bone tissue regeneration. However, no information is reported so far on the effectiveness of applying *in vivo* a mechanical loading on cell-seeded scaffold with respect to bone formation in a bone site. In our study, we were interested in human bone progenitor cells due to their low immunogenicity, sensitivity to mechanical loading and capacity to differentiate in osteogenic human bone progenitor cells. The latest capacity allowed us to test two different bone cell fates originated from the same cell type. Therefore, the general aim of this study was to assess the outcome on bone formation when human bone progenitor cells or osteogenic human bone progenitor cells are combined with early and delayed mechanical loading inside bone tissue engineering scaffolds. As scaffold control, we used a scaffold without cells, named cell-free scaffold. Surprisingly, we found in our study that (1) the best solution for bone regeneration is the combination of cell-free scaffolds and delayed mechanical loading and (2) the timing of the mechanical application is crucial and dependent on the cell types inside the implanted scaffolds.

Keywords: Bone tissue engineering, scaffold, cell therapy, human bone progenitor cells, osteogenic human bone progenitor cells, early and delayed mechanical loading, microCT imaging.

3.2 Introduction

The clinical need for alternative bone substitutes to bone auto- and allografts is an actual challenge for researcher to develop simple, safe and easy-to-use bone tissue engineering (BTE) scaffolds. Several approaches have been combined such as the use of different biomolecules delivery (Bose et al. 2012), bone cell types (Owen et al. 1987; Pittenger et al. 1999; Krebsbach et al. 1999; Phinney et al. 1999; Montjovent et al. 2004; Krattinger et al. 2011; Wu et al. 2015) or the application of mechanical loading (Roshan-Ghias et al. 2010; Roshan-Ghias, Lambers, et al. 2011; Boerckel, Uhrig, et al. 2011).

Bone affiliated cells, such as mesenchymal stem cells (MSCs), human bone progenitor cells (hBPCs), and bone marrow-derived MSCs, have shown their potential for BTE in several *in vitro* studies, by differentiating into mineralized cells under osteogenic conditions (Owen et al. 1987; Pittenger et al. 1999; Krebsbach et al. 1999; Phinney et al. 1999; Montjovent et al. 2004; Krattinger et al. 2011; Wu et al. 2015). Under different experimental and *in vivo* implantation conditions, those cells have demonstrated their capacity to induce bone formation when implanted with BTE scaffolds. For mentioning but a few, Serafini et al. (Serafini et al. 2014) have highlighted the ability of bone marrow-derived MSCs to form bone marrow and hematopoietic niches when implanted in heterotopic sites, whereas others studies have shown an increase in bone formation when implanted in bone sites (Yasko et al. 1992; Srouji & Livne 2005; Jäger et al. 2007; Montjovent et al. 2008; Dupont et al. 2010; Xu et al. 2010; Liu et al. 2013; Corre et al. 2015).

In parallel, it has long been known that mechanical loading plays an important role in the regulation of bone architecture and properties (Turner et al. 1994; Forwood et al. 1996; Robling et al. 2006; Robling & Turner 2009; Roshan-Ghias et al. 2010; Dupont et al. 2010; Boerckel, Uhrig, et al. 2011; Roshan-Ghias, Lambers, et al. 2011; Boerckel, Kolambkar, et al. 2011; Boerckel et al. 2012). Roshan-Ghias and Boerckel especially demonstrated *in vivo* (Roshan-Ghias et al. 2010; Roshan-Ghias, Lambers, et al. 2011; Boerckel et al. 2012) that the temporal onset of mechanical loading on bone formation was crucial, as the application of early mechanical loading, applied few days post-implantation, was seen to be ineffective or moderated compared to delayed mechanical loading, applied several weeks.

Three previously *in vivo* studies completed in our laboratory were combined in this work. In the first work they have shown that hBPCs-seeded in poly(L-lactic acid) (PLA)/5% ß – tricalcium phosphate (ß–TCP) scaffolds promote bone repair (Montjovent et al. 2008). Furthermore, in the second work they have described that early mechanical loading increases modestly bone formation inside PLA/5% ß–TCP scaffolds (Roshan-Ghias et al. 2010). In the latest one, they have demonstrated that delayed mechanical loading accelerates bone formation and decelerates bone resorption inside PLA/5% ß–TCP scaffolds (Roshan-Ghias, Lambers, et al. 2011). As the present work stands at the intersection of two main functions of bone, namely the biological and mechanical functions, we explored the impact of early and delayed loading mechanical loading on three different conditions using the same type of scaffolds, characterized by the absence or presence of mechano-sensitive cells (Mammoto et al. 2012). In this work, we were interested in using hBPCs due to their low immunogenicity and capacity for osteogenic differentiation into mature osteoblasts, refereed to as osteogenic hBPCs (hOBPCs). The choice to use these two cell types was driven by the complex healing and regeneration mechanism of bone involving various cell fates (Amini et al. 2012). The capacity of these hBPCs to

differentiate into hOBPCs allows us to test two different bone cell fates *in vivo* originally derived from the same type of cell. To the best of our knowledge, this is the first work that investigates the effect on bone regeneration when cell therapy and mechanical loading are combined in BTE scaffolds.

Therefore, the first aim of this study was to evaluate the potential for BTE of hBPCs-seeded PLA/5% β-TCP scaffolds and hOBPCs-seeded PLA/5% β-TCP scaffolds in a long-term *in vivo* study. The second aim of this study was to assess the effect of early and delayed mechanical loading on cell-free (CF), hBPCs-seeded scaffolds (CS scaffolds) and hOBPCs-seeded scaffolds (OCS scaffolds) on bone formation after 12 weeks of implantation in femoral condyles of rats.

Based on microCT images and histological analysis, we first showed in this work that CF scaffolds induced a significantly higher amount of newly formed bone compared to CS and OCS scaffolds, independently of the mechanical loading conditions. Secondly, we demonstrated that early mechanical loading had a positive effect on bone formation inside CS scaffolds and a negative one inside OCS scaffolds, while it had no repercussion in CF scaffolds. Finally, we presented that delayed loading increased significantly the amount of bone formation in both CF and CS scaffolds.

3.3 Materials and Methods

3.3.1 Cell Culture and Scaffold

For this *in vivo* study, hBPC were seeded and cultured in PLA/5% ß-TCP as described in Chapter 2 (see sections 2.3.1 and 2.3.2). We used the same scaffold conditions, namely CF, CS and OCS scaffolds, than in Chapter 2 (see Fig. 3.1). For the study in which early mechanical loading was compared to no loading, only CF and CS scaffolds were marked with ruby beads at their top and at their bottom. The aim and the protocol of this marking are described in the Supporting Information (sub-section 3.7.1). The scaffolds preparation and seeding protocols were the same than those described in Chapter 2, section 2.3.2.2.
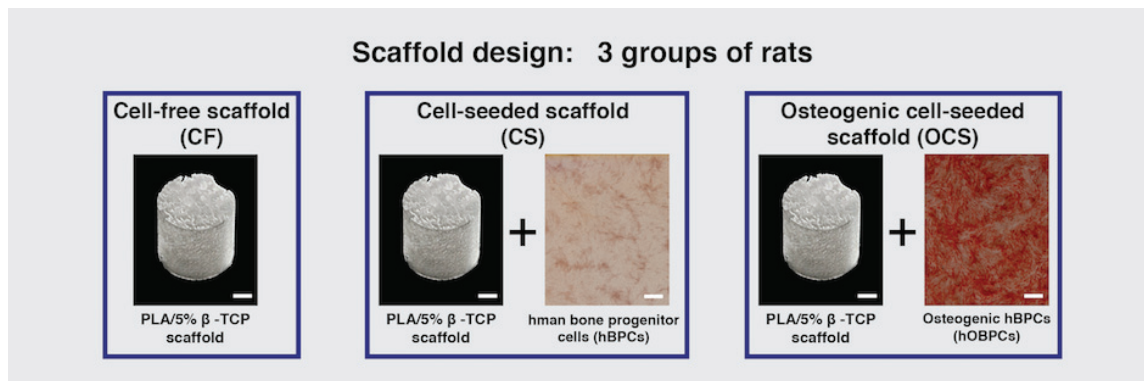
Figure 3.1 Experimental conditions of scaffolds. Cell-free (CF), cell-seeded (CS) and osteogenic cell-seeded (OCS) poly(L-lactic acid)/5% ß-tricalcium (PLA/5% β-TCP) scaffolds were prepared for this study. For CS scaffolds, human bone progenitor cells (hBPCs) were cultured in standard medium and seeded in PLA/5% β-TCP scaffolds 3 days before implantation. In the case of OCS scaffolds, hBPCs were seeded in PLA/5% β-TCP scaffolds and cultured in differentiation osteogenic medium for 2 weeks before implantation to obtain osteogenic hBPCs (hOBPCs). On the photographs, hBPCs and hOBPCs are stained with Alizarin Red S to reveal the mineralization in red. The detection of the presence of extracellular matrix mineralization shows the differentiation capacity of hBPC into hOBPCs (scale bar: 1 mm, picture of the scaffold adapted from A. Roshan-Ghias thesis).

3.3.2   *In Vivo* Study

3.3.2.1   Study Design

Tissue engineering PLA/5% β-TCP scaffolds were implanted in a pre-drilled hole in both femoral condyles of female rats, a commonly used animal model in the field of bone tissue engineering. The study included 5 experimental groups with 5 to 6 animals assigned to each group. Each experimental group corresponded to a scaffold condition and a loading condition. For scaffold conditions, we implanted either CF, CS or OCS scaffolds bilaterally, while for the mechanical loading aspects, we defined 2 conditions: early and delayed mechanical loadings. The early loading was applied over the total acute phase of inflammation whereas the delayed mechanical loading covered the late inflammation phase as well as the start of cell proliferation in the wound healing process. In both mechanical loading conditions one leg of each rat received an external 5 minutes controlled mechanical loading, while the contra-lateral leg was used as internal control (no loading during the 5 minutes session). In the early mechanical loading, the application of the mechanical loading started 2 days post-implantation, while the delayed mechanical loading started 14 days post-implantation. A longitudinal *in vivo* micro-computed tomography (microCT) imaging follow-up was performed to evaluate the bone formation inside the different scaffold conditions and loading cases. The study timelines are shown in Fig. 3.2.
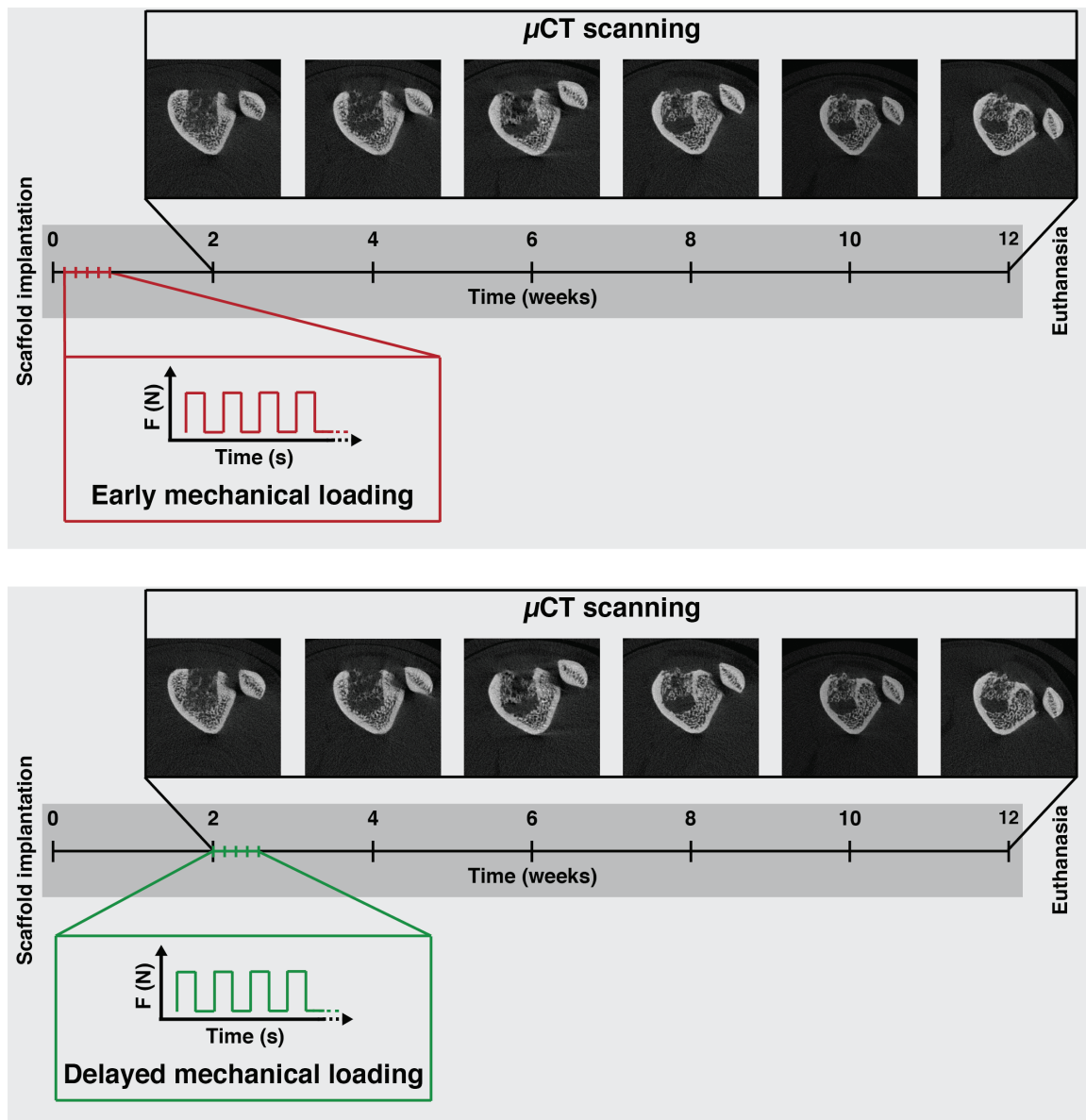
Figure 3.2 *In vivo* **study designs over 12 weeks with the different mechanical loading conditions.** Each experimental group of rats was implanted with one type of scaffold (CF, CS or OCS) on both femoral condyles. Two different mechanical loading were designed and applied for each scaffold condition. The loading designs are (1) early mechanical loading in red or (2) delayed mechanical loading in green, which started at 2 or 14 days after scaffold implantation on one leg, respectively. The rats were scanned over 12 weeks, every two weeks, starting at week 2.

3.3.2.2   Animal Model and Surgical Procedure

The animal model (Wistar female) rat and the surgical procedure were identical to the ones described in Chapter 2 (sections 2.3.5.2 and 2.3.5.3 respectively). In this study, no blood samples were drawn.

3.3.2.3 *In vivo* Mechanical Loading

After the surgery, one leg of each rat received a controlled mechanical loading (10 N at 4 Hz for 5 min, every two days over a period of 9 days) using a machine developed in our laboratory (Stadelmann et al. 2009) and previously used in other studies (De Souza et al. 2005; Fritton et al. 2005). The contra-lateral leg of the rat was used as a control (no external loading) as shown in Fig. 3.3. The loading parameters were based on a study described elsewhere (Roshan-Ghias et al. 2010; Roshan-Ghias, Arnoldi, et al. 2011). The application of the external loading started after 2 days post-implantation, which we defined as an early mechanical loading. In the case of delayed loading, the same loading parameters were applied than in the early loading case, but it started 14 days after implantation. For both loading conditions, the rats were kept under anesthesia during the loading sessions and were free to move between the sessions.
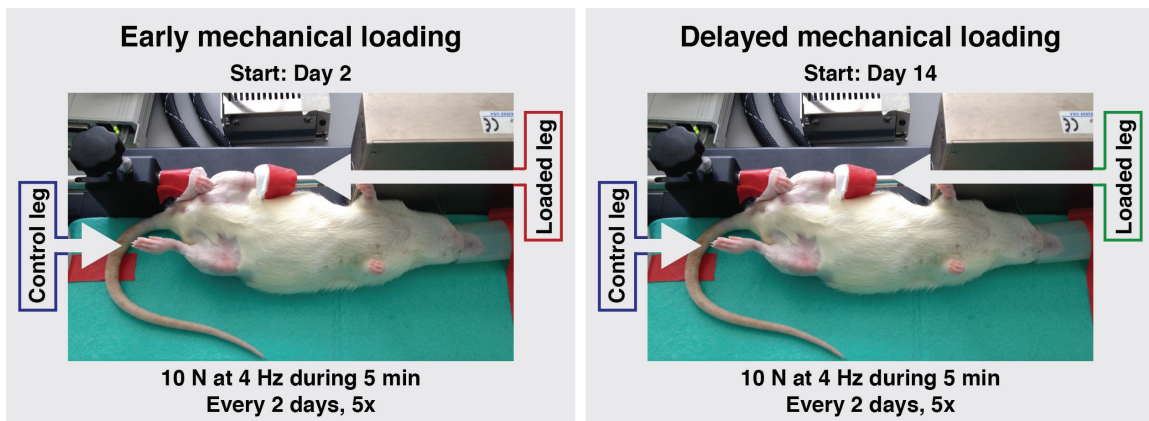
Figure 3.3 Early and delayed mechanical loading designs. The rat lay on its back during a loading session while it was maintained under anesthesia. The rat underwent five loading sessions, one session every two days, for both loading conditions. In the early mechanical loading design (left panel, red), the first session started 2 days post-implantation. In the delayed mechanical loading design (right panel, green), the first session started 14 days post-implantation. The contra-lateral leg (blue) was not subjected to mechanical loading and used as control.

3.3.3 *In Vivo* MicroCT Imaging and Data Analysis

A longitudinal *in vivo* microCT imaging of both rat's femurs were performed using a SkyScan 1076 scanner (Bruker microCT, Kontich, Belgium). The scans were done at weeks 2, 4, 6, 8, 10 and 12 after scaffolds implantation for static and dynamic bone histomorphometry, except for OCS scaffold group. The timepoint after 6 weeks of implantation was left out due to a source breakdown of the microCT. The rats were kept under Isoflurane anesthesia during the scans and were euthanized with an intracardiac injection of pentobarbital (Esconarkon, Streuli Pharma SA, Uznach) after their last scan after 12 weeks of implantation. The chosen scan frequency had no impact on the structural bone parameters as described elsewhere (Brouwers et al. 2007). Each leg was scanned separately and introduced in a plastic tube to stretch and fix it during scanning. All animals were scanned with the same scan parameters for each timepoint. The parameters were as follows: 0.5 mm aluminum

filter, 80 kV voltage, 120 μA current, exposure time of 360 ms and 0.5° rotation step with a pixel resolution of 18 μm.

The reconstruction and analysis of implanted scaffolds were done using NRecon and CTan software respectively, both provided by Skyscan (Bruker microCT). For the reconstruction, a ring artifact correction of 4 and beam hardening of 20% were used, without smoothing. The obtained output for each leg was image stacks of cross-sections in 8-bit bitmap format. The determination of the volume of interest and the dynamic histomorphometry were done on Amira® (FEI Visualization Sciences Group, Burlington, USA). As the scaffold is not visible on the microCT images, because its density is lower than the one of the bone, we determined the volume of interest (VOI) as a cylinder with the same dimension than the scaffold (3 mm of diameter and 3 mm of height). After having made a 3D reconstruction with Amira®, the bone of the first time point was manually placed around the VOI (Fig. 3.4). The coordinate system of the first time point was transformed into the coordinate system of the VOI. All following datasets (weeks 4, 6, 8, 10 and 12 of the same leg) were loaded to Amira® (FEI Visualization Sciences Group) for registration and segmentation (Fig. 3.4) using a custom script adapted from a published script (Kettenberger et al. 2014). The static and dynamic bone parameters inside the scaffold were then measured. For the static bone parameters, the bone volume density, also named bone volume over the total volume (BV/TV), the trabecular thickness (Tb.Th), the trabecular separation (Tb.Sp) and the trabecular number (Tb.N) were quantified for the bone morphology and structure assessment inside the scaffold.

Concerning the dynamic bone parameters, the percentage of bone formation (BF) and bone resorption (BR) were determined based on segmented three-gray values datasets from consecutive time points of registered pairs of microCT scans. BF and BR values were excluded from the analysis, when their value was outside of an interval of 1.5 times the quartile range. The gray-values correspond to resorbed (only first dataset), quiescent (both datasets) and forming (only second dataset) bone. The BF and the BR are both given in percent per day. The BF was calculated as the ratio of formed volume to the sum of the quiescent and resorbed bone volume divided by the number of days between two successive scans, namely 14 days:

$$\text{BF (\%)} = \frac{(BV/TV)_{formed}}{(BV/TV)_{quiescent} + (BV/TV)_{resorbed}} * \frac{1}{14}$$

The BR was calculated as the ratio of the resorbed volume to the sum of the quiescent and resorbed bone volume divided by the number of days between two scans:

$$\text{BR (\%)} = \frac{(BV/TV)_{resorbed}}{(BV/TV)_{quiescent} + (BV/TV)_{resorbed}} * \frac{1}{14}$$
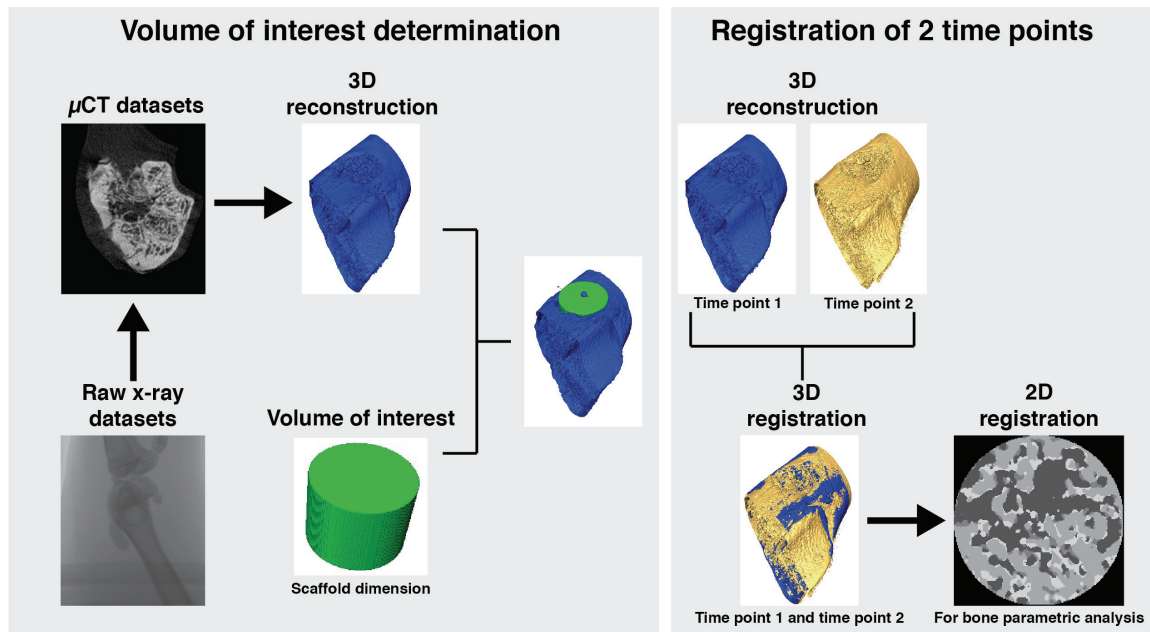
Figure 3.4 Description from the microCT imaging to the bone parameters analysis. The x-rays datasets are first reconstructed in 2D datasets before the 3D reconstruction. The bone is then placed and orientated manually around the volume of interest, which is a cylinder with the same dimensions than the implanted scaffold. An automated algorithm registers pairs of microCT scans from consecutive time points. The time points are then compared voxel by voxel by assigning different gray values to bone present only on the first (resorbed bone), only on the second (formed bone) or on both datasets (quiescent bone) as described elsewhere (Kettenberger et al. 2014).

3.3.4   Histology

The implanted femoral condyles were dehydrated by immersing them in a series of ethanol (EtOH, VWR, Dietikon, Switzerland) solutions with ascending concentration (70%, 80%, 90%, 96%, 100%) as described in Chapter 2, sub-section 2.3.5. Each immersion lasted 24 h. After clearing the sample in toluene (VWR), 1 x 24 h followed by 1 x 48 h of immersion, all femur samples were embedded by infiltration with methylmethacrylate (MMA, 100 mL, Sigma-Aldrich, ST Louis, USA) and 0.5% bis(tert-butylcyclohexyl) peroxydicarbonate (Perkadox 16, Dr Grogg Chemie AG, Deisswil, Switzerland) at 4°C during 5 days. For the polymerization, 100 mL of MMA, 20-25 mL of dibutylphtalate (DBP, Sigma-Aldrich) and 1% of Perkadox 16 (Dr Grogg Chemie AG) were prepared and the samples were polymerized at room temperature (RT) over 3 weeks. After polymerization, the MMA were cut with a diamond-coated inner diameter saw (Leica SP 1600, Leica Microsystems, Wetzlar, Germany) to slices of around 180 µm thickness. Four to five of these preparations were cut and attached to custom-made opaque OMMA microscope slides (Semadeni, Ostermundingen, Switzerland) with acrylic glue (Loctite, 401, Henkel, Düsseldorf, Germany). They were then ground to around 80-100 µm thicknesses with a grinding machine (Pedemax-2, Sturers, Willich, Germany) before staining. The surface of thick slides was etched with 1% formic acid (AppliChem, Darmstadt, Germany) before being stained with 0.1% toluidine blue (VWR). Images were taken with an upright light microscope (DM 5500, Leica Microsystems). Based on the stained sections, semi-quantitative and qualitative evaluations were performed, where the quality of bone formation and cellular events were

interpreted. Bone formation (score: 0 to 8), bone reaction (score: 0 to 3) and interface (score: 0 to 4) as well as the interstitial tissue quality (score: 0 to 8) were evaluated inside the scaffold. The osteoblast activation and shape, the osteoclast activation, the presence of multinuclear giant cells and presence of fibrous capsule were observed and commented. The percentage of fibrous tissues and the number of blood vessels were evaluated inside the scaffold. Statistical analysis using student t-test was carried out on the semi-quantitative evaluation. A p-value of less than 0.05 was considered as significant.

3.3.5   Numerical Modeling

The stiffness of the newly formed bone inside CF and CS scaffolds were evaluated based on microCT images. Only the early and no mechanical loading conditions were considered at weeks 2, 4, 6, 8, 10 and 12 after scaffolds implantation. The VOI determination as well as the registration were done on Amira® (FEI Visualization Sciences Group) as described in section 3.3.3. After the registration and transformation, the image stacks of each bone sample of each time point were saved without segmentation. The images were then opened with CTan, where only the centered half of the original VOI was selected to reduce the computational cost. For the finite element analysis (FEA), we used a custom FEA solver (FAIM 6.0, Numerics88 Solutions Ltd., Calgary, Alberta, Canada) on a desktop workstation (MacPro, Apple Inc. Cupertino, CA, USA). The images were binarized and each voxel was converted to a hexahedral element, using the voxel conversion approach (Müller & Rüegsegger 1995; van Rietbergen et al. 1995). All elements were given isotropic linear elastic material properties with a Poisson's ratio of 0.3 and homogeneous Young's modulus of 6829 MPa (MacNeil & Boyd 2008). In order to avoid floating elements, a connectivity filter was applied before running the simulation. All degrees of freedom of the bottom of the VOI (medial part of the bone inside the scaffold) were constrained, while a uniaxial compression was simulated on the top of the VOI (lateral part of the bone inside the scaffold) up to 1% strain. The simulation evaluated the bone stiffness of the mineralized bone inside the implanted scaffold.

3.3.6   Statistical Analysis

Statistical analysis within the different scaffold groups (CF, CS and OCS) and loading conditions (early mechanical loading, delayed mechanical loading and no loading) were performed using a series of flexible and powerful statistical models called Generalized Additive Mixed Models (GAMMs), which are already used and described elsewhere (Roshan-Ghias, Lambers, et al. 2011). The GAMMs, based on original values, use a semi-parametric model to capture the highly non-linear trend of the response variable in time. Outliers were excluded from the analysis, when their value was outside of an interval of 1.5 times the quartile range. For each condition (*e.g.* CF scaffold with early loading), a curve is adjusted to the response variable in order to obtain a flexible model, capable of capturing the trend of the response variable in time. After capturing such a trend, it would be easier to compare two groups based of predicted values of separately fitted model. Based on the obtained predicted curves and at each time point, the difference between predicted values for two conditions (*e.g.* CF under an early mechanical loading vs CF without mechanical loading) were assessed using the confidence interval of predicted values of adjusted curves. The confidence interval was constructed to have coverage of 95% (equivalent to $\alpha = 0.05$). The gray zone on the graphics represents the regions in which two predicted values are well separated from each other. As the analyzed datasets are from a longitudinal study, the advantage of GAMM, compared to standard

statistical tests, is that the significant difference can be detected for a time frame, and not only for each time point, with an error margin of 5%. All statistical analysis were done in R (R Development Code Team 2010).

3.4 Results

3.4.1 *In Vivo* Study: Early Mechanical Loading

3.4.1.1 MicroCT Based Static Morphometry

For all static bone parameters, the results for CF, CS and OCS scaffolds are shown in separate graphs. In each graph no loading and early mechanical loading conditions are compared for each scaffold condition. Gray areas display significant differences between conditions. The p-values analysis of BV/TV between all scaffold and mechanical loading conditions are detailed in Tab. S3.5 under section 3.7.3 (Supporting Information; part of the table: Early loading vs no mechanical loading: Experimental groups of rat (EL)). The calculations of the percentage increase or decrease between the different conditions are based on their mean values.

First, we observed a gradual increase of BV/TV over the entire duration of the study in all scaffolds (Fig. 3.5). The results show that BV/TV inside CF scaffolds, in both early mechanical loading and no loading conditions, is significantly higher than inside CS or OCS scaffolds (Fig. 3.5). This difference has already been observed after the first scanning session at week 2; BV/TV was at approximately 14% for CF scaffolds independently of the loading conditions. In the CS and OCS scaffold conditions, BV/TV was between 3 and 4%. Furthermore, after 12 weeks of implantation, BV/TV was 36% lower inside CS scaffolds than inside CF scaffolds when subjected to an early mechanical loading. For both scaffold conditions, a decrease by 57% was observed when no mechanical loading was applied. When comparing BV/TV inside CF scaffolds to OCS scaffolds, a decrease by 58% and by of 28% were seen under early and no mechanical loading conditions, respectively. Regarding the results between CS and OCS scaffolds, we noticed an inversed effect of the early mechanical loading and no loading conditions. In the case of CS condition, early mechanical loading had a positive effect and started to significantly increase BV/TV from week 6 until week 12. At this later timepoint a increased by 48% was observed. In contrast early mechanical loading condition had a negative impact on the bone formation in the case of OCS scaffolds. A significant lower BV/TV was observed starting from week 6 to week 12. Indeed, after 12 weeks of implantation, 41% less BV/TV was observed when early mechanical loading was applied. The only condition where early mechanical loading had no impact on the bone formation, was in the CF scaffold condition.
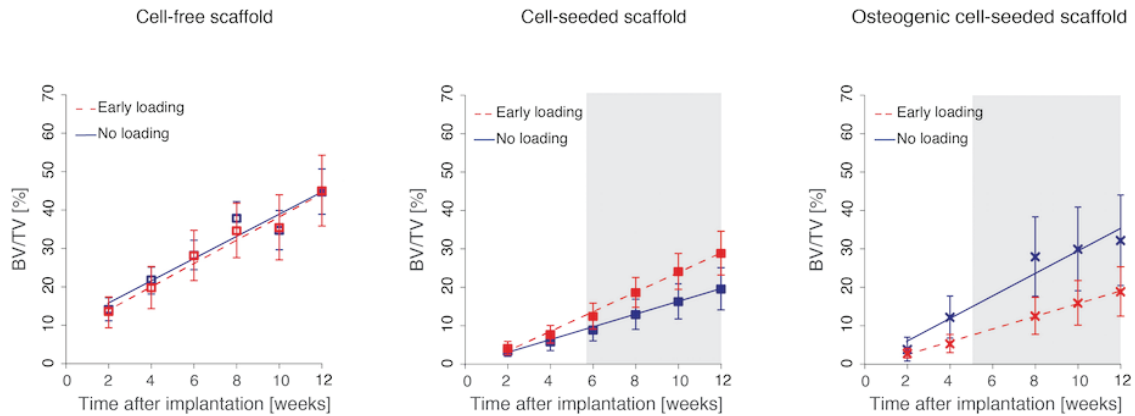
Figure 3.5 Bone volume over tissue volume (BV/TV) evolution inside different scaffold conditions over 12 weeks. CF scaffolds are represented by empty squares (□), CS scaffolds are shown by filled squares (■) and OCS scaffolds are crosses (✕). The lines represent the fitted GAMM model. The no loading groups are illustrated by solid blue line while the early mechanical loading groups are drawn in dashed red lines. The gray zone on the graphics shows the time span where a significant difference exists between the two groups (n=5–6).

The other bone parameters, Tb.Th, Tb.Sp and Tb.N are in accordance with the behavior of BV/TV for all three scaffold conditions; Tb.Th and Tb.N gradually increased over time while Tb.Sp decreased (Fig. 3.6). Regarding Tb.Th, the values are in the same range for all conditions over the entire duration of the experiment, except inside OCS scaffold. In this scaffold condition, Tb.Th significantly increased starting at week 6 when no loading was applied. No significant difference was observed between the loading conditions inside CF and CS scaffolds. Tb.Sp was twice time higher inside CS and OCS scaffolds compared to CF scaffolds over the entire experimental duration. Moreover, it was significantly higher in the case of no loading compared to early mechanical loading conditions for CS scaffolds from week 4 on. No significant difference was observed in the case of CF and OCS scaffolds between the loading conditions. Finally, inside CF scaffolds the values of Tb.N were more than doubled compared to CS and OCS scaffolds. In both cell conditions, a significant difference was observed between early mechanical loading and no loading conditions.
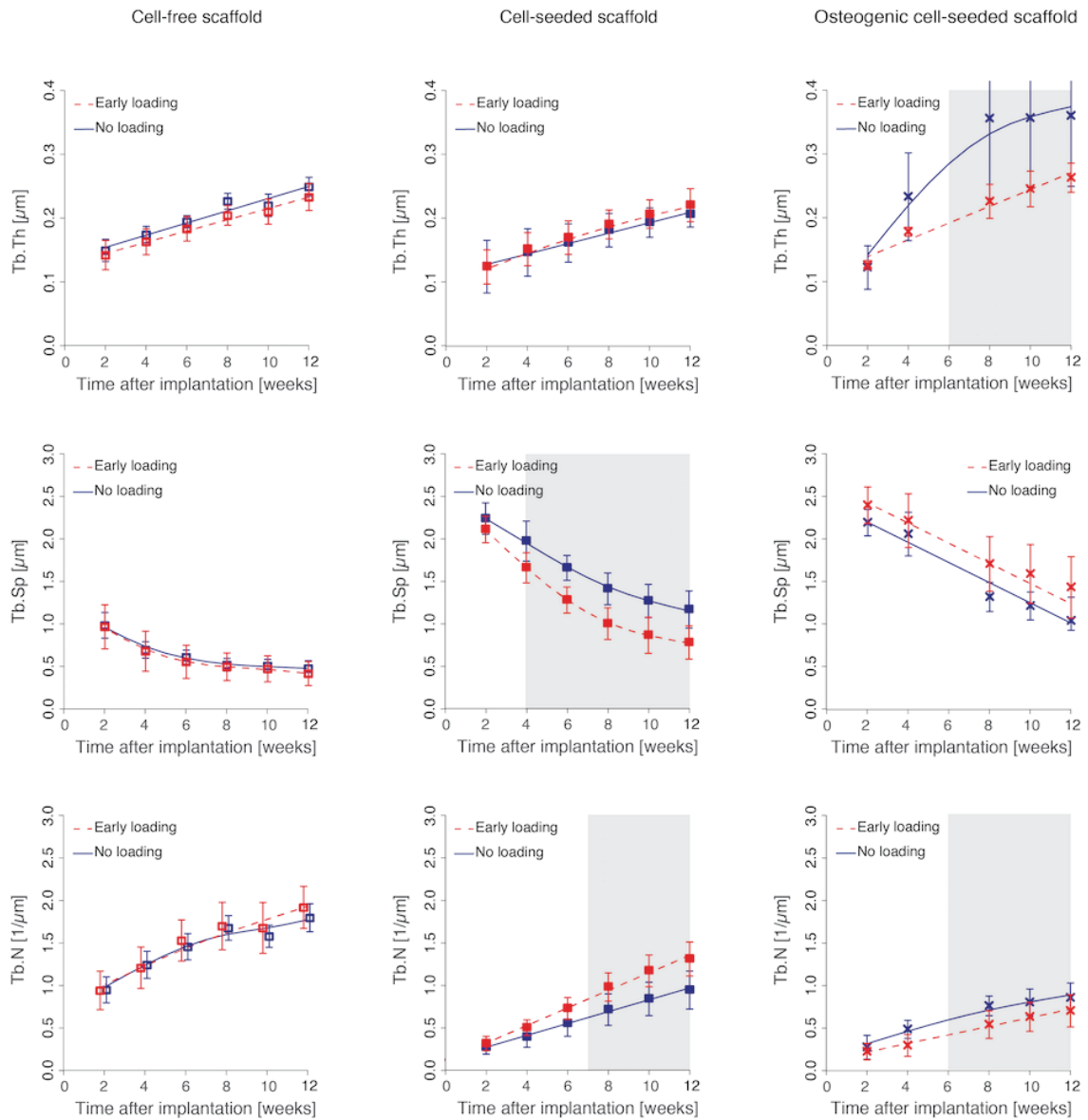
Figure 3.6 Evolution of trabecular thickness (Tb.Th), trabecular separation (Tb.SP) and trabecular number (Tb.N) inside different scaffold conditions over 12 weeks. CF scaffolds are represented by empty squares (□), CS scaffolds by filled squares (■) and OCS scaffolds are crosses (✕). The lines represent the fitted GAMM model. The no loading groups are illustrated by solid blue line while early mechanical loading groups are drawn in dashed red lines. The gray zone on the graphics shows the time span where a significant difference exists between the two groups (n=5–6).

3.4.1.2   MicroCT Based Dynamic Bone Morphometry

For both dynamic bone parameters, namely BR and BF, an overall decrease over time span was observed in all conditions as shown in Fig. 3.7. For CF scaffolds, no significant difference was seen for both BR and BF, except for BR at the period from 6 to 8 weeks after implantation. Early mechanical loading did not influence BR of CS scaffolds while BF was significantly higher between weeks 2 to 4 after implantation. In the case of OCS scaffolds, BR and BF were significantly lower in early mechanical loading condition between the period between weeks 2 to 10 and weeks 2 to 8 respectively. The effect of OCS scaffolds without mechanical loading had a greater influence on BR and BF than in the other scaffold conditions.
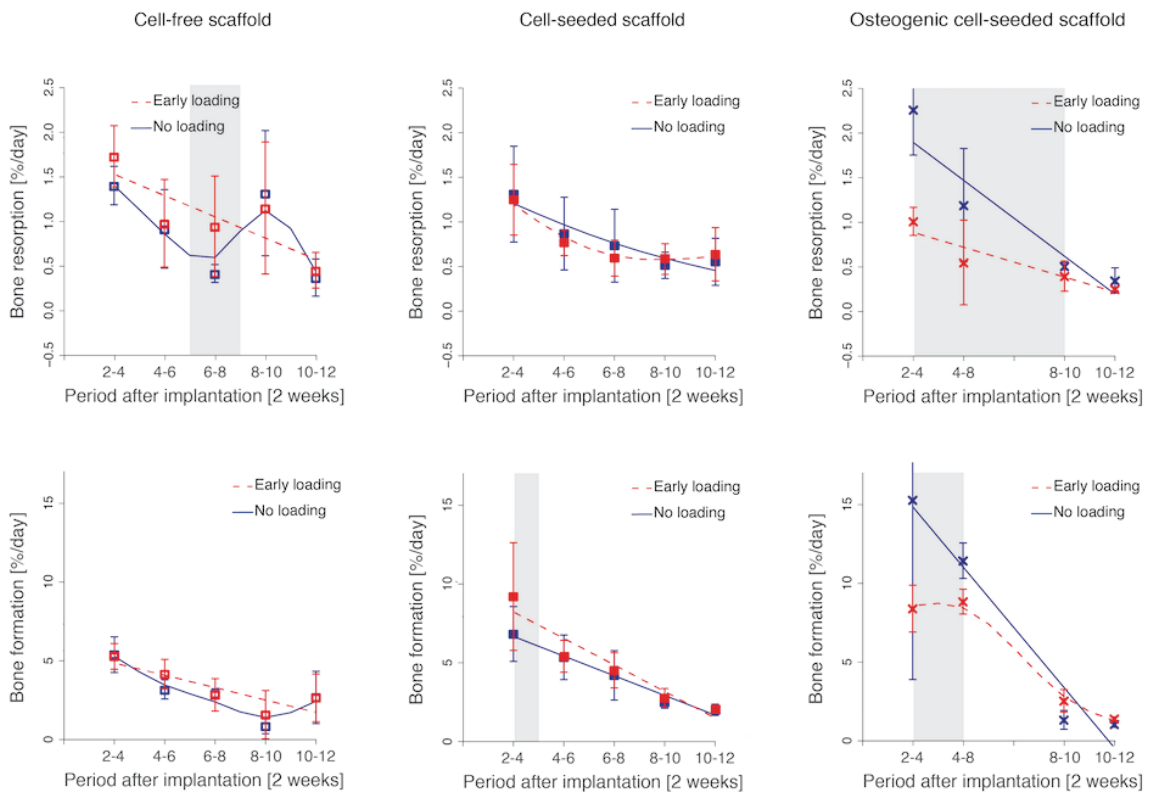
Figure 3.7 Evolution of bone resorption and formation inside different scaffold conditions over 12 weeks. CF scaffolds are represented by empty squares (□), CS scaffolds by filled squares (■) and OCS scaffolds are crosses (✕). The lines represent the fitted GAMM model. The no loading groups are illustrated by solid blue line while early mechanical loading groups are drawn in dashed red lines. The gray zone on the graphics shows the time span where a significant difference exists between the two groups (n=5–6).

In Fig. 3.8, a representative volume rendered visualization is shown between two time points for one femoral condyle implanted with CF, CS or OCS scaffolds. The depicted images were picked randomly. For each scaffold condition, both no loading and early mechanical loading conditions are shown. This visualization illustrates well the bone growth dynamic, influenced by the BR (in red) and BF (in green) over time. The difference in terms of bone formation between the different scaffold conditions and mechanical loading conditions are nicely visible. The bone started to grow from the bottom and the sides of the scaffold's hole.
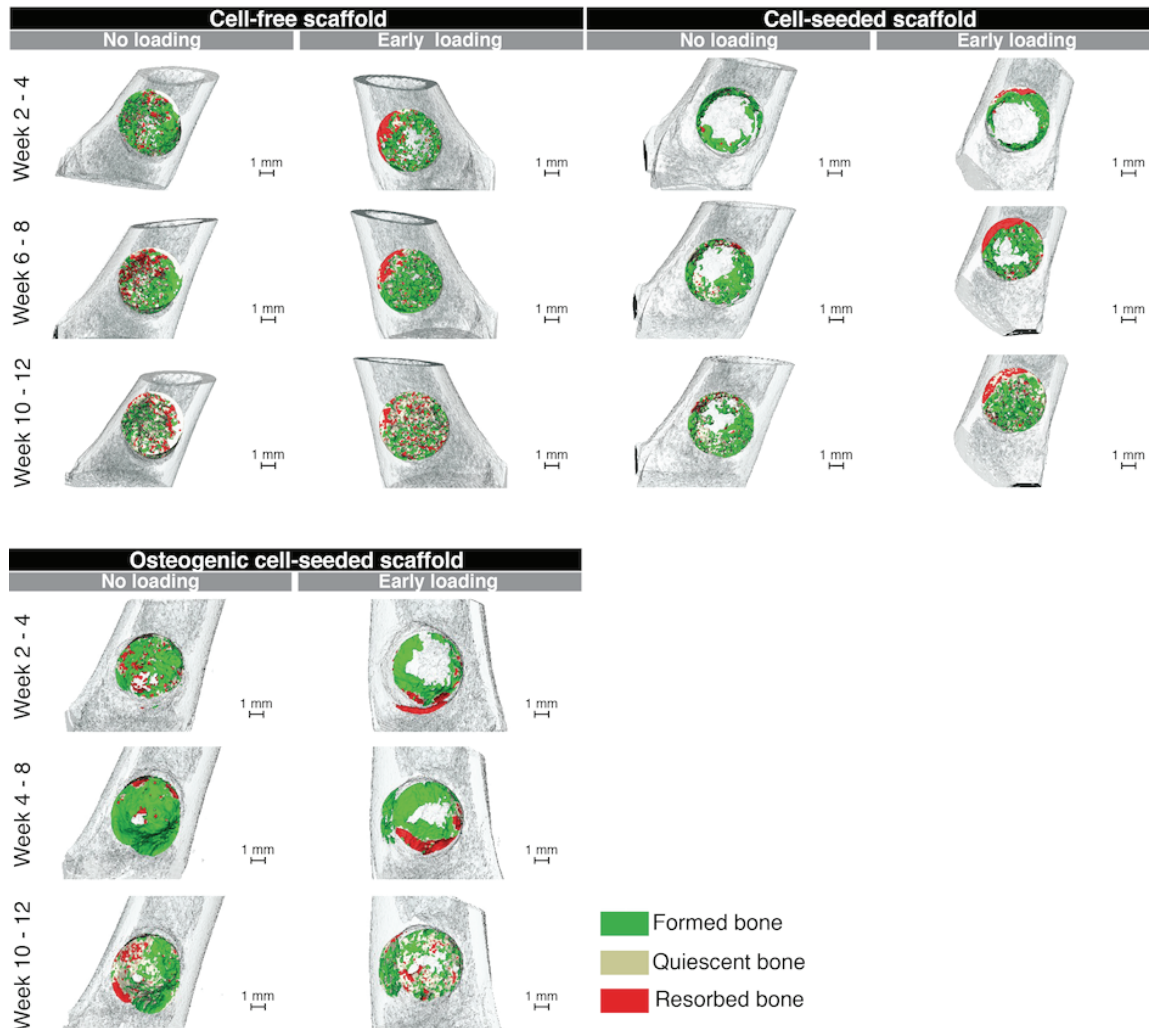
Figure 3.8 Three-dimensional images of implanted scaffolds inside femoral condyles. The resorbed bone and the formed bone are shown in red and green respectively, while the quiescent bone and the cortical bone are shown in off-white and transparent gray respectively. The data were collected from two chronological successive microCT scans as described in sub-section 3.3.3. Three out of five data time points are represented in the graphic. Because of a breakdown the microCT source, the time in-between scans is 4 weeks instead of 2 for the second data of OCS scaffolds compared to the CF and CS scaffold conditions.

3.4.1.3 Histological Analysis

Histological imaging is still considered as the gold standard for analyzing bone formation. It is often used as a complementary method to microCT histomorphometry, to assess cellular activity, scaffold integration and bone reaction, which are not visible on microCT images. We therefore did semi-quantitative and qualitative evaluations, summarized in Tab. S3.1 and Tab. S3.2 under section 3.7.2 (Supporting Information). The corresponding images of the histological slides of CF, CS and OCS scaffolds after 12 weeks of implantation are shown in Fig 3.9, 3.10 and 3.11 respectively. Concerning the difference in terms of color on the histology slides, it was affected by the change of Toluidine Blue batches between different staining sessions of histology slides. This change may have influenced the color intensity on the slides even by following the same staining protocol without having an impact on the evaluation and interpretation of the slides.

In Tab. S3.1, semi-quantitative evaluation of bone formation, bone reaction, interface quality and interstitial quality are summarized. By bone reaction, we mean the bone maturity and similarity to cortical bone. The total score is defined as the sum of scores of all evaluated parameters per condition, to give an overall evaluation of the bone tissue. In between different scaffolds and mechanical loading conditions, no difference was found for bone-scaffold interface and the qualitative evaluation of the interstitial tissue. However, trends were observed regarding the bone formation, the bone reaction and the total scores. For both loading conditions, CF scaffolds showed a higher bone formation than inside CS and OCS scaffolds. A small difference was also observed between no loading and early mechanical loading conditions in terms of bone formation inside CS and OCS scaffolds. This observed trend in bone formation is in accordance with the total score and confirms the results obtained by microCT scanning for CF and CS scaffolds. For OCS scaffolds, the trend on histology is inversed compared to the results obtained by microCT scanning. Furthermore, we generally observed a physiological bone formation: It formed from the bottom and then grew from the sides inside the scaffolds in all conditions. Based on the other evaluated parameters (bone reaction, interface and interstitial tissue), all scaffolds integrated well inside the surrounding bone tissue. A direct and clear scaffold-bone contact was noticed in all three scaffold conditions.

Regarding the cellular events (Tab. S3.2) after 12 weeks of implantation, we observed some more active osteoblasts in the case of CS and OCS scaffolds, especially where bone was forming. For all conditions, a normal range of multinuclear giant cells was evaluated. Furthermore, an increased numbers of blood vessels were noticed in the case of CS scaffolds. We observed a similar percentage of fibrous tissue (5 and 15%) in CF and CS scaffolds for both loading conditions. In the case of OCS scaffolds, 5-15% and 10-75% of fibrous tissue were observed in no loading and early mechanical loading conditions, respectively. As in chapter 2, the fibrous tissue did not form any fibrous capsule around CS and OCS scaffolds.

With respect to the maturity of the remodeled bone and bone marrow inside the scaffolds, we noticed a total maturity of both inside CF scaffolds independently of the loading conditions (Fig.3.9). The less mature state of the bone inside CS and OCS scaffolds compared to CF is in accordance with the higher number of observed blood vessels and the higher osteoblast activation. As the bone is still in a modeling phase, a higher osteoblast activity is needed as well as more nutrient and oxygen supply, represented by the higher number of present blood vessels.
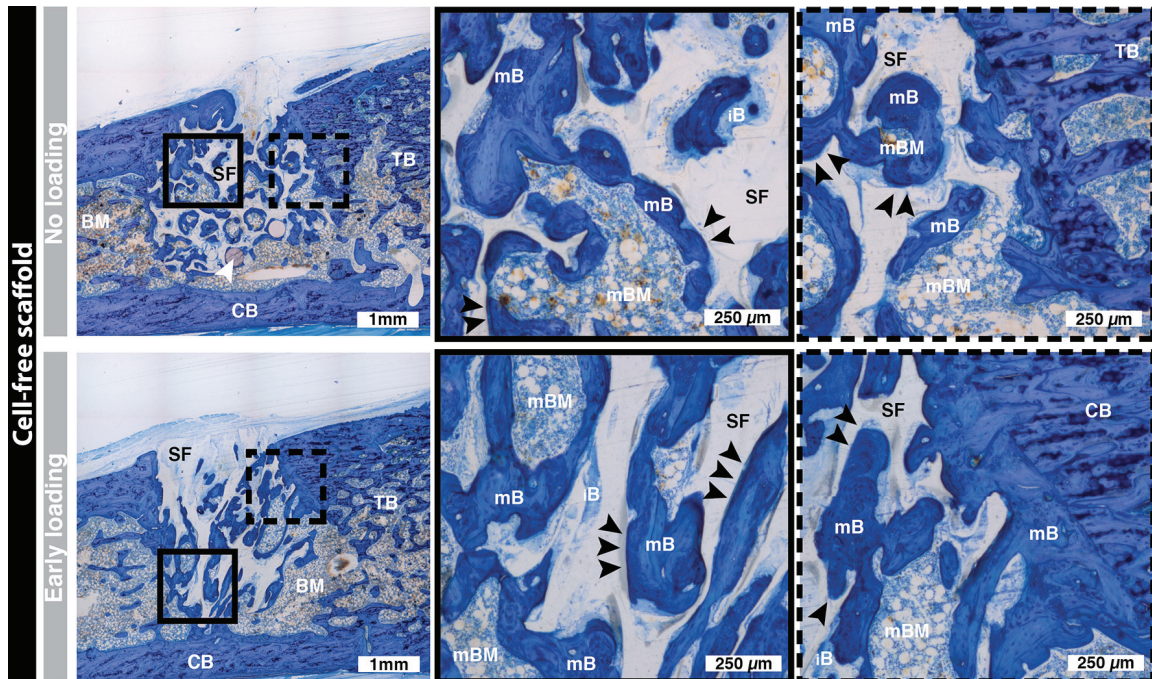
Figure 3.9 Toluidine blue stained sections of CF scaffolds after 12 weeks of implantation. On the top of the figure, no loading condition is shown and the early mechanical loading condition is illustrated at the bottom. The different tissues and the scaffolds are shown using the following abbreviations: Trabecular bone (TB), cortical bone (CB), bone marrow (BM), scaffold (SF), mature bone remodeling inside the scaffold (mB), mature bone marrow inside the scaffold (mBM) and immature bone (iB). The black arrows indicate examples of region where the scaffold is well integrated and the white arrows point at ruby beads.

Concerning the bone maturity in CS scaffolds, immature to mature bone was observed under early mechanical loading condition. In the case of no loading, less mature bone was observed. We noticed less active bone marrow in early loading conditions and no bone marrow formation in the case of no mechanical loading condition. The activity and maturity of the bone marrow are determined by the presence of fatty structure. This difference is well illustrated in Fig. 3.10.
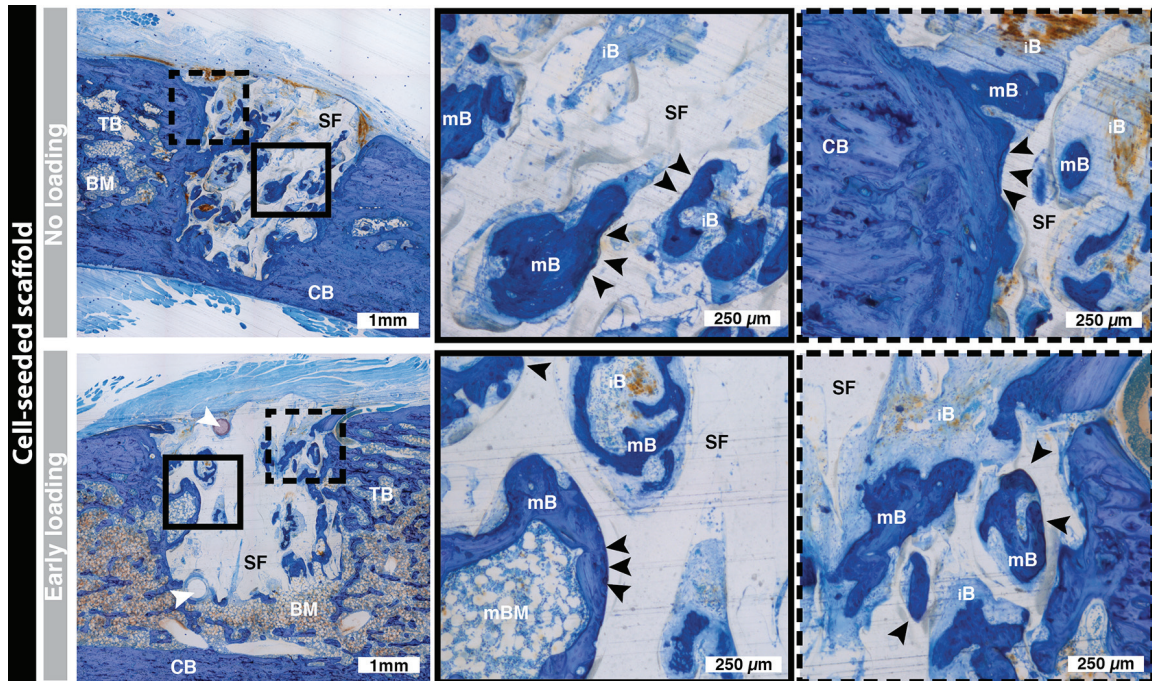
Figure 3.10 Toluidine blue stained sections of CS scaffolds after 12 weeks of implantation. On the top of the figure, no loading condition is shown and the early mechanical loading condition is illustrated at the bottom. The different tissues and the scaffolds are shown using the following abbreviations: Trabecular bone (TB), cortical bone (CB), bone marrow (BM), scaffold (SF), mature bone remodeling inside the scaffold (mB), mature bone marrow inside the scaffold (mBM) and immature bone (iB). The black arrows indicate examples of region where the scaffold is good integrated and the white arrows point at ruby beads. The sections were cut in the coronal plane.

In OCS scaffolds, independently of the mechanical loading conditions, no bone marrow activity or rare fatty structure was observed as shown in Fig. 3.11. Few mature bone tissue and some more immature bone were noticed. Consequently, from an increase in bone maturation, we can classify the different scaffolds type from OCS, CS to CF scaffolds.
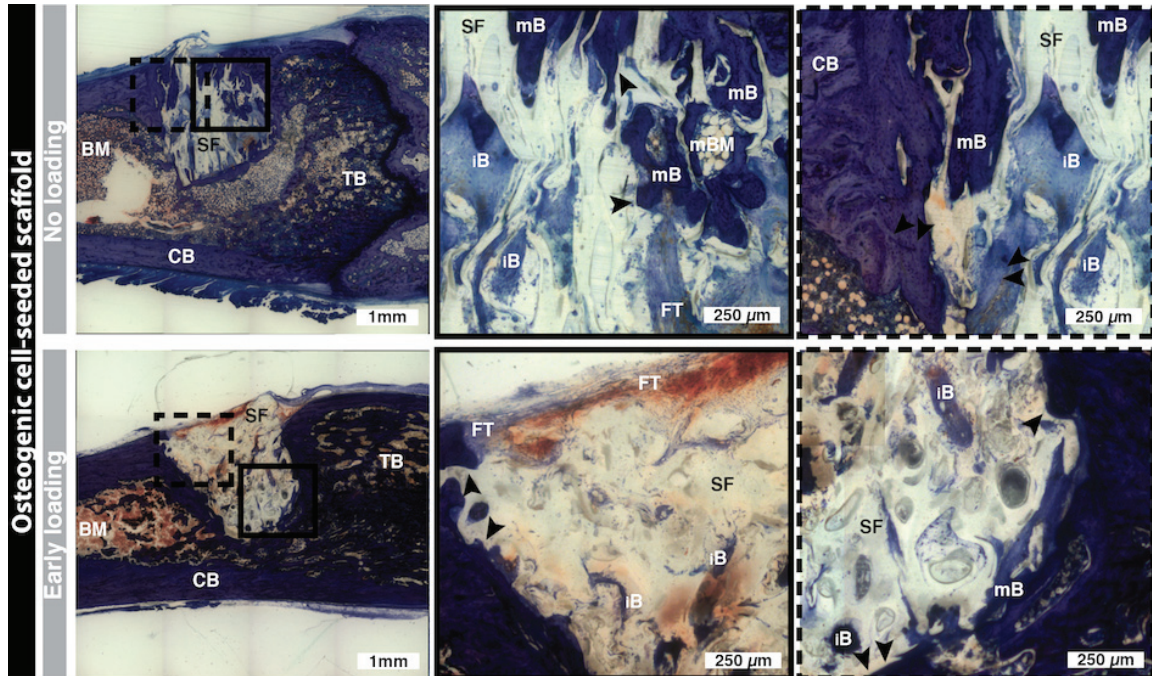
Figure 3.11 Toluidine blue stained sections of CS scaffolds after 12 weeks of implantation. On the top of the figure, no loading condition is shown and the early mechanical loading condition is illustrated at the bottom. The different tissues and the scaffolds are shown using the following abbreviations: Trabecular bone (TB), cortical bone (CB), bone marrow (BM), scaffold (SF), mature bone inside the scaffold remodeling (mB), mature bone marrow inside the scaffold (mBM), immature bone (iB) and fibrous tissue (FT). The black arrows indicate examples of region where the scaffold is good integrated. The sections were cut in the coronal plane.

3.4.1.4   Numerical Modeling

The mechanical properties of the mineralized bone inside CF and CS scaffolds are shown in Fig. 3.12. The stiffness of the formed bone inside OCS scaffolds was not evaluated as discussed later in section 3.5. As for BV/TV, bone stiffness had a linear increase from the start until the end of the study in both CF and CS scaffolds and mechanical loading conditions. Here as well, the absence of hBPCs was beneficial in terms of bone stiffness than with them. Inside implanted CF scaffolds, early mechanical loading had no influence on the mechanical behavior. Unlike, early mechanical loading improved the mechanical properties of CS scaffolds from week 6 until the end of the study.
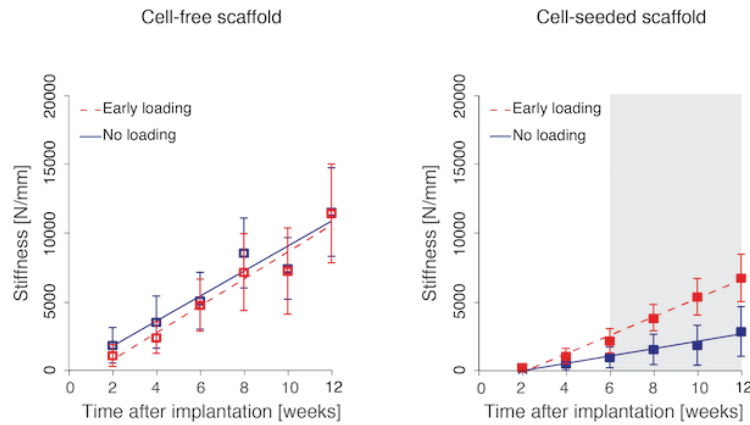
Figure 3.12 Stiffness evaluation of the mineralized bone inside CF and CS scaffolds after 12 weeks of implantation. CF scaffolds are represented by empty squares (□) and CS scaffolds are shown by filled squares (■). The lines represent the fitted GAMM model. No loading groups are illustrated by solid blue line while early mechanical loading groups are drawn in dashed red lines. The gray zone on the graphics shows the time span where a significant difference exists between the two groups (n=6).

3.4.2 *In vivo* study: Delayed Mechanical Loading

3.4.2.1 MicroCT Based Static Bone Morphometry

Each graph depicts the pairwise delayed mechanical loading and no loading conditions of CF and CS scaffolds. As for early mechanical loading condition in the previous described *in vivo* study, BV/TV, Tb.Th and Tb.N generally and gradually increased over the entire period of the study. In accordance with the other bone parameters, Tb.Sp decreased between 2 weeks and 12 weeks after implantation (Fig. 3.13 and 3.14). A significantly higher amount of formed bone was observed inside CF scaffolds compared to CS scaffolds, independently of the mechanical loading conditions. Significant differences between groups are highlighted in gray in the figures, and the p-values analyses in between each scaffold and loading conditions of BV/TV are detailed in Tab. S3.5 under sub-section 3.7.3 (Supporting Information; part of the table: Delayed loading vs no mechanical loading: Experimental groups of rat (DL)). Delayed mechanical loading increased significantly the amount of formed bone inside both CF and CS scaffolds as shown in Fig. 3.13. In the case of CS scaffolds, the significant increase started from week 8, while for CF scaffolds, it started from week 5. After 12 weeks of implantation, the bone formation increased by 26% inside CS scaffolds and by 32% inside CF scaffolds when delayed loading was applied compared to no loading.
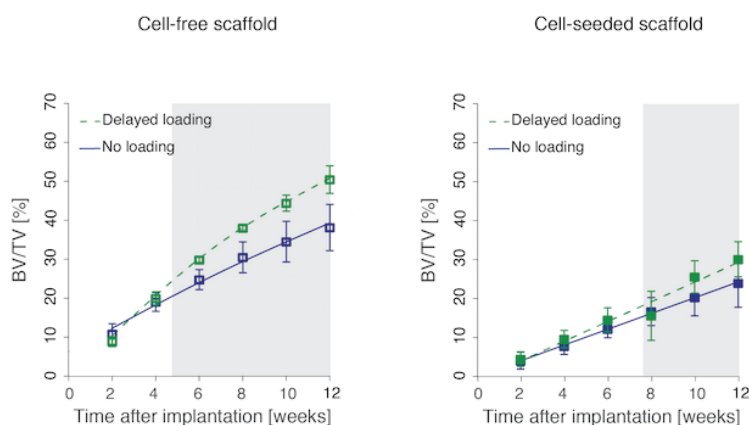
Figure 3.13 BV/TV evolution inside different scaffold and mechanical conditions over 12 weeks. CF scaffolds are represented by empty squares (□) and CS scaffolds by filled squares (■). The lines represent the fitted GAMM model. No loading groups are illustrated by solid blue line while delayed mechanical loading groups are drawn in dashed green lines. The gray zone on the graphics shows the time span where a significant difference exists between the two groups (n=5–6).

The other bone parameters, Tb.Th, Tb.Sp and Tb.N are consistent with the behavior of BV/TV for all conditions (Fig. 3.14). In CS scaffolds, no significant difference was observed between no loading and delayed mechanical loading conditions for Tb.Th and Tb.N. After 10 weeks of implantation, less Tb.Sp was noticed inside CS scaffolds when a delayed mechanical loading was applied. For CF scaffolds, a greater Tb.Th and Tb.N was observed for delayed mechanical loading after 6 weeks of implantation until the end of the study, while a lower Tb.Sp was seen between week 4 and 6 post-implantation when subjected to delayed mechanical loading. Regarding the range of values, we noticed significant

lower values for Tb.Th and Tb.N in CS scaffolds than in CF scaffolds, whereas higher values were observed for Tb.Sp.
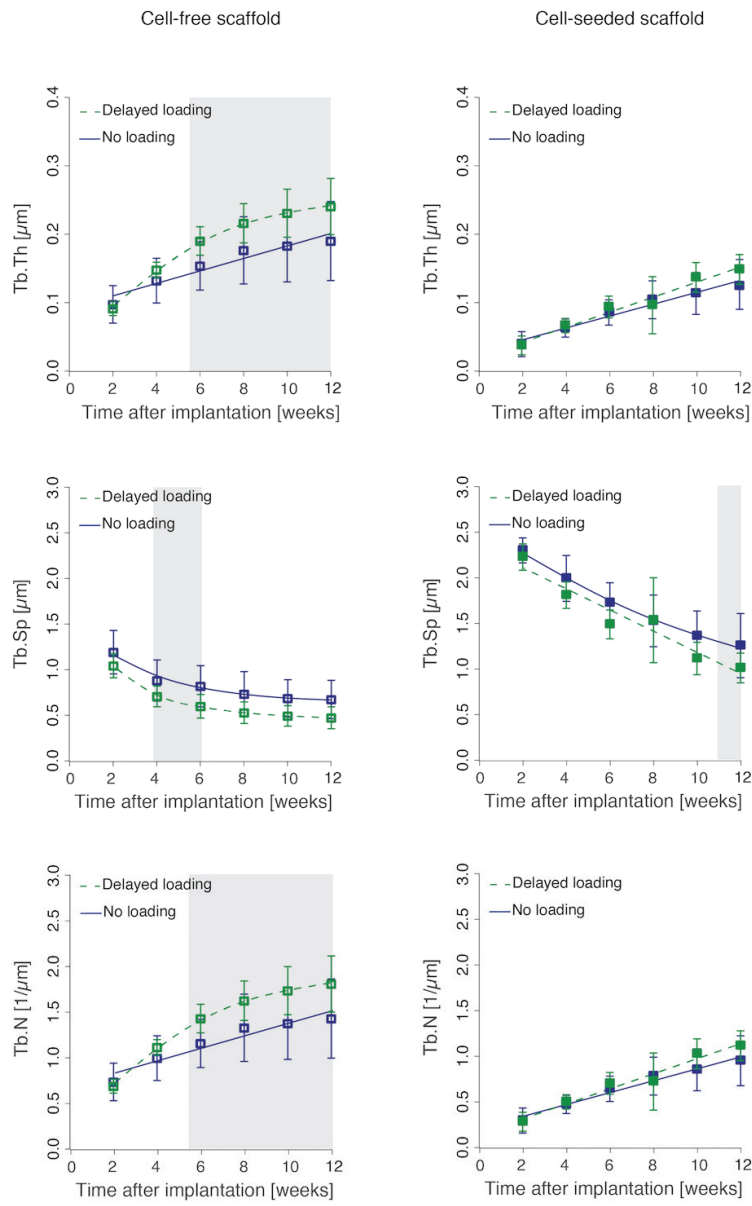
Figure 3.14 Evolution of Tb.Th, Tb.SP and Tb.N inside different scaffolds and mechanical loading conditions over 12 weeks. CF scaffolds are represented by empty squares (□) and CS scaffolds by filled squares (■). The lines represent the fitted GAMM model. No loading groups are illustrated by solid blue line while delayed mechanical loading group is drawn in dashed green lines. The gray zone on the graphics shows the time span where a significant difference exists between the two groups (n=5–6).

3.4.2.2 MicroCT Based Dynamic Bone Morphometry

Over the entire *in vivo* study, a decrease of BR and BF was seen for all conditions as shown in Fig. 3.15. In CF scaffolds, BR was lower under delayed mechanical loading between weeks 4 to 8, while BF was significantly higher between weeks 2 to 4. In CS scaffolds, delayed mechanical loading had no impact on BR or BF.
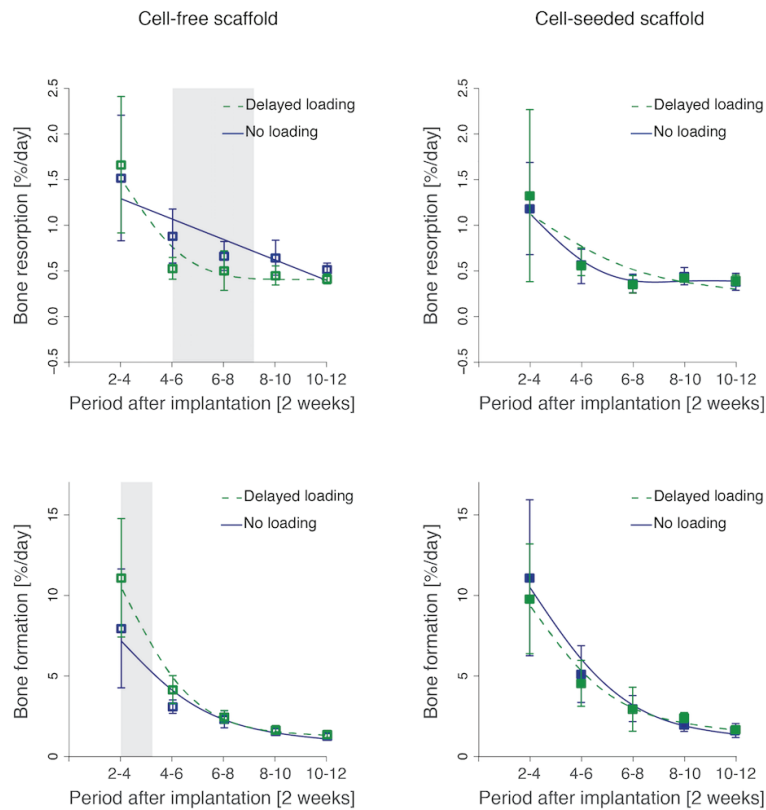
Figure 3.15 Evolution of bone resorption and formation inside the different scaffolds and mechanical loading conditions over 12 weeks. CF scaffolds are represented by empty squares (□) and CS scaffolds by filled squares (■). The lines represent the fitted GAMM model. No loading groups are illustrated by solid blue line while delayed mechanical loading group is drawn in dashed green lines. The gray zone on the graphics shows the time span where a significant difference exists between the two groups (n=5–6).

In Fig. 3.16, a representative volume rendered visualization is shown between two time points for one femoral condyle implanted with CF or CS scaffolds. The depicted images were picked randomly. For each scaffold condition, no loading and delayed mechanical loading conditions are shown. As in sub-section 3.4.1.2, this visualization illustrates well the bone growth dynamic, influenced by the bone resorption (in red) and formation (in green) over time. The difference in terms of bone formation between the different scaffold conditions and mechanical loading conditions are nicely visible.
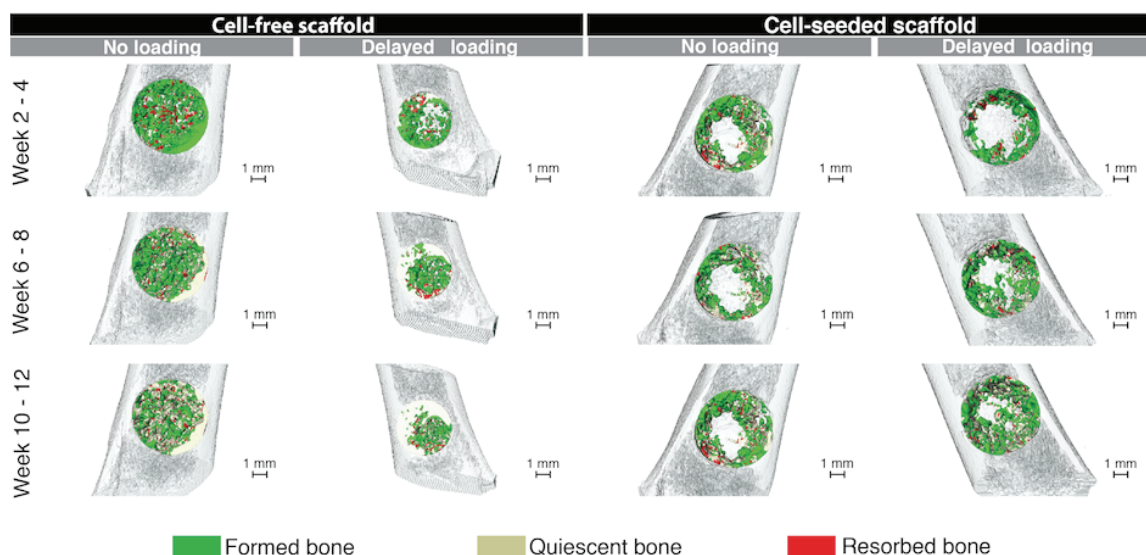
Figure 3.16 Three-dimensional images of implanted scaffolds inside femoral condyles. The resorbed bone and the formed bone are shown in red and green respectively, while the quiescent bone and the cortical bone are shown in off-white and transparent gray respectively. The data were collected from two chronological successive microCT scans as described in sub-section 3.3.3. Three out of five data points are represented in the graphic.

3.4.2.3   Histological Analysis

The semi-quantitative and qualitative evaluations of this study are summarized in Tab. S3.3 and Tab. S3.4 under section 3.7.2 (Supporting Information), respectively. Representative histological slides for each scaffold condition (CF and CS) after 12 weeks of implantation are shown in Fig. 3.17 and 3.18, respectively. In each figure, the corresponding delayed and no mechanical loading conditions are depicted for each scaffold condition.

In Tab. S3.3, semi-quantitative evaluation of bone formation, bone reaction, interface quality and interstitial quality are summarized. In between different scaffolds and mechanical loading conditions, no significant statistical difference was found for bone formation, bone reaction, bone-scaffold interface and the qualitative evaluation of the interstitial tissue. However, trends were observed regarding total scores. For both loading conditions, CF scaffolds showed a higher total of scores than inside CS scaffolds. A higher score was as well observed for the bone formation in the delayed mechanical loading condition than in the no loading condition inside CF scaffolds. As in the previous study, all different scaffolds integrated well inside the surrounding bone tissue; a direct and clear scaffold-bone contact was noticed in both scaffold conditions.

Regarding the cellular events (Tab. S3.4), we observed some more active osteoblasts in the case of CS than in CF scaffolds. These activated osteoblasts were especially noticed in the region where bone was forming. For all conditions, a normal range of multinuclear giant cells was observed whereas a higher number of blood vessels were noticed in the case of CS scaffolds. In addition, we observed about 5% to 15% of fibrous tissue in all conditions, except for no loading condition inside CS scaffolds, which contained a higher amount comprised between 10% and 50%.

Finally, we noticed a full maturity of modeled bone and bone marrow inside CF scaffolds independently of the loading condition (Fig.3.17). In contrast, in CS scaffolds, immature to mature bone was observed in both loading conditions. We noticed less active bone marrow, which is determined by the presence of fatty structure as shown in Fig. 3.18. The difference in maturity between CF and CS scaffolds is confirmed by the different cellular events, such as higher osteoblast activation and number of observed blood vessels in CS scaffolds compared to CF scaffolds.
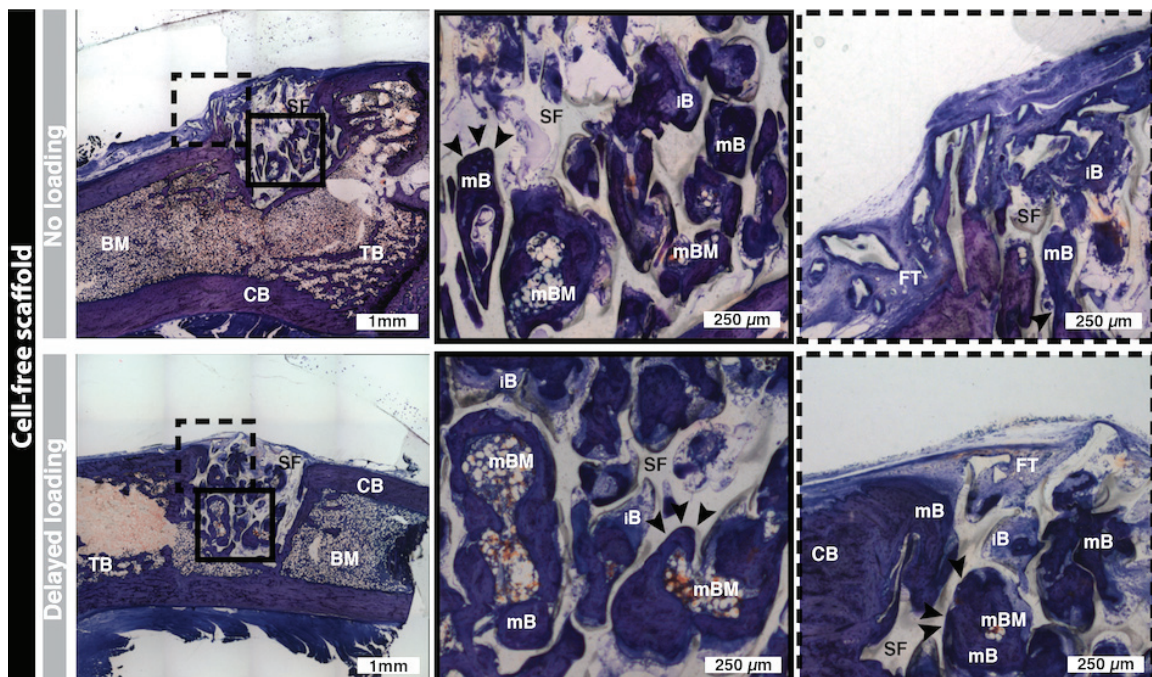
Figure 3.17 Toluidine blue stained sections of CF scaffolds after 12 weeks of implantation. On the top of the figure, no loading condition is shown and the delayed mechanical loading condition is illustrated at the bottom. The different tissues and the scaffolds are shown using the following abbreviations: Trabecular bone (TB), cortical bone (CB), bone marrow (BM), scaffold (SF), mature bone remodeling inside the scaffold (mB), mature bone marrow inside the scaffold (mBM), immature bone (iB) and fibrous tissue (FT). The black arrows indicate examples of region where the scaffold is well integrated. The sections were cut in the coronal plane.
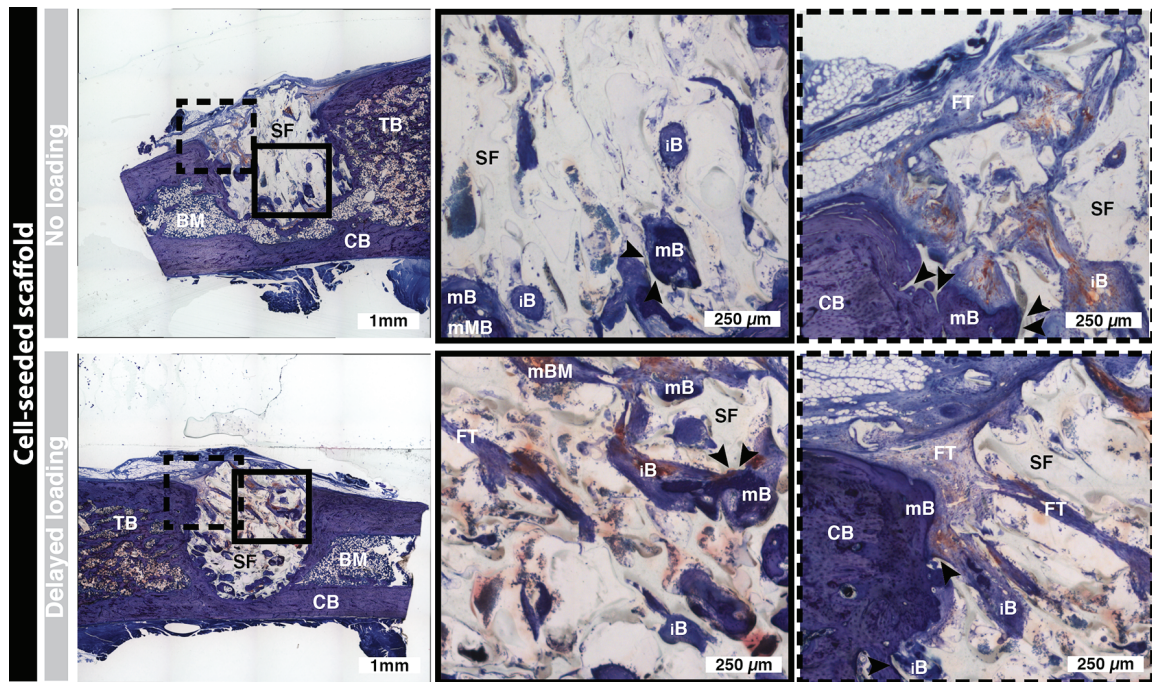
Figure 3.18 Toluidine blue stained sections of CS scaffolds after 12 weeks of implantation. On the top of the figure, no loading condition is shown and the delayed mechanical loading condition is illustrated at the bottom. The different tissues and the scaffolds are shown using the following abbreviations: Trabecular bone (TB), cortical bone (CB), bone marrow (BM), scaffold (SF), mature bone inside the scaffold remodeling (mB), mature bone marrow inside the scaffold (mBM), immature bone (iB) and fibrous tissue (FT). The black arrows indicate examples of region where the scaffold is well integrated.

3.5   Discussion

Several studies have shown positive effects on bone formation inside different types of BTE scaffolds, which were seeded with various bone affiliated cells, such as bone marrow preparations, bone marrow-derived mesenchymal stem cells or osteoblasts (Yasko et al. 1992; Srouji & Livne 2005; Jäger et al. 2007; Montjovent et al. 2008; Xu et al. 2010; Dupont et al. 2010; Boerckel, Kolambkar, et al. 2011; Corre et al. 2015). The choice of these bone affiliated cells is driven by the complex healing and regeneration mechanisms of bone in which different and various cell fates are involved (Amini et al. 2012). In this work, we were interested in hBPCs as they have low immunogenicity and have the capacity for osteogenic differentiation due to their multipotency and fetal cellular origin (Montjovent et al. 2004; Montjovent et al. 2008; Krattinger et al. 2011; Hirt-Burri et al. 2011). We therefore not only analyzed the effect of hBPCs, but also its osteogenic differentiated fate, namely hOBPCs.

Based on Montjovent's study, in which bone was significantly increased inside scaffolds treated with hBPC in immuno-competent rats, we excluded the potential immune rejection of xenograft cells. Therefore, we preferred immuno-competent rats in order to make sure that the obtained results would be due to experimental conditions rather than due to the use of another animal strain.

Considering the generated results, the immuno-competent rat model deserves further consideration in combination with hBPCs for future studies.

In parallel, other studies have demonstrated the importance of temporal onset of mechanical loading on bone formation inside BTE scaffolds (Roshan-Ghias et al. 2010; Boerckel, Uhrig, et al. 2011; Roshan-Ghias, Lambers, et al. 2011; Boerckel et al. 2012). The study of Roshan-Ghias et al. has demonstrated that early mechanical loading has a moderate effect inside CF scaffolds whereas a delayed mechanical loading shows a significant improvement of bone formation (Roshan-Ghias et al. 2010; Roshan-Ghias, Lambers, et al. 2011). Interestingly, in the study conducted by Boerckel et al., they have shown that early mechanical loading disrupts neovasculature ingrowth and therefore prevents bone formation whereas delayed mechanical loading stimulated neovascular network remodeling and enhances bone regeneration (Boerckel, Uhrig, et al. 2011).

As to our knowledge, the combination of bone cell types seeded within scaffolds and mechanical loading has not been investigated yet in bone regeneration, we evaluated the osteogenic effect of hBPCs and hOBPCs-seeded scaffolds compared to CF scaffolds when stimulated by early or delayed mechanical loadings. We therefore implanted different scaffolds, namely CF, CS and OCS scaffolds, in pre-drilled bone defects in femoral condyles of rats. We then evaluated the evolution of bone formation over 12 weeks by microCT scans and histological analysis. Two major key findings of this work are (1) that the quantitatively highest amount of bone was formed in CF scaffolds compared to CS and OCS scaffold and that (2) the timing of the mechanical application was crucial and dependent on the biological conditions inside the implanted scaffold.

In our study, we first observed that significantly less bone was formed inside CS and OCS scaffolds than in CF scaffolds over the entire duration of the different studies. This significant difference started already after 2 weeks of implantation. In our study, implanted CS and OCS scaffolds in femoral condyles of rats delayed the formation of bone in all mechanical loading conditions compared to CF scaffolds, as the analysis of the static and dynamic bone parameters indicated. When examining more closely the time needed to form the same volume of mineralized bone inside different scaffolds, we observed that for CS under early mechanical loading and OCS without mechanical loading, it took twice more time than for CF scaffolds. Indeed, the equivalent amount of formed bone after 6 weeks in CF scaffolds was reached after 12 weeks post-implantation inside CS scaffolds. Furthermore, the histological evaluation confirmed the observed delay and showed a clear trend that the maturation state of newly formed bone and bone marrow was more advanced inside CF scaffolds than inside CS and OCS scaffolds after 12 weeks of implantation. A similar difference in maturity state was noticed between CS and OCS scaffolds; less bone marrow activity and more immature bone were observed in OCS scaffolds compared to CS scaffolds.

These results of CF scaffolds inducing better bone regeneration than CS and OCS scaffolds are in contradiction with the data published by Montjovent (Montjovent et al. 2008), in which they have shown that hBPCs-seeded scaffolds improved significantly bone formation in femoral condyles after 2 months of implantation in femoral condyles of rats. A potential explanation could be the difference in the treatment of CF scaffolds before implantation, as the same scaffold condition and cell type were used. In our study, CF scaffolds were sonicated just after having wet them to eliminate air bubbles and increase the surface energy of the hydrophobic scaffolds. In the experiments of Montjovent et al., they have implanted hydrophobic PLA/5% ß-TCP scaffolds in a dry state

(Montjovent et al. 2008). The attractiveness of the scaffold's surface was therefore different for the cells between the studies. Furthermore, the induced fibrous tissue formation due to hBPCs and hOBPCs at 3, 7 and 14 days of implantation (see Chapter 2), is a plausible explanation for the delay in bone formation inside CS and OCS scaffolds compared to CF scaffolds.

When comparing the obtained results with other publications on BTE using cell therapy, several differences in technical and experimental designs have been observed, which affect the final outcomes on bone formation. In general, a positive effect on bone formation have been demonstrated when bone affiliated cells were used, as described elsewhere (Yasko et al. 1992; Srouji & Livne 2005; Jäger et al. 2007; Montjovent et al. 2008; Xu et al. 2010; Dupont et al. 2010; Boerckel, Kolambkar, et al. 2011; Liu et al. 2013; Corre et al. 2015). The major contrasts between the described studies and the one presented here are the different used scaffolds (PLA/5% β-TCP, hydrogels, porcine collagen combined with TCP, bicalcium phosphate, PLC, bioactive glass collagen hyaluronic acid phosphatidylserine, to name but a few), cell fate (BPCs, amniotic fluid stem cells, stromal MSCs), cell origin (human, allogeneic or syngeneic), defect type (partial or large), implantation site (femoral, tibial or cranial), immuno-competence of the animals (immuno-competent or immunodeficient) or the use of growth factors such as BMP-2 (lack or addition). Furthermore, other important parameters could influence the outcome of a BTE *in vivo* study. One of these parameters is the dose-effect relationship of the quantity of seeded cells *in vivo* (Carlier et al. 2014; Wu et al. 2015). It has been demonstrated that the cellular type and the amount of consumed oxygen are tightly linked. In our study, the different cell fates and concentrations of hBPCs and hOBPCs inside the scaffold just before implantation may have affected the oxygen consumption level, which could have influenced the final BV/TV outcome. It could therefore be interesting to analyze the oxygen consumption of hBPCs and hOBPCs at the same seeding concentration *in vitro* and test different seeding concentrations *in vivo* to study how this concentration could influence the final amount of formed bone in our model. Another crucial key player for a successful bone healing, as described elsewhere (Carlier et al. 2014), are the timing of treatment, such as administration of formation factors or cells, as well as the quality of the host environment. Using an *in silico* model, they have demonstrated that the optimization of the treatment strategy of bone defects was depended on the sensitive and linked mechanisms combining complex non-linear oxygen-dependent dynamics of blood vessels formation, oxygen supply, angiogenic growth factor production, cell differentiation, proliferation and oxygen consumption. Based on the optimization of treatment strategy described by Carlier et at. (Carlier et al. 2014), it could be interesting to combine both mechanical loading conditions with growth factors and hBPCs and hOBPCs several days or weeks after scaffold implantation for an even better bone regeneration than what we observed in our study. Additionally, Corre et al. (Corre et al. 2015) have determined that the combination between biphasic calcium phosphate scaffolds and syngeneic mesenchymal stromal cells in different osteogenic differentiation states, did not improve bone formation, but reached a similar level of bone formation than biphasic calcium phosphate scaffolds alone and analogous total bone marrow grafts respectively. Their results have shown that using biphasic calcium phosphate scaffolds without cells is a simpler and safer way to go as we showed in our study. However, it remains difficult to make a thorough comparison between the different studies, as different scaffolds and cell systems were combined in animal models with unlike immune competences.

Then, we also noticed in our study different bone formation behaviors inside CS, OCS and CF scaffolds when subjected to early or delayed mechanical in comparison to no loading (Figures in

sections 3.4.1 and 3.4.2, Tab. S3.5 in sub-section 3.7.4 (Supporting Information)). In the case of CF scaffolds, no difference was observed between early mechanical loading and no loading condition, for which the amount of newly formed bone reached 45%. In the same scaffold and loading conditions, Roshan-Ghias et al. (Roshan-Ghias et al. 2010) have shown a significant but moderate increase in the amount of formed bone after 13 weeks of implantation, when early mechanical loading was applied compared to no loading. Our results did not suggest such a trend after 12 weeks of implantation. This difference could be explained by the improvement of surgical techniques (fixation of leg, automated drilling system, …) and different surgical operators.

When early mechanical loading was applied to CS scaffolds, it increased the amount of formed bone, which was quite expected. Thanks to their multipotency, hBPCs have similar capacities to differentiate into osteoblasts under certain mechanical and environmental conditions than MSCs. It has been demonstrated several times that MSCs or bone marrow-derived MSCs appeared to be osteogenic when they were grown on firm gels that mimic precalcified bone (Engler et al. 2006; Discher et al. 2009). These mechanical sensitive cells have also shown to express early osteogenic markers with an increased mineralized matrix deposition, when subjected to cyclic tensile or compressive loading (Mauney et al. 2004; Sumanasinghe et al. 2006; Haudenschild et al. 2009; Delaine-Smith & Reilly 2012). Early mechanical loading surely induced the secretion of these osteogenic markers by hBPCs *in vivo*, which resulted in an increase of bone formation.

In contrast, we found that early mechanical loading had a negative effect on OCS scaffolds and significantly decrease in bone formation. A potential explanation can be suggested by two *in vitro* studies (Kadow-Romacker et al. 2009; Kadow-Romacker et al. 2013). In these studies, Kadow-Romacker et al. have demonstrated that small changes in duration of frequency of mechanical stimulations had significant consequences on the behavior of osteoblast- and osteoclast-like cells in single or co-culture conditions. In both studies, a three-point bending mechanical stimulation with different frequencies and durations was applied on osteoblast- and osteoclast-like cells either in single or in co-culture on dentin slices. Under the same stimulation condition, single culture of osteoclast-like cells did not influence the resorption activity, while in co-culture with osteoblast-like cells, an increase of resorption activity was observed. Based on these studies, one can propose that not only the duration and frequency of mechanical loading affects cell behavior, but also the cell type and the interaction with other cell types are as well crucial. Making the parallel between these *in vitro* studies and *in vivo* study presented here, we can hypothesize that the osteogenic cell fate of hOBPCs, which received the same early mechanical loading than implanted hBPCs, interacted differently with its surrounding tissue under this specific mechanical loading condition. This activity therefore resulted in a decrease of bone formation compared to no loading condition.

Furthermore, we noticed that the results obtained with OCS scaffolds, especially for BV/TV, Tb.Th, BF and BR, showed higher standard deviations than with CF and CS scaffold conditions. We think that this variation is mainly due to the preparation of the different types of cells before seeding into the scaffolds. In the case of CF scaffolds, no biological material was added, whereas CS scaffolds were pre-seeded with hBPCs 3 days before implantation. OCS scaffolds were seeded 14 days before implantation and were cultured within an osteogenic differentiation culture medium. The preparation conditions between the three types of scaffolds were therefore totally different. As for the preparation of OCS scaffolds the culture time was longer with several culture medium changes, a higher variation between OCS scaffolds could occur compared to CS scaffolds. It is thus important to

keep in mind when using biological content, that the possible variations due to preparation procedures influence the final output of a BTE scaffold.

We also analyzed the effect of delayed mechanical loading on CF and CS scaffolds. As in the previous study, significant higher bone volume inside CF scaffolds was observed compared to CS scaffolds, independently of the loading conditions, from 5 weeks post-implantation. The same trend has previously been shown by Roshan-Ghias et al. (Roshan-Ghias et al. 2010; Roshan-Ghias, Lambers, et al. 2011). Like for early mechanical loading, BV/TV increased significantly in CS scaffolds when subjected to delayed mechanical loading. As for the study with early mechanical loading, the static and dynamic bone parameters as well as the histological analysis are in accordance with the previously described observation based on BV/TV for scaffold and loading conditions.

The different effects of early or delayed mechanical loading on CF, CS or OCS scaffolds could be explained by the absence or presence of different cell types, based on the histology results after 3 days of implantation (see Chapter 2). When early mechanical loading was applied (2 days after implantation) the pores of CF scaffolds were empty or filled with red blood cells (see Chapter 2), whereas the pores of CS or OCS scaffolds were partially colonized with hBPCs or hOBPCs and extracellular matrix. In the case of delayed mechanical loading, the loading was applied 14 days after implantation. Based on the histology results in Chapter 2, CF scaffolds were filled with immature and some mature bone tissue, whereas CS and OCS scaffolds were filled with, fibrous tissue, immature bone tissue and potentially hBPCs and hOBPCs, respectively. The biological materials were therefore different between CF, CS and OCS scaffolds when subjected to early and delayed mechanical loadings. As both loading conditions were transmitted by fluid flow to the cells present inside scaffolds, the different amount of formed bone inside CF, CS and OCS scaffolds might reflect the secretion of different growth factors and signaling molecules of host or xenograft cells to the surrounding tissue.

For early mechanical loading experiments, bone stiffness inside CF and CS scaffolds has been assessed by finite element analysis, in which a uniaxial compression was applied on the lateral side of the formed bone inside scaffolds. We observed that the modeled stiffness of the mineralized bone showed a similar trend than BV/TV. As the input files used for the finite element analysis were based on the same microCT images than the ones used for BV/TV evaluation, the similarity in terms of results between BV/TV and stiffness are not surprising. As neither scaffold's mechanical properties nor tissues' mechanical properties were taken into account, due to technical limitations for scaffold visualization (see sub-section 3.7.1 in Supporting information), the obtained results do not fully represent the complexity of this system. Before refining the finite element analyses to a more physiologically-close model, we analyzed if early mechanical loading influenced BV/TV in a specific anatomic axis of the rat inside the scaffolds. For this purpose, BV/TV of CF scaffolds was evaluated in the distal, proximal, anterior and posterior axes in both mechanical loading conditions. The results are shown in Fig. S3.1 under sub-section 3.7.3 (Supporting information) and they demonstrated no difference between distal, proximal, anterior and posterior axes in both mechanical loading conditions. Therefore, no finite element analysis was further conducted for all scaffold conditions. For a future study, to obtain a more physiologically-close model, we propose that the axial compression should not be applied on the lateral part of the formed bone inside the scaffold, but on the anterior axes of the animal's leg like in the *in vivo* experiment. Then, the scaffold should contain a contrast agent with a different density than bone, for better visualization and distinction with the

bone for finite element analysis. With these changes, the modelization of mechanical properties of the implanted scaffold and newly formed mineralized bone, augmented by the applied mechanical loading on the leg, could be improved.

Finally, it would be interesting to analyze in more details the bone quality inside the different scaffold conditions in the long term. As bone quality includes the geometric and material factors contributing to its strength (Donnelly 2011), microCT scanning, Raman microspectroscopy and finite element analysis could be combined for comprehensive interpretation. MicroCT imaging provides the characterization of macroscopic geometry and microarchitecture, while Raman microspectroscopy evaluates the physiochemical components of the formed bone (Donnelly 2011). As Raman microspectroscopy is a noninvasive technique applicable for *in vivo* studies, it could be used in parallel with a longitudinal microCT study. This microspectroscopy would allow to measure mineral/matrix ratio (related to bone material density), mineral crystallinity (related to mineral quality) and cross-linking within the organic phase (related to collagen quality) (Draper et al. 2005). Lastly, finite element modeling would allow us to assess the properties of the bone-scaffold construct in a more accurate and realistic way by taking into account the above-suggested modifications. Furthermore, it would be interesting to extend the actual *in vivo* studies to 20 or 30 weeks of implantation to see when the amount of formed bone inside CS and OCS scaffolds reaches the same amount than inside CF scaffolds and how the different biological conditions used for the scaffolds affect on long-term the quality of the bone.

3.6   Conclusion

The complex healing and regeneration mechanisms of bone, which includes bone cells in different cell fate states, secretion of growth factors or mechanical stimulations, result in a variety of strategies for BTE. In this work, we combined for the first time fetal cells seeded within scaffolds and mechanical loading applied at different time points after implantation. Our goal was therefore to evaluate the effect of these different conditions on the amount of formed bone inside scaffolds seeded with hBPCs and hOBPCs compared to cell-free scaffolds when early and delayed mechanical loadings were applied. In the first part of the present study, we showed that the amount of formed bone inside CS and OCS scaffolds was significantly lower than inside CF scaffolds independently of the mechanical loading conditions, which could be explained by the presence of fibrous tissue in CS and OCS scaffolds at 3, 7 and 14 days of implantation compared to CF scaffolds. In the second part, we noticed that early mechanical loading had no effect on CF scaffolds compared to no loading condition, while we observed a significant improvement in bone formation inside CS scaffolds and a significant decrease in OCS scaffolds. The contrary effect of early loading inside CS and OCS scaffolds could be explained by the different differentiation state of hBPCs and hOBPCs. The secretion of growth factors and biomolecules was certainly different when the same mechanical loading was applied as it results in bone formation and bone resorption for CS and OCS, respectively. In terms of mechanical properties modeling of newly formed bone inside CF and CS scaffolds, we observed that the modeled bone stiffness was significantly higher in CF scaffolds than in CS scaffolds, and that early mechanical loading enhanced the modeled stiffness of bone inside the CS scaffolds only. In a third part, we observed in both CF and CS scaffold conditions a bone formation increase starting from 5 weeks or 8 weeks post-implantation, respectively. Taken all together, the *in vivo* results indicate that

CF scaffold approach, independently of the mechanical loading conditions used here, represents a clinically relevant alternative for BTE compared to CS and OCS scaffolds. The application of early mechanical loading would have been of advantage for the patient, as it would have allowed a fast mobilization in order to regain a good life quality. However, CF scaffolds combined with delayed loading is finally the best option in terms of qualitative bone regeneration. Even if there is still a long and challenging path to follow in order to reach a stable and satisfactory bone formation for clinical application, this latest approach has the merits to be simple and safe from a clinical point of view, without additional costs and increasing regulatory restriction due to the use of cells.

3.7 Supporting Information

3.7.1 Scaffold Marking with Ruby Beads

Initially, we wanted to mark the PLA/5% β-TCP scaffold with ruby beads, because once implanted in the bone and scanned with the *in vivo* parameters, the scaffold was not visible anymore on the microCT images. The main idea was to be able to distinguish between the newly formed bone inside the scaffold and the scaffold itself for a numerical model analysis. In this model, the aim was to assess the mechanical properties of the implanted scaffold, augmented by the applied mechanical loading on the leg. Our hypothesis was that mechanically loaded scaffold would augment its mechanical strength due to an optimization of the bone formation in the scaffold's weakest spots.

Therefore, for CF and CS scaffolds in our first *in vivo* experiment, in which early mechanical loading was studied, we marked each scaffold with two 300 µm and one 400 µm ruby beads (Sandoz & Fils SA, Cugy, Switzerland) at its bottom and with three 300 µm ruby beads at its top. The beads were heated up and glued in the scaffold. The microCT scans showed that this technique did not obstruct the pores or glued them together. Once marked, the scaffolds were scanned using a SkyScan 1076 scanner (Bruker microCT) with the following parameters: no filter, 40 kV voltage, 150 µA current, exposure time of 650 ms and 0.25° rotation step with a pixel resolution of 9 µm. The scaffolds were then sterilized by ethylene oxide at the CHUV (Lausanne, Switzerland). The reconstruction were performed with the NRecon and Amira® (FEI Visualization Sciences Group) as described in sub-section 3.2.3. On Amira®, the pixel sizes of the scaffold were resized from 9 µm to 18 µm.

Once the animals were implanted and scanned, and the microCT images reconstructed on Amira®, we observed either a loss of one to five beads or bead motion. The loss and bead motion occurred between the time of scaffold marking and the implantation. As during the surgery, the scaffold was press-fitted inside the hole, the surfaces were sometimes slightly impaired. Therefore, a mapping between the scaffolds before implantation and the implanted scaffold was not possible. For further *in vivo* studies, the scaffold marking was left out.

3.7.2 Histological Evaluation

The semi-quantitative evaluation of bone formation and scaffold integration for CF, CS and OCS under no loading and early mechanical loading conditions is shown in Tab. S3.1 and its corresponding qualitative evaluation of cellular events is summarized in Tab. S3.2. No statistical significance was observed between different conditions of each parameter. The trend for both semi-qualitative and quantitative evaluation confirms the results obtained by microCT scanning.

Table S3.1 Semi-quantitative evaluation of bone formation and scaffold integration based on histology slides. Each parameter was evaluated with a separate score system. The scores of all parameters were summed up and summarized under *Total* (n=2-3).

Scaffold	Mechanical loading	Bone formation (0-8)	Bone reaction (0-3)	Interface (0-4)	Interstitial tissue (0-4)	Total
CF	No loading	6.33 ± 1.53	2.67 ± 0.58	4.0 ± 0.0	3.67 ± 0.58	16.67 ± 2.68
	Early loading	5.67 ± 1.15	2.67 ± 0.58	4.0 ± 0.0	4.0 ± 0.0	16.33 ± 1.73
CS	No loading	3.67 ± 1.53	2.67 ± 0.58	4.0 ± 0.0	3.0 ± 0.0	13.33 ± 2.10
	Early loading	4.33 ± 0.58	3.0 ± 0.0	4.0 ± 0.0	3.33 ± 0.58	14.66 ± 1.15
OCS	No loading	3.67 ± 2.08	2.0 ± 1.0	2.67 ± 1.15	1.67 ± 1.15	10.0 ± 5.39
	Early loading	4.33 ± 0.58	2.0 ± 1.0	3.33 ± 0.58	2.67 ± 0.58	12.33 ± 2.73

Table 3.2 Qualitative evaluations of histology slides. The cellular events were evaluated from rare, few, some or many and the bone marrow activity as no activity, few fatty structure up to totally mature (n=2-3).

Scaffold	Mechanical loading	Osteoblast activation	Presence of multinuclear giant cells	Number of vessels approximation	Fibrous tissue approximation (%)	Bone marrow activity
CF	**No loading**	Few	Few to normal range	< 20	5 - 15%	Totally mature
	Early loading	Few	Few	< 20	5 - 10%	Totally mature
CS	**No loading**	Some, where bone is forming	Few to normal range	20 - 30	5 - 10%	No activity to few fatty structure
	Early loading	Some, where bone is forming	Few to normal range	20 - 30	5 - 15%	Immature to mature bone
OCS	**No loading**	Some, where bone is forming	Few to normal range	> 20	10-75%	No activity to few fatty structure
	Early loading	Some, where bone is forming	Few to normal range	> 20	15-50%	No activity to few fatty structure

The semi-quantitative evaluation of bone formation and scaffold integration for CF and CS under no loading and delayed mechanical loading conditions is shown in Tab. S3.3 and its corresponding qualitative evaluation of cellular events is summarized in Tab. S3.3. No statistical significance was observed between different conditions of each parameter. The trend for both semi-qualitative and quantitative evaluation confirms the results obtained by microCT scanning.

Table S3.3 Semi-quantitative evaluation of bone formation and scaffold integration based on histology slides. Each parameter was evaluated with a separate score system. The scores of all parameters were summed up and summarized under *Total* (n=2-3).

Scaffold	Mechanical loading	Bone formation (0-8)	Bone reaction (0-3)	Interface (0-4)	Interstitial tissue (0-4)	Total
CF	No loading	6.0 ± 1.41	3.0 ± 0.0	4.0 ± 0.0	4.0 ± 0.0	17 ± 1.41
	Delayed loading	7.5 ± 0.71	3.0 ± 0.0	4.0 ± 0.0	4.0 ± 0.0	18.5 ± 0.71
CS	No loading	6.0 ± 1.41	3.0 ± 0.0	3.5 ± 0.71	3.5 ± 0.71	16 ± 2.82
	Delayed loading	6.0 ± 2.82	3.0 ± 0.0	4.0 ± 0.0	4.0 ± 0.0	12.33 ± 2.73

Table S3.4 Qualitative evaluations of histology slides. The cellular events were evaluated from rare, few, some or many and the bone marrow activity as no activity, few fatty structure up to totally mature (n=2-3).

Scaffold	Mechanical loading	Osteoblast activation	Presence of multinuclear giant cells	Number of vessels approximation	Fibrous tissue (%)	Bone marrow activity
CF	No loading	Few	Few to normal range	< 5	5 – 10%	Totally mature
	Delayed loading	Few	Few to normal range	< 5	5 – 10%	Totally mature
CS	No loading	Some, where bone is forming	Few to normal range	< 15	15 – 50%	Immature to mature bone
	Delayed loading	Some, where bone is forming	Few to normal range	< 15	10 – 15%	Immature to mature bone

3.7.3   Bone Volume Density Analysis Inside Scaffold in Four Anatomic Axes

BV/TV inside implanted CF scaffolds in the distal, proximal, anterior and posterior axes of the rats were analyzed, based on microCT images obtained under early and no mechanical loading conditions. The femurs of the rats were all oriented using Amira® (FEI Visualization Sciences Group) and the VOI of the four axes were defined in CTan (Bruker microCT). The statistical analysis was tested with the GAMM in R (R Development Code Team 2010) (n=6), where all conditions were compared one to each other. In Fig. S3.1, BV/TV for CF scaffolds with an early and no mechanical loading conditions is shown for each physiological axis. No statistical difference was observed between early mechanical loading and no loading condition in all four axes, as well as between the physiological axes. Early mechanical loading did therefore not impact the bone formation in a specific physiological axis. Due to this observation, BV/TV of CS and OCS were not analyzed.
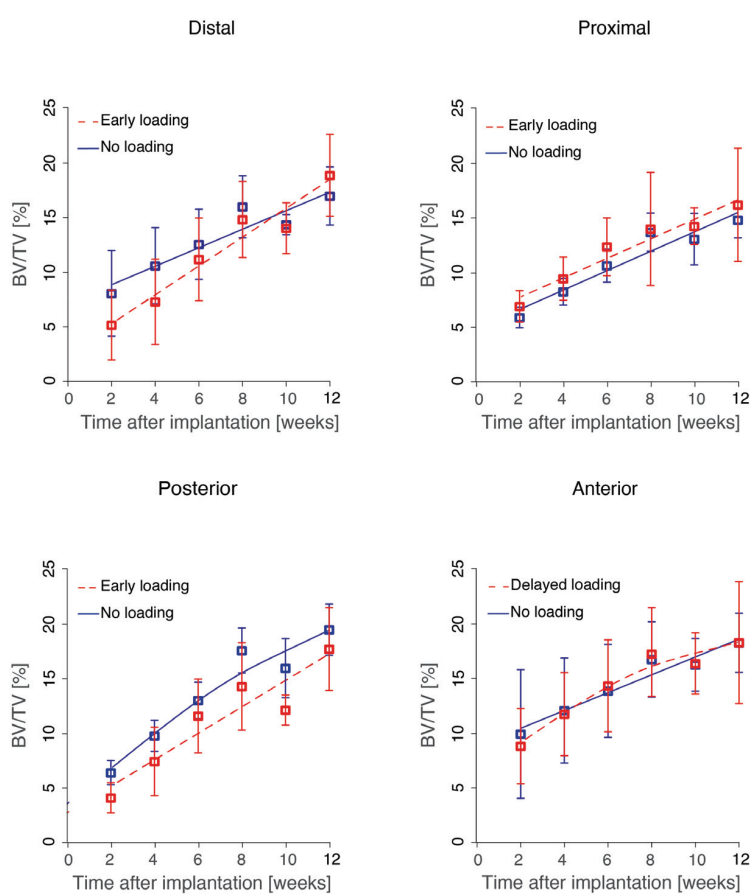

Figure S3.1 Bone volume density in the distal, proximal, posterior and anterior directions in implanted CF scaffolds between early mechanical loading and no loading (n=6).

3.7.4 P-Values of Bone Volume Density Between Different Scaffolds and Mechanical Loading Conditions

Tab. S3.5 summarizes the p-values between all scaffold conditions and mechanical conditions of the static bone parameter BV/TV. On the top, the p-values between scaffold conditions of each *in vivo* study, namely early and delayed loading, are presented. At the bottom, the p-values of scaffold conditions between early and delayed loading are listed.

Table S3.5 P-values summary of bone volume density between the different scaffold conditions and mechanical loading conditions.

P-values of BV/TV (%) between CF, CS and OCS scaffolds

Early vs no mechanical loading: Experimental groups of rat (EL)

Cond. 1	Cond. 2	Week 2	Week 4	Week 6	Week 8	Week 10	Week 12
□	■ (blue)	5.74E-08	1.06E-11	5.55E-16	00E-00	00E-00	00E-00
□	X	3.01E-02	1.96E-02	1.13E-02	1.12E-02	1.11E-02	1.29E-02
□	□ (red)	3.37E-01	3.54E-01	3.79E-01	4.10E-01	4.44E-01	4.76E-01
□	■ (red)	3.14E-07	8.77E-09	3.56E-10	5.27E-11	4.59E-11	1.73E-10
□	X	1.42E-06	2.23E-09	1.3E-12	1.33E-15	1.11E-02	1.29E-02
■ (blue)	X	4.66E-01	4.62E-01	4.60E-01	4.57E-01	4.56E-01	4.55E-01
■ (blue)	□ (red)	3.01E-04	6.50E-06	7.14E-08	6.79E-10	1.06E-11	4.40E-13
■ (blue)	■ (red)	4.06E-01	1.09E-01	4.49E-02	7.68E-03	9.46E-04	9.98E-05
■ (blue)	X	2.15E-01	8.27E-02	2.2E-02	4.67E-03	9.93E-04	2.69E-04
X	□ (red)	0.60E-01	4.45E-02	3.48E-02	3.06E-02	3.09E-02	3.52E-02
X	■ (red)	2.55E-01	1.94E-01	1.43E-01	1.07E-01	8.48E-02	7.23E-02
X	X	2.12E-01	8.45E-02	2.41E-02	5.59E-03	1.30E-03	3.82E-04
□ (red)	■ (red)	6.10E-04	1.30E-04	2.93E-05	8.63E-06	3.96E-06	2.95E-06
□ (red)	X	1.25E-01	4.36E-02	1.07E-02	2.81E-03	1.34E-03	1.23E-03
■ (red)	X	3.89E-01	1.79E-01	5.88E-02	1.38E-02	2.61E-03	4.60E-04

P-values of BV/TV (%) between CF and CS scaffolds

Delayed vs no mechanical loading: Experimental groups of rat (DL)

Cond. 1	Cond. 2	Week 2	Week 4	Week 6	Week 8	Week 10	Week 12
□	■ (blue)	1.02E-04	00E-00	00E-00	00E-00	00E-00	00E-00
□	□ (green)	1.08E-01	1.72E-01	1.30E-03	00E-00	00E-00	00E-00
□	■ (green)	4.84E-01	2.92E-01	1.25E-01	4.32E-02	1.79E-02	1.1E-02
■ (blue)	□ (green)	3.2E-04	00E-00	00E-00	00E-00	00E-00	00E-00
■ (blue)	■ (green)	4.84E-01	4.84E-01	2.92E-01	4.31E-02	1.79E-02	1.11E-02
□ (green)	■ (green)	1.84E-04	1.67E-06	1.92E-08	5.79E-10	9.05E-11	1.79E-10

P-values of BV/TV (%) between all conditions

Early vs delayed vs no mechanical loading: Comparison between experimental groups of rat of different *in vivo* studies (EL vs DL)

EL	DL	Week 2	Week 4	Week 6	Week 8	Week 10	Week 12
□	□	9.77E-02	8.50E-02	7.25E-02	5.37E-02	3.48E-02	2.46E-02
□	■ (blue)	3.00E-01	1.97E-01	1.18E-01	6.66E-02	3.77E-02	2.26E-02
□	□ (green)	2.18E-03	1.98E-01	1.17E-01	5.20E-03	1.15E-03	1.64E-03
□	■ (green)	1.0E-04	00E-00	00E-00	00E-00	00E-00	00E-00
■ (blue)	□ (blue)	3.01E-05	4.98E-08	6.87E-011	1.70E-13	1.78E-15	4.44E-16
■ (blue)	■ (blue)	3.02E-01	1.97E-01	1.17E-01	6.66E-02	3.77E-02	2.26E-02
■ (blue)	□ (green)	3.43E-05	4.44E-16	00E-00	00E-00	00E-00	00E-00
■ (blue)	■ (green)	2.17E-01	5.34E-01	6.91E-03	5.05E-04	2.56E-05	1.17E-06
X	□	8.38E-02	8.38E-02	6.65E-02	6.62E-02	7.46E-02	1.08E-01
X	■ (blue)	3.00E-01	1.69E-01	7.97E-02	3.35E-02	1.45E-02	7.32E-03
X	□ (green)	1.87xE-01	2.09E-02	1.21E-03	1.34E-04	6.95E-05	1.24E-04
X	■ (green)	2.91E-01	2.32E-01	1.82E-01	1.47E-01	1.28E-01	1.22E-01

EL	DL	Week 2	Week 4	Week 6	Week 8	Week 10	Week 12
□ (red)	□	2.93E-01	2.17E-01	2.37E-01	1.84E-01	1.25E-01	8.15E-02
□ (red)	■ (blue)	9.58E-04	6.04E-06	2.67E-06	1.29E-07	1.11E-08	2.26E-09
□ (red)	□ (green)	7.89E-02	4.58E-01	1.46E-01	3.76E-02	2.13E-02	2.38E-02
□ (red)	■ (green)	2.81E-04	9.40E-05	1.11E-05	2.37E-06	1.38E-06	1.99E-06
■ (red)	□ (blue)	1.04E-04	9.13E-06	1.87E-06	1.00E-06	1.50E-06	7.06E-06
■ (red)	■ (blue)	3.05E-01	2.89E-01	2.74E-01	2.64E-01	2.57E-01	2.53E-01
■ (red)	□ (green)	3.01E-04	6.50E-06	7.14E-08	6.79E-10	1.06E-11	4.40E-13
■ (red)	■ (green)	1.90E-04	2.77-011	00E-00	00E-00	00E-00	00E-00
X	□	1.94E-04	1.45E-06	8.51E-09	7.94E-11	2.41E-12	6.87E-13
X	■ (blue)	2.98E-01	2.06E-01	1.33E-01	8.26E-02	5.18E-02	3.44E-02
X	□ (green)	5.87E-04	5.87E-04	5.58E-11	00E-00	00E-00	00E-00
X	■ (green)	2.80E-01	9.29E-02	1.68E-02	2.06E-03	2.98E-04	7.69E-05

Legend:
- ■ (blue) No loading
- ■ (red) Early loading
- ■ (green) Delayed loading
- □ Cell-free scaffold
- ■ Cell-seeded scaffold
- X Osteogenic cell-seeded scaffold

Shading:
- ■ ≤ 1.0E-04
- 1.0E-04 < ■ ≤ 1.0E-03
- 1.0E-03 < ■ ≤ 1.0E-02
- 1.0E-02 < ■ ≤ 5.0E-02

3.8   Acknowledgements

3.9   References

Amini, A.R., Laurencin, C.T. & Nukavarapu, S.P., 2012. Bone tissue engineering: recent advances and challenges. *Critical Reviews in Biomedical Engineering*, 40(5), pp.363–408.

Boerckel, J.D. et al., 2012. Effects of *in vivo* mechanical loading on large bone defect regeneration. *Journal of Orthopaedic Research*, 30(7), pp.1067–1075.

Boerckel, J.D., Kolambkar, Y.M., et al., 2011. Effects of protein dose and delivery system on BMP-mediated bone regeneration. *Biomaterials*, 32(22), pp.5241–5251.

Boerckel, J.D., Uhrig, B.A., et al., 2011. Mechanical regulation of vascular growth and tissue regeneration in vivo. *Proceedings of the National Academy of Sciences of the United States of America*, 108(37), pp.E674–E680.

Bose, S., Roy, M. & Bandyopadhyay, A., 2012. Recent advances in bone tissue engineering scaffolds. *Trends in Biotechnology*, 30(10), pp.546–554.

Brouwers, J.E.M., Van Rietbergen, B. & Huiskes, R., 2007. No effects of *in vivo* micro-CT radiation on structural parameters and bone marrow cells in proximal tibia of wistar rats detected after eight weekly scans. *Journal of Orthopaedic Research*, 25(10), pp.1325–1332.

Carlier, A. et al., 2014. Size does matter: An integrative *in vivo-in silico* approach for the treatment of critical size bone defects F. M. Gabhann, ed. *PLoS Computational Biology*, 10(11), p.e1003888.

Corre, P. et al., 2015. Direct comparison of current cell-based and cell-free approaches towards the repair of craniofacial bone defects – A preclinical study. *Acta Biomaterialia*, 26, pp.306–317.

De Souza, R.L. et al., 2005. Non-invasive axial loading of mouse tibiae increases cortical bone formation and modifies trabecular organization: A new model to study cortical and cancellous compartments in a single loaded element. *Bone*, 37(6), pp.810–818.

Delaine-Smith, R.M. & Reilly, G.C., 2012. Mesenchymal stem cell responses to mechanical stimuli. *Muscles, Ligaments and Tendons Journal*, 2(3), pp.169–180.

Discher, D.E., Mooney, D.J. & Zandstra, P.W., 2009. Growth factors, matrices, and forces combine and control stem cells. *Science*, 324(5935), pp.1673–1677.

Donnelly, E., 2011. Methods for assessing bone quality: A review. *Clinical Orthopaedics and Related Research*, 469(8), pp.2128–2138.

Draper, E.R. et al., 2005. Novel assessment of bone using time-resolved transcutaneous Raman Spectroscopy. *Journal of Bone and Mineral Research*, 20(11), pp.1968–1972.

Dupont, K.M. et al., 2010. Human stem cell delivery for treatment of large segmental bone defects. *Proceedings of the National Academy of Sciences*, 107(8), pp.3305–3310.

Engler, A.J. et al., 2006. Matrix elasticity directs stem cell lineage specification. *Cell*, 126(4), pp.677–689.

Forwood, M.R. et al., 1996. Increased bone formation in rat tibiae after a single short period of dynamic loading *in vivo*. *The American Journal of Physiology*, 270(3 Pt 1), pp.E419–E423.

Fritton, J.C. et al., 2005. Loading induces site-specific increases in mineral content assessed by microcomputed tomography of the mouse tibia. *Bone*, 36(6), pp.1030–1038.

Haudenschild, A.K. et al., 2009. Pressure and distortion regulate human mesenchymal stem cell gene expression. *Annals oBiomedical Engineering*, 37(3), pp.492–502.

Hirt-Burri, N. et al., 2011. Biologicals and fetal cell therapy for wound and scar management. *ISRN Dermatology*, 2011(1), pp.1–16.

Jäger, M. et al., 2007. Bone healing and migration of cord blood-derived stem cells into a critical size femoral defect after xenotransplantation. *Journal of Bone and Mineral Research : the Official Journal of the American Society for Bone and Mineral Research*, 22(8), pp.1224–1233.

Kadow-Romacker, A. et al., 2009. Effect of mechanical stimulation on osteoblast- and osteoclast-like cells *in vitro*. *Cells Tissues Organs*, 190(2), pp.61–68.

Kadow-Romacker, A. et al., 2013. Slight changes in the mechanical stimulation affects osteoblast- and osteoclast-like cells in co-culture. *Transfusion Medicine and Hemotherapy*, 40(6), pp.441–447.

Kettenberger, U. et al., 2014. Does locally delivered Zoledronate influence peri-implant bone formation? - Spatio-temporal monitoring of bone remodeling *in vivo. Biomaterials*, 35(37), pp.9995–10006.

Krattinger, N. et al., 2011. Regulation of proliferation and differentiation of human fetal bone cells. *European Cells and Materials*, 21, pp.46–58.

Krebsbach, P.H. et al., 1999. Bone marrow stromal cells: Characterization and clinical application. *Critical Reviews in Oral Biology & Medicine*, 10(2), pp.165–181.

Liu, Y. et al., 2013. Integration of a calcined bovine bone and BMSC-sheet 3D scaffold and the promotion of bone regeneration in large defects. *Biomaterials*, 34(38), pp.9998–10006.

MacNeil, J.A. & Boyd, S.K., 2008. Bone strength at the distal radius can be estimated from high-resolution peripheral quantitative computed tomography and the finite element method. *Bone*, 42(6), pp.1203–1213.

Mammoto, A., Mammoto, T. & Ingber, D.E., 2012. Mechanosensitive mechanisms in transcriptional regulation. *Journal of Cell Science*, 125(13), pp.3061–3073.

Mauney, J.R. et al., 2004. Mechanical stimulation promotes osteogenic differentiation of human bone marrow stromal cells on 3-D partially demineralized bone scaffolds *in vitro*. *Calcified Tissue International*, 74(5), pp.458–468.

Montjovent, M.-O. et al., 2004. Fetal bone cells for tissue engineering. *Bone*, 35(6), pp.1323–1333.

Montjovent, M.-O. et al., 2008. Human fetal bone cells associated with ceramic reinforced PLA scaffolds for tissue engineering. *Bone*, 42(3), pp.554–564.

Müller, R. & Rüegsegger, P., 1995. Three-dimensional finite element modelling of non-invasively assessed trabecular bone structures. *Medical Engineering and Physics*, 17(2), pp.126–133.

Owen, M.E., Cavé, J. & Joyner, C.J., 1987. Clonal analysis in vitro of osteogenic differentiation of marrow CFU-F. *Journal of Cell Science*, 87 (Pt 5), pp.731–738.

Phinney, D.G. et al., 1999. Plastic adherent stromal cells from the bone marrow of commonly used strains of inbred mice: Variations in yield, growth, and differentiation. *Journal of Cellular Biochemistry*, 72(4), pp.570–585.

Pittenger, M.F. et al., 1999. Multilineage potential of adult human mesenchymal stem cells. *Science*, 284(5411), pp.143–147.

R Development Code Team, 2010. *R: A language and environment for statistical computing*, Vienna: R Foundation for Statistical Computing.

Robling, A.G. & Turner, C.H., 2009. Mechanical signaling for bone modeling and remodeling. *Critical Reviews in Eukaryotic Gene Expression*, 19(4), pp.319–338.

Robling, A.G., Castillo, A.B. & Turner, C.H., 2006. Biomechanical and molecular regulation of bone remodeling. *Annual Reveiw of Biomedical Engineering*, 8(1), pp.455–498.

Roshan-Ghias, A. et al., 2010. *In vivo* cycling loading as potent stimulatory signal for bone formation inside tissue engineereing scaffolds. *European Cells and Materials*, 19, pp.41–49.

Roshan-Ghias, A., Arnoldi, J., et al., 2011. *In vivo* assessment of local effects after application of bone screws delivering bisphosphonates into a compromised cancellous bone site. *Clinical Biomechanics*, 26(10), pp.1039–1043.

Roshan-Ghias, A., Lambers, F.M., et al., 2011. *In vivo* loading increases mechanical properties of scaffold by affecting bone formation and bone resorption rates. *Bone*, 49(6), pp.1357–1364.

Serafini, M. et al., 2014. Establishment of bone marrow and hematopoietic niches in vivo by reversion of chondrocyte differentiation of human bone marrow stromal cells. *Stem Cell Research*, 12(3), pp.659–672.

Srouji, S. & Livne, E., 2005. Bone marrow stem cells and biological scaffold for bone repair in aging and disease. *Mechanisms of Ageing and Development*, 126(2), pp.281–287.

Stadelmann, V.A. et al., 2009. 3D strain map of axially loaded mouse tibia: A numerical analysis validated by experimental measurements. *Computer Methods in Biomechanics and Biomedical Engineering*, 12(1), pp.95–100.

Sumanasinghe, R.D., Bernacki, S.H. & Loboa, E.G., 2006. Osteogenic differentiation of human mesenchymal stem cells in collagen matrices: Effect of uniaxial cyclic tensile strain on bone morphogenetic protein (BMP-2) mRNA expression. *Tissue Engineering*, 12(12), pp.3459–3465.

Turner, C.H., Forwood, M.R. & Otter, M.W., 1994. Mechanotransduction in bone: Do bone cells act as sensors of fluid flow? *The FASEB Journal*, 8(11), pp.875–878.

van Rietbergen, B. et al., 1995. A new method to determine trabecular bone elastic properties and loading using micromechanical finite-element models. *Journal of Biomechanics*, 28(1), pp.69–81.

Wu, H. et al., 2015. The dose-effect relationship between the seeding quantity of human marrow mesenchymal stem cells and *in vivo* tissue-engineered bone yield. *Cell Transplantation*, 24(10), pp.1957–1968.

Xu, C. et al., 2010. A novel biomimetic composite scaffold hybridized with mesenchymal stem cells in repair of rat bone defects models. *Journal of Biomedical Materials Research Part A*, 95(2), pp.495–503.

Yasko, A.W. et al., 1992. The healing of segmental bone defects, induced by recombinant human bone morphogenetic protein (rhBMP-2): A radiographic, histological and biomechanical study in rats. *Journal of Bone and Joint Surgery*, 74(5), pp.659–670.

Chapter 4

Accomplishments, Future Works and Conclusion

4.1 Accomplishments

The approaches to use osteogenic cells and mechanical loading as therapies in bone tissue engineering (BTE) have separately been shown to be promising (Robling et al. 2002; Srouji & Livne 2005; Jäger et al. 2007; Montjovent et al. 2008; Dupont et al. 2010; Xu et al. 2010; Roshan-Ghias et al. 2010; Roshan-Ghias et al. 2011; Boerckel et al. 2011; Boerckel et al. 2012; Amini et al. 2012; Liu et al. 2013). So far, the combination of these two main strategies inside a tissue engineering scaffold has not been analyzed in a bone tissue, but only in ectopic sites such as under the skin (Duty et al. 2007). The main objective of this thesis was to assess the effect of cell therapies combined with different temporally applied mechanical loadings on bone formation inside tissue engineering scaffolds implanted in femoral condyles of rats. Indeed, our main goal was to find a scaffold providing an adequate compromise between friendly-to-use for surgeons, safe, with minimal regulatory constraints and with minimal surgical and rehabilitation costs for the patient.

We therefore studied the combination of three *in vivo* studies in rats previously completed in our laboratory. These studies highlighted the potential of (1) human bone progenitor cells (hBPCs) seeded in poly(L-lactic acid) (PLA)/5% ß – tricalcium phosphate (ß–TCP) scaffolds (Montjovent et al. 2008), (2) early mechanical loading on bone formation inside PLA/5% ß–TCP scaffolds (Roshan-Ghias et al. 2010) and (3) delayed mechanical loading on bone formation inside PLA/5% ß–TCP scaffolds (Roshan-Ghias et al. 2011) for BTE. We focused our work on two main aspects: (1) the evaluation of the potential triggered immune reaction of hBPCs-seeded scaffolds (CS) and osteogenic hBPCs (hOBPCs)-seeded scaffolds (OCS) compared to scaffolds without cells (CF) early after their implantation and (2) the investigation of the impact of early and delayed mechanical loading on implanted CF, CS and OCS scaffolds.

We first demonstrated that the xenograft systems, composed of hBPCs- or hOBPCs-seeded PLA/5% ß-TCP scaffolds, affected the surrounding tissue. A temporary fibrous tissue formed partially around CS and OCS scaffolds than around CF scaffolds. Based on histological evaluation of immune cells, we observed that CS and OCS scaffolds did not trigger particular specific immune reaction after 3, 7 and 14 days of implantation in immuno-competent rats, compared to CF scaffolds. However, the fibrous tissue formation was seen to be more important in OCS than in CS scaffolds. This higher amount of fibrous tissue suggests that hBPCs and hOBPCs secrete specific growth factors or cytokines at different concentration by inducing distinct amount of fibrous tissue. Based on these observations, we hypothesize that the presence of fibrous tissue in CS and OCS scaffolds is directly induced by the secretion of specific growth factors (*e.g.* CTGF) from the xenograft cells rather than by a reaction of the host's immune system due to the xenogeneic origin of the cells. To confirm *in vitro* and *in vivo* experiments would be required to investigate the signaling mechanism between the hBPCs or hOBPCs and the surrounding tissue (see sub-section 4.2.1). In parallel, we also noticed a higher amount of mature bone in CF scaffolds than in CS and OCS scaffolds after 14 days of implantation, based on histological evaluation.

We then confirmed that CF scaffolds induced a significantly higher amount of formed bone than in CS and OCS scaffolds performed under the same implantation and scaffold conditions than in the first *in vivo* study. This significant higher amount of bone was visible already after 2 weeks of implantation and lasted the entire duration of the experiment. Based on histological evaluation, we also showed that no fibrous capsule was visible after 12 weeks of implantation of CS and OCS scaffolds.

Consequently, the fibrous tissue, observed after 2 weeks of implantation (see chapter 2), was partially replaced by immature and mature bone inside CS and OCS scaffolds. Therefore, we can propose that the observed delay in bone formation inside CS and OCS scaffolds after 12 weeks of implantation results from the time needed for the body's host to remodel the fibrous tissue into bone tissue.

We also characterized the impact of mechanical loading and particularly its temporal onsets on bone regeneration in CF, CS and OCS scaffolds. We observed that early mechanical loading had no impact on the amount of formed bone inside CF scaffolds after 12 weeks of implantation, whereas delayed mechanical loading significantly increased it compared to no mechanical loading condition. Furthermore, we noticed that independently of the mechanical loading conditions, significantly higher amount of bone was formed in CF scaffolds than in the two cell-seeded types of scaffolds. Focusing on cell-seeded scaffolds, we showed that early mechanical loading had a positive influence on the bone formation inside CS scaffolds compared to no mechanical loading. In the case of OCS scaffolds, the early mechanical loading had a negative effect. These different behaviors on bone remodeling could potentially be explained by the different cell fates of hBPCs and hOBPCs. The transmission of fluid flow of the surrounding bone to hBPCs and hOBPCs seeded within scaffolds might affect differentially the expression of markers and growth factors. Therefore, it could results in an increase or decrease of bone formation inside CS or OCS scaffolds respectively. Like in the early mechanical loading, the delayed mechanical loading was seen to increase the amount of formed bone in CS scaffolds. In this case, the statistical difference in bone formation was observed to start after 8 weeks of implantation, whereas it started after 6 weeks of implantation for early mechanical loading. Lastly, we looked at the time needed to notice an impact of mechanical loading between the last mechanical loading session and its significant effect on bone formation. In the case of CS and OCS scaffolds, we noticed an interval of 5.5 weeks when subjected to an early mechanical loading. In the case of CF scaffolds, this interval was reduced to 3 weeks when subjected to a delayed mechanical loading.

Furthermore, a finite element analysis was used to evaluate the bone stiffness inside CF and CS scaffolds. In this model, a uniaxial compression was applied on the lateral side of the formed bone inside the implanted scaffold. Equivalent results were observed between BV/TV and bone stiffness evaluation. As both analyses were based on the same microCT images, the similarity is not surprising. For future experiments, a more physiological-mimicking model might bring more differentiated results. Specifically, the compression should be applied on the anterior axes of the animal's leg as in the *in vivo* experiments. The visualization of the scaffold as well as it distinction from bone would be a further improvement of the finite element model. To distinguish clearly the scaffold from the bone, a contrast agent could be added to the scaffold. For this purpose the scaffold should contain a contrast agent with a different density than bone. Thanks to this improvement, the property of the scaffold itself could be added to the model and be more realistic.

Finally, the results of this thesis allowed us to evaluate the bone formation outcome of different types of scaffolds for each loading condition, as recapitulated in Fig. 4.1. This bone formation outcome is defined as the ratio between the volumes of formed bone in early or delayed loading, over the internal no mechanical loading conditions:

Bone formation outcome $= \frac{(BV/TV)_{early\ loading}}{(BV/TV)_{no\ loading}}$ or $\frac{(BV/TV)_{delayed\ loading}}{(BV/TV)_{no\ loading}}$

This analysis highlighted that early mechanical loading accelerated twice the formation of bone in CS scaffolds, had a no effect on CF scaffolds and accelerated bone resorption in OCS scaffolds. We also found that delayed mechanical loading slightly increased the bone formation rate of ~30% after 12 weeks of implantation in CF scaffolds (ratio of 1.3) whereas it has a neutral-to-positive effect on CS scaffolds (ratio around 1).
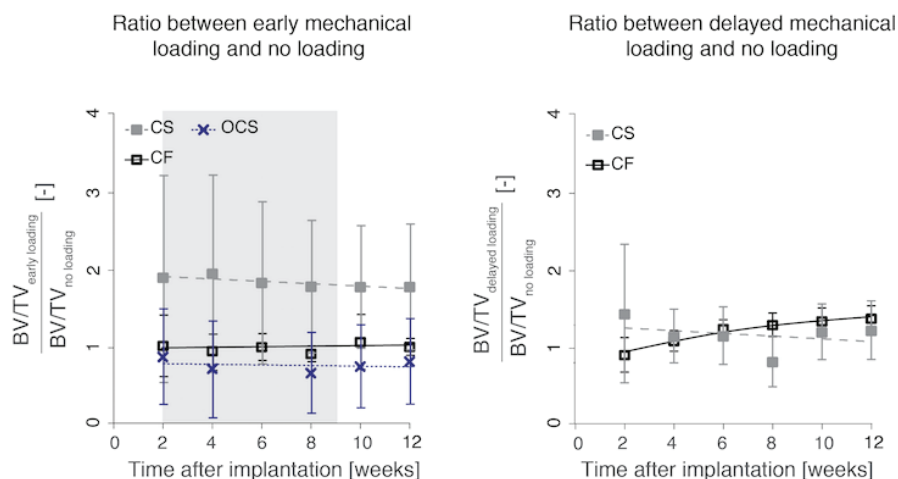

Figure 4.1 Ratios of BV/TV between early or delayed mechanical loading over no loading conditions for each scaffold condition. CF scaffolds are represented by black empty squares (□), CS scaffolds by filled squares (■) and OCS scaffolds by blue crosses (✕). The lines represent the fitted GAMM model. BV/TV ratios of CF groups are illustrated by solid black line, CS groups are drawn in dashed gray lines while OCS are pictured in small blue dots. The gray zone on the graphics shows the time span where a significant difference exists between CF and CS groups. No significant difference was observed between OCS and CF groups, whereas between OCS and CS groups a significant difference was seen from the start until the end of the study (not shown) (n=5–6).

These findings suggest that beyond the total amount of formed bone volume in the scaffolds, the speed of bone formation can further be modulate by applying an appropriate mechanical loading. Consequently, although the bone volume was significantly higher inside CF scaffolds than inside CS or OCS scaffolds, the maximum speed of bone formation was reached in CS scaffolds under early mechanical loading. This statement might be highly relevant in the context of larger bone defects for example. Indeed, critical size bone defects treated with CF scaffolds might suffer from the limited migration rate of endogenous cells, which might take few days to weeks to entirely fill the scaffold and initiate bone regeneration. Such delay, not present when using cell-seeded scaffolds, may promote the choice toward a strategy based on CS scaffolds combined with early mechanical loading, which might then become competitive to a CF scaffold therapy.

4.2   Future Experimental Works

For both aims of this thesis, further experiments should be conducted to detail the underlying mechanisms of the findings.

4.2.1 *In Vitro* and *in Vivo* Quantification of CTGF Secretion and its Impact on Fibrous Tissue Formation

Among other growth factors, connective growth factors (CTGF) have been shown to be strongly involved in the formation of fibrous tissue (Moussad & Brigstock 2000; Lee et al. 2010). Therefore, *in vitro* experiments quantifying the secretion of CTGF of hBPCs and rat BPCs (rBPCs) would be insightful before, during and after osteogenic differentiation. Indeed, these experiments would give a first piece of proof that the fibrous tissue formation observed at the early stage of implantation could be induced by the temporal secretion of CTGF by hBPCs and hOBPCs instead of the immune system as discussed in Chapter 2. Thanks to these experiments we might find out that (1) hBPCs do express CTGF, that (2) a secretion increase is observed during the osteogenic differentiation of hBPCs, and that (3) hOBPCs secrete a higher amount of CTGF than hBPCs after their terminal differentiated state (14 days in culture). For this experiment, we would use rat and human bone-derived mesenchymal stem cells (MSCs) as controls. Furthermore, it would also be interesting to evaluate the effect of added CTGF to the cell culture medium and compare our results with those obtained by Lee et al. (Lee et al. 2010). In their study, they have shown that human MSCs differentiated into fibroblasts induced by an extra addition of CTGF. They have also described that MSCs fail to differentiate into osteoblasts in the addition of CTGF when cultured in an osteogenic differentiation medium.

Additional *in vivo* experiments using syngeneic rBPCs or bone-derived rat MSCs should be performed to give the final proof that the observed fibrous tissue after 3, 7 and 14 days after implantation of CS and OCS was effectively induced by hBPCs and hOBPCs, respectively. In the case of lack of fibrous tissue formation using rBPCs or bone-derived rat MSCs, we would then know that the fibrous tissue formation was driven by the immune system, responding to xenograft cells implantation. Hypothesizing that it is the case, it would be interesting then to make a long-term *in vivo* experiment using rBPCs or bone-derived rat MSCs to evaluate the bone formation density compared to CF scaffolds. If in this last experiment a lower amount of bone density was observed using different types of cells originating from rat, it would confirm that PLA/5% ß–TCP scaffold used in this study is a system having the required quality to be applied in clinics without cell therapy. If on the other hand, this *in vivo* experiment would show a significant increase in bone density inside scaffolds seeded with rat affiliated cells, a potential clinical application of hBPCs in human could be reconsidered.

4.2.2 Optimization of the Imaging and Numerical Modeling for Bone Quality Evaluation

In this thesis we numerically modeled the bone stiffness inside CF and CS scaffolds without taking into account the scaffold's geometry and mechanical property due to technical issues. Specifically, we did not find an accurate way to mark and visualize the scaffold on microCT scans once implanted, as initially expected. Such technique would have been particularly useful to evaluate if the augmentation of a mechanically loaded scaffold would optimize the bone formation to increase the mechanical properties of the scaffolds in its weakest spots. As a possible solution, a scaffold combined with a contrast agent could be used to differ its density from the bone one, and be better determined on microCT scans. Once the difference between scaffold and newly formed bone could be distinguished, the according mechanical properties could be implemented in a finite element model. Also axial compression could be applied in the same physiological axis than in the *in vivo* experiments as discussed in Chapter 3. Furthermore, as the bone stiffness and geometry is not the only thing needed to assess the bone quality and strength in regeneration, it would be valuable to

complete this analysis with other techniques focusing on the material factors (Donnelly 2011). For example, Raman microspectroscopy could be used complementary to microCT imaging to assess the physiochemical component of the newly formed bone, such as the mineral crystallinity, cross-linking and mineral/matrix ratio (Draper et al. 2005). A more complete characterization of bone quality inside CF and CS scaffolds could be elaborated by combining microCT images, Raman microspectroscopy and finite element analysis in an *in vivo* study extended to 20 or 30 weeks after implantation.

4.2.3   Scaffold Processing for Histological Evaluation

In this work, we used PLA/5% ß–TCP scaffolds for all *in vivo* experiments. As this scaffold cannot be softened and can only be cut when embedded in MMA resin, we were restricted to the use of color stains for histological analysis, such as Toluidine blue stain. The development of a proper protocol to soften the scaffold without altering the bone samples would open the possibility of demineralizing them and embedding them in paraffin. Contrary to MMA resin, immunohistostaining and specific DNA and RNA sequences labeling are feasible on paraffin fixed samples. As we have seen in Chapter 2, we tried to optimize the embedment material by changing it in order to label a specific DNA sequence using *in situ* hybridization, with a relatively low success level. Should a better scaffold processing for immunohistochemistry in PLA/5% β-TCP scaffolds be possible, it would be interesting to (1) visualize implanted cells and (2) evaluate in a more precise way the immune reaction by targeting specific cytokines, growth factors and extracellular matrix components.

4.3   Conclusion

To conclude, we demonstrate specifically for this study, that CF scaffolds are the best solution for BTE when combined with delayed mechanical loading, followed by early mechanical loading or no loading. Continuing the ranking of the analyzed solutions, we saw that early mechanical loading in CS scaffolds was equivalent in terms of bone formation after 12 weeks of implantation than OCS scaffolds without mechanical loading. These two conditions were still significantly higher than the last options, namely CS scaffolds without mechanical loading or OCS scaffolds under early mechanical loading. Even if there is still a long and challenging path to follow in order to reach a stable and satisfactory bone formation for clinical application in the tested systems, CF scaffolds combined with delayed mechanical loading has the merits to be simple and safe from a clinical point of view, without additional costs and increasing regulatory restriction due to the use of cells. Based on these conclusions, it is of long-term advantage for the patient to achieve a better bone formation density by delaying the start of its mobilization and rehabilitation, rather than by loading the operated site hastily. On the other hand, application of early mechanical loading might be beneficial in specific cases where a cell-seeded scaffold-based therapy would be preferred, perhaps for the treatment of critically large bone defects.

4.4 References

Amini, A.R., Laurencin, C.T. & Nukavarapu, S.P., 2012. Bone tissue engineering: recent advances and challenges. *Critical Reviews in Biomedical Engineering*, 40(5), pp.363–408.

Boerckel, J.D. et al., 2012. Effects of *in vivo* mechanical loading on large bone defect regeneration. *Journal of Orthopaedic Research*, 30(7), pp.1067–1075.

Boerckel, J.D. et al., 2011. Mechanical regulation of vascular growth and tissue regeneration in vivo. *Proceedings of the National Academy of Sciences of the United States of America*, 108(37), pp.E674–E680.

Donnelly, E., 2011. Methods for assessing bone quality: A review. *Clinical Orthopaedics and Related Research*, 469(8), pp.2128–2138.

Draper, E.R. et al., 2005. Novel assessment of bone using time-resolved transcutaneous Raman Spectroscopy. *Journal of Bone and Mineral Research*, 20(11), pp.1968–1972.

Dupont, K.M. et al., 2010. Human stem cell delivery for treatment of large segmental bone defects. *Proceedings of the National Academy of Sciences*, 107(8), pp.3305–3310.

Duty, A.O., Oest, M.E. & Guldberg, R.E., 2007. Cyclic mechanical compression increases mineralization of cell-seeded polymer scaffolds in vivo. *Journal of Biomechanical Engineering*, 129(4), pp.531–539.

Jäger, M. et al., 2007. Bone healing and migration of cord blood-derived stem cells into a critical size femoral defect after xenotransplantation. *Journal of Bone and Mineral Research : the Official Journal of the American Society for Bone and Mineral Research*, 22(8), pp.1224–1233.

Lee, C.H. et al., 2010. CTGF directs fibroblast differentiation from human mesenchymal stem/stromal cells and defines connective tissue healing in a rodent injury model. *The Journal of Clinical Investigation*, 120(9), pp.3340–3349.

Liu, Y. et al., 2013. Integration of a calcined bovine bone and BMSC-sheet 3D scaffold and the promotion of bone regeneration in large defects. *Biomaterials*, 34(38), pp.9998–10006.

Montjovent, M.-O. et al., 2008. Human fetal bone cells associated with ceramic reinforced PLA scaffolds for tissue engineering. *Bone*, 42(3), pp.554–564.

Moussad, E.E. & Brigstock, D.R., 2000. Connective tissue growth factor: what's in a name? *Molecular Genetics and Metabolism*, 71(1-2), pp.276–292.

Robling, A.G. et al., 2002. Improved bone structure and strength after long-term mechanical loading is greatest if loading Is separated into short bouts. *Journal of Bone and Mineral Research*, 17(8), pp.1545–1554.

Roshan-Ghias, A. et al., 2010. *In vivo* cycling loading as potent stimulatory signal for bone formation inside tissue engineereing scaffolds. *European Cells and Materials*, 19, pp.41–49.

Roshan-Ghias, A. et al., 2011. *In vivo* loading increases mechanical properties of scaffold by affecting bone formation and bone resorption rates. *Bone*, 49(6), pp.1357–1364.

Srouji, S. & Livne, E., 2005. Bone marrow stem cells and biological scaffold for bone repair in aging and disease. *Mechanisms of Ageing and Development*, 126(2), pp.281–287.

Xu, C. et al., 2010. A novel biomimetic composite scaffold hybridized with mesenchymal stem cells in repair of rat bone defects models. *Journal of Biomedical Materials Research Part A*, 95(2), pp.495–503.

Curriculum Vitae

Tanja HAUSHERR

In couple + 1x 🍼 1x 👤
28.12.1984, Swiss

French and Swiss German, native   Native   Fluent

Avenue de Bel-Air 93
1814 La Tour-de-Peilz
Switzerland
+41 (0) 79 793 29 03
hausherr.tanja@gmail.com

EDUCATION

PhD Candidate in Biotechnology & Bioengineering   2012-2016
Swiss Federal Institute of Technology, EPFL (Lausanne, Switzerland)
In vivo mechanical loading combined with a bone-tissue engineering scaffold (Prof. D. P. Pioletti)

Master of Sicence in Bioengineering & Biotechnology   2009-2011
Swiss Federal Institute of Technology, EPFL (Lausanne, Switzerland)
2D stem cells culture on microfluidic-generated hydrogel microbeads (Prof. M. P. Lutolf)

Bachelor of Life Sicences & Technology   2004-2009
Swiss Federal Institute of Technology, EPFL (Lausanne, Switzerland)
Intraperitoneal drug delivery for prevention of postoperative adhesion (Prof. J. A. Hubbell)

SKILL PROFILE

General laboratory skills
Mammalian and stem cell culture, DNA and RNA extraction, PCR and RT-PCR, histology on resin (from embedment to staining), work in P1 and P2 biosafety level, transduction of mammalian cells with lentiviruses, immunohistochemistry and fluorescent staining

In vivo experimental skills
Basic surgery and care, SC and IP injections, scaffold implantation in femoral condyles, organs harvesting, microCT scanning

Tissue engineering related skills
Functionalization of hydrogels, microfluidic hydrogel beads generation, cell culture in 3D biomaterials
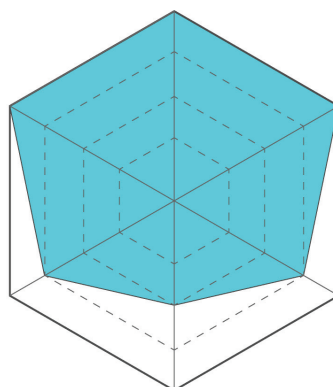
Acquired general working skills
Data and statistical analysis, team and project management, teaching

Imaging skills
Stereomicroscope, widefield microscope, brightfield and fluorescent microscope, confocal microscope and microCT scanning

Programming skills
C, C++, Latex, MATLAB, R, AMIRA and Abaqus

PROFESSIONAL PROFILE

I am an energetic and open-minded person who has developed a mature and responsible approach to any task or situation that I am presented with. Through my undergraduate and graduate education, I have acquired an excellent multidisciplinary knowledge. I have developed skills allowing me to lead research project as well as developed an analytical dexterity essential for product development. I am excellent in working with others and getting the best out of my co-workers to achieve a certain objective in time and with excellent quality.

CONFERENCES

European Society of Biomechanics
Oral presentation — June 2015

Swiss Society for Biomaterials & Regenerative Medicine
Poster — April 2015

OTHER EXPERIENCES

June 2014 - Jan. 2016 — **Co-founder and treasurer**
Life Sciences PhD association (ADSV), EPFL

Research Day on Translational Musculoskeletal Biomechanics
Oral presentation — June 2014

PUBLICATIONS

2013 —

T. C. Hausherr, H. Majd, D. Joss, A. Müller, D. P. Pioletti, M. A. M. Gijs and Ch. Yamahata, *Capillary-vavled-based platform towards cell-on-chip mechanotransduction assays,* Sensors and Actuators B-Chemical, 188, pp. 1019-1025

S. Allazetta, **T. C. Hausherr**, M. P Lutolf, *Microfluidic synthesis of cell-type-specific artificial matrix hydrogels,* Biomacromolecules, 14(4), pp. 1122-1131

RESEARCH EXPERIENCES

PhD candidate
Laboratory of Biomechanical Orthopedics, EPFL
Prof. D. P. Pioletti
In vivo bone tissue engineering
March 2012 - Present

Research assistant
Laboratory of Microsystems (LMIS2), EPFL
Prof. M. A. M. Gijs
Bio-MEMS in vitro characterization
Aug. 2011 - March 2012

Intern
Laboratory of Stem Cell Bioengineering, EPFL
Prof. M. P. Lutolf
PEG hydrogel characterization
Feb. 2010 - Aug. 2010

Sept. 2007 - Jan. 2012 — **Teacher** (children, teenagers, adults)
Netpune, Hip-hop dance school, Switzerland

Sept. 2005 - Jun. 2006 — **Responsible for sponsors**
Yearbook association, EPFL

June 2005 - Jan. 2011 — **Nursing assistant** (1 week-end/month + holidays)
Phare-Elim, home for seniors, Switzerland

120